

HCN4 pacemaker channels as potential therapeutic targets based on their novel structural properties



TECHNISCHE
UNIVERSITÄT
DARMSTADT

Vom Fachbereich Biologie der Technischen Universität Darmstadt
zur Erlangung des akademischen Grades
eines Doctor rerum naturalium (Dr. rer. nat.)
genehmigte Dissertation von

Atiyehsadat Sharifzadeh

IRAN


1. Referent/Referentin: Prof. Dr. Gerhard Thiel
2. Referent/Referentin: Prof. Dr. Anna Moroni

Tag der Einreichung: 08/03/2023

Tag der mündlichen Prüfung: 24/04/2023

Darmstadt 2023

D17



Atiyehsadat Sharifzadeh: HCN4 pacemaker channels as potential therapeutic targets based on their novel structural properties
Darmstadt, Technische Universität Darmstadt,
Jahr der Veröffentlichung der Dissertation auf TUprints: 2023
Tag der mündlichen Prüfung: 24/04/2023
Veröffentlicht unter CC BY-SA 4.0 International
<https://creativecommons.org/licenses/>

Table of contents

Abstract	7
Zusammenfassung.....	8
Overview	10
1. Introduction.....	12
1.1 Eukaryotic membrane proteins: Challenging molecules for structural biology/biochemistry	12
1.2 HCN channels	13
1.2.1 Tissue and Cellular Expression Pattern of HCN Channels	14
1.2.2 Functional role of HCN channels in nervous and cardiac tissues	16
1.2.3 Dysfunction of HCN channels.....	16
1.2.3.1 HCN1 and disease.....	17
1.2.3.2 HCN2 and disease.....	17
1.2.3.3 HCN4 and disease.....	18
1.2.4 Structural features of HCN channels.....	20
1.2.4.1 Architecture of HCN1 channels.....	20
1.2.5 So similar, so different: The cAMP sensitivity	22
PART I	24
2.1 Materials and methods (part I and II)	25
2.1.1 Constructs.....	25
2.1.2 Protein expression and membrane isolation	25
2.1.3 Protein purification in LMNG/CHS	26
2.1.4 Protein purification in amphipols.....	26
2.1.5 Thermal denaturation assay	27
2.1.6 Thermal shift of GFP-HCN4 Holo following Mg ²⁺ removal assay	28
2.1.7 Setting of a fast screening system for ligand binding to purified GFP-HCN4	28
2.1.8 Monitoring cyclic di-GMP binding to the GFP-HCN4 pacemaker channel using the thermal shift assay.....	29
2.2 The cryo-EM structure determination of HCN4 with and without cAMP bound	30
2.2.1 HCN4 response to cAMP: a structural view	31
2.2.2 The closed and open pore structure of HCN4.....	34
2.2.3 Selectivity and permeation in HCN	36
References.....	37

PART II	44
3. Monitoring ligand binding to purified HCN4 channels	45
3.1 Detection of cyclic di-GMP binding to the HCN4 pacemaker channel	49
References.....	53
PART III	60
4. Isolation of state-dependent nanobodies against HCN4 channels using a yeast surface display platform	61
Abstract	61
4.1 Introduction.....	62
4.1.1 Nanobodies	62
4.2 Materials and Methods	66
4.2.1 Constructs	66
4.2.2 Preparation of antigens.....	66
4.2.3 Naïve yeast library growth and induction of protein expression	66
4.2.4 Nanobody expression test	67
4.2.5 Procedure of selection using MACS and FACS	67
4.2.6 Fast-screening method for identifying the sequences over-represented	69
4.2.7 Cloning the isolated nanobody genes into bacterial vector	70
4.2.8 Expression and purification of isolated nanobodies in E.coli	71
4.2.9 SDS-PAGE and Western Blot analysis.....	72
4.2.10 Nanobody Labelling.....	72
4.2.11 Analysis the interaction affinity and the dissociation constant (KD) using Microscale Thermophoresis (MST)	72
4.2.12 Binding check assay.....	73
4.2.13 Monitoring the interaction of Nb19, 34 and 68 with the HEK cells expressing GFPHCN4 using the analytical FACS.....	73
4.2.14 Electrophysiology	74
4.3 Results	75
4.3.1 Checking the quality of nanobodies' expression on the surface of yeast	75
4.3.2 Selection procedure using iterative MACS and FACS.....	76
4.3.3 Isolation of clones	81
4.3.4 Expression and purification of nanobodies for functional studies	84
4.3.5 Functional characterization of nanobodies in HEK293T cells	87
4.3.5.1 Effect of nanobodies from the extracellular side	87




4.3.5.2 Effect of nanobodies from the intracellular side	98
4.3.6 Monitoring the interaction of Nb19, 34 and 68 with HCN4 using biochemical assays	99
.....	
4.3.7 Conclusions.....	104
References.....	108
Declaration of own work.....	117
EHRENWÖRTLICHE ERKLÄRUNG	118
CURRICULUM VITAE	119

Abstract

Over the past few years, single particle cryogenic electron microscopy (cryo-EM) has made impressive impacts on the research field of structural biology of large eukaryotic membrane proteins. These are, indeed, challenging proteins for structural biology as they have a low yield of expression and thus purification. Their low purification yield originates from the fact that they require an expression in complex cell systems, such as mammalian cell lines. These systems provide them with the suitable physiological environment for their proper maturation but limit their over-expression. This makes them generally not suitable for classical methods of structural biology such as X-ray and NMR. But in the advent of improved cryo-EM methods it turned out that even a small amount of pure protein may often be sufficient for structural studies with this new technology. In this context, the present PhD thesis is focused on setting the procedure for the expression and for the subsequent purification of a large eukaryotic protein in mammalian HEK293F. The purified protein of interest, the Hyperpolarization activated and Cyclic Nucleotide regulated (HCN4) pacemaker channel, was eventually used to obtain high resolution structures of the channel in the open and closed state by cryo-EM. This allowed to unravel the structural determinants of key phenomena of HCN channel function such as gating/ion permeation, and the HCN4 specific cyclic nucleotide-dependent modulation. Furthermore, the protocol of HCN4 purification that I have set here has also opened in combination with the structural information the possibility of performing biochemical studies with the full-length protein. This led to the identification and characterization of drugs, which can modulate HCN function in an isoform specific manner. Here I show the successful use of purified HCN4 to detect and quantify ligand binding with molecules whose interaction with the channel protein was so far impossible with classical biochemistry. The most important outcome of this work is the use of purified HCN4 as a bait in a yeast displayed nanobody library. This screening endeavour resulted in the discovery of new nanobodies, which can modulate with high affinity HCN channel function in an isoform specific manner. This may eventually lead to the first HCN4 specific drug for targeting cardiac arrhythmias related to the malfunction of this pacemaker channel.

Zusammenfassung

In den letzten Jahren hat vor allem die Einzelpartikel-Tiefemperatur-Elektronenmikroskopie (cryo-EM) erheblichen Einfluss auf die Strukturbiologie von großen Membranproteinen aus Eukaryoten gewonnen. Die entsprechenden Proteine sind vor allem wegen ihrer geringen Ausbeute in der Expression und der folgenden Aufreinigung eine große Herausforderung für Strukturbiologen. Die geringe Ausbeute bei der Proteinreinigung ist in der Regel darauf zurückzuführen, dass die Proteine in komplexen Zellsystemen, z. B. Säugerzellen, exprimiert werden müssen. Während diese Systeme eine geeignete physiologische Umgebung für die korrekte Faltung der Proteine ermöglichen, sind sie andererseits für die geringe Ausbeute verantwortlich. Aus den genannten Gründen sind großen Membranproteinen meist nicht zugänglich für klassische Methoden der Strukturbiologie wie Röntgen-Kristallographie oder NMR. Im Rahmen, der sich ständig verbessernden Methoden in der cryo-EM Technik hat sich jedoch herausgestellt, dass mit dieser Technik selbst geringe Mengen an gereinigtem Protein ausreichen können, um Strukturstudien durch führen zu können. In diesem Kontext beschäftigt sich die vorliegende Arbeit mit der Ausarbeitung von Protokollen, die eine Expression mit folgender Aufreinigung von einem großen eukaryotischen Membranprotein in der Säugerzelllinie HEK293F ermöglichen. Die Aufreinigung des Proteins von Interesse, der hyperpolarization activated and cyclic nucleotide regulated (HCN4) Schrittmacherkanal, wurde in Folge genutzt, um mittels cryoEM hochauflösenden Strukturen des Kanals im offenen und geschlossenen Zustand zu gewinnen. Dies eröffnete Einblicke in die strukturellen Besonderheiten des Proteins, die die funktionellen Eigenarten von HCN Kanälen wie Kanalschalten / Ionendurchtritt und die HCN4 spezifische Modulation durch zyklische Nucleotide, erklären. Das Protokoll zur Aufreinigung von HCN4, das ich hier etabliert habe, erlaubte in Kombination mit den Strukturdaten, ebenfalls die Möglichkeit biochemische Experimente mit dem Volllängenprotein durchzuführen. Diese haben zur Identifizierung und Charakterisierung von Wirkstoffen geführt, die in der Lage sind, die Funktion der HCN Kanäle in einer Isoform-spezifischen Weise zu modulieren. Ich präsentiere hier den erfolgreichen Einsatz von gereinigtem HCN4 zur Detektion und Quantifizierung von Liganden-Bindung mit Wirkmolekülen, die bisher mit konventionellen Methoden nicht möglich war. Das wichtigste Ergebnis aus dieser Arbeit ist die Nutzung von gereinigtem HCN4 Protein als Köder zum



Durchmustern einer Hefe Nanobody display Bibliothek. Diese Durchmusterung führte zur Isolation eines neuen Antikörpers, der in der Lage ist, mit hoher Affinität die Funktion des Kanals in einer Isoform-spezifischen Weise zu modulieren. Daraus resultiert die Entwicklung des ersten HCN4 spezifischen Wirkstoffes, der das Potential hat um in Zukunft eingesetzt zu werden, um Herzrhythmusstörungen, die auf einer Fehlfunktion dieses Kanals beruhen, zu korrigieren.


Overview

The present PhD thesis, which is focused on the establishment of a robust procedure for production and purification of HCN4, let our laboratory to publish a recent work, which constitutes Chapter I of the thesis: “Gating movements and ion permeation in HCN4 pacemaker channels “ (Saponaro, Bauer, et al., 2021). By studying on the structure-function relationship on the pacemaker channel, the work describes the atomistic details of the cyclic nucleotide-dependent modulation of HCN channels and highlights HCN4 subtype-specific features. Moreover, it contributes mechanistic understanding on HCN channel gating, and ion permeation.

Identification of HCN isotype-specific differences offers excellent opportunities for the rational design of drugs. In this light, Chapter II presents the results of a recent publication (Saponaro, Sharifzadeh, et al., 2021) in which I have adapted a screening system, based on fluorescent thermal shift assay, to detect binding of small molecules to the purified GFP-tagged HCN4 protein. This system was useful to detect binding of Ivabradine, the unique commercially available HCN blocker, to HCN4 proteins purified with the pore in the open state. Chapter II ends with unpublished data showing the first biochemical evidence of the binding between HCN4 channels and c-di-GMP, a molecule representing, nowadays, the only example of an isotype specific drug for HCN channels.

In Chapter III, I will present the results of another screening strategy that I adopted to find subtype-specific drugs. In this approach, purified HCN4 protein in either open or closed pore conformation is used to screen a yeast surface display platform to select nanobodies that specifically target the open or the closed configuration of the HCN4 pore. This approach relies on the multi-copy display of nanobodies on the yeast cell surface, applying the given protein as an antigen, and using a cell-based selection scheme by Magnetic Cell Sorting (MACS) and Fluorescence-Activated Cell Sorting (FACS) that allows straightforward and rapid identification of conformationally selective nanobodies.

Overall, I used the benefit of purifying HCN4 in the open and close pore conformations together with the thermal shift assay and yeast surface display platform as tools for screening the specific binders to pacemaker HCN4 channels. In the future, cryo-EM structures of HCN4



- binder (either molecule or nanobody) complex will provide further details on their interaction, thus facilitating the rational design of more potent drugs.

1. Introduction

1.1 Eukaryotic membrane proteins: Challenging molecules for structural biology/biochemistry

Biochemistry and structural biology of eukaryotic membrane proteins are challenging because they usually require large amounts of purified protein. This limit is due to their obliged expression in a complex cell system, mammalian cells, which provide them with the physiological environment for their proper maturation. Indeed, eukaryotic membrane proteins often require post translational modifications, such as N-linked glycosylation, and a near native lipid environment, for instance with high levels of cholesterol. These features are typical of mammalian and not of yeast and insect cells, other two systems frequently used for expression of eukaryotic proteins. The low yield of purification is the reason why biochemical characterization of eukaryotic membrane proteins, like for instance protein - ligand interaction studies, is preferentially performed on the isolated soluble domains rather than on the full-length proteins. The same obstacle has been experienced in structural biology. Nonetheless, the technology employed in biochemistry and structural biology of membrane proteins has over the past few years significantly improved with tremendous impacts on understanding large eukaryotic membrane proteins. Single particle cryogenic electron microscopy (cryo-EM) has recently revolutionized structural biology. In this case the obstacle of a low yield of purification of eukaryotic membrane proteins is overcome by the fact that cryo-EM requires very small amounts of purified protein. But also, the biochemical methods of membrane proteins have been improved. In particular, the fusion of the target protein with fluorescent proteins, like GFP, significantly improved the sensitivity of methods employed for detecting ligand – protein interaction.

The present thesis will take advantage of the above cited technologies to characterize HCN4 pacemaker channels as potential therapeutic targets.

1.2 HCN channels

HCN channels, the molecular correlate of the I_f/I_h currents, are mammalian membrane proteins that play important roles in several physiological processes and various pathological conditions (Baruscotti & DiFrancesco, 2004; Gareth et al., 2005; Robinson & Siegelbaum, 2003). They belong to the superfamily of voltage-dependent ion channels and they serve as nonselective voltage-gated cation channels in the plasma membranes of heart and brain cells. In neurons, the current is called hyperpolarization-activated current (I_h) and controls a wide array of functions, such as rhythmic activity and excitability (Pape & McCormick, 1989). In the heart, the current through HCN channels is called "funny" current (I_f) because of its opposite voltage dependency to most other heart currents (D. DiFrancesco, 2006). In this work, the term I_f will be used.

The HCN channels have unique features compared to other voltage-gated channels: they are less selective for K^+ ions and possess a significant permeability to sodium; on average HCN channels conduct 1 Na^+ ion per 4 K^+ ions (D. DiFrancesco, 1993). Indeed, the small sodium permeation is critical because it contributes to the depolarization of the membrane potential and in this way to the initiation of a subsequent action potential following a strong hyperpolarizing stimulus. HCN channels are primarily activated by membrane hyperpolarization in contrast to most other voltage-gated potassium (K_v) channels which are activated by membrane depolarization (Baruscotti et al., 2012; Flynn & Zagotta, 2018). Their voltage dependent activation is further modulated by the direct binding of nucleotides to the cyclic nucleotide binding domain (CNBD) in the cytosol. (J. C. DiFrancesco & DiFrancesco, 2015), and

These channels are encoded by four HCN channel genes (HCN1, HCN2, HCN3, and HCN4) that share about 60% sequence identity, which increases up to 89-90% in the core transmembrane regions and the cytosolic regions (Santoro et al., 1998). Indeed, the four mammalian subtypes (HCN1-4) show the main biophysical properties of I_f current but vary in voltage dependence, as well as activation time constants (τ) that are inversely related to the magnitude of the hyperpolarization. Typical values of the half-activation potential ($V_{1/2}$) are: -70 mV for HCN1, -95 mV for HCN2, -77 mV to -95 mV for HCN3 and -100 mV for HCN4. Among the four subtypes, HCN1 exhibits the fastest activation kinetics upon hyperpolarization

(Stieber et al., 2005; Wahl-Schott & Biel, 2009). The subtypes also differ from one another in their response to cyclic nucleotides (Robinson and Siegelbaum, 2003; Fürst & D'Avanzo, 2015; Stieber et al., 2005; C. Wahl-Schott & Biel, 2009). The activation of HCN2 and HCN4 for example is potentiated much more by cAMP than that of HCN1 channels. The HCN3 channel, unlike other HCN subtypes, is not modulated at all by intracellular cAMP (Stieber et al., 2005).

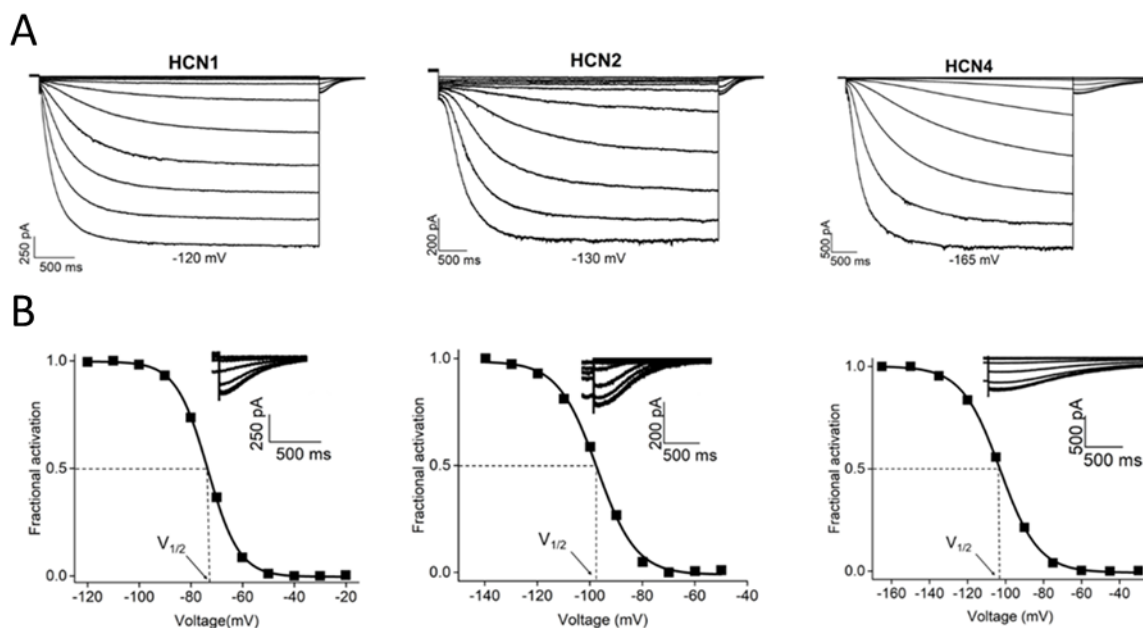



Figure 1.1. Biophysical properties of HCN homotetramers expressed in HEK293T cells. A. Representative current trace elicited by HCN1 (left), HCN2 (center) and HCN4 (right). HCN1 has the fastest activation and deactivation kinetics and reaches saturation at more depolarized potentials compared to HCN2 and HCN4 which also shows the slowest kinetics. **B.** Activation curves of HCN1, HCN2 and HCN4 extrapolated from normalized tail current amplitude plotted against the preconditioning hyperpolarizing voltage step used to activate the current. Fitting activation curves with a Boltzmann equation provides the half-maximal potential ($V_{1/2}$) indicated with the black arrow. Inset shows an enlargement of tail currents used to fit the activation curve (Data has been generated in our lab by Roberta Castelli).

1.2.1 Tissue and Cellular Expression Pattern of HCN Channels

The expression pattern of HCN1-4 channel isoforms markedly differs in various regions and displays distinct biophysical properties. The expression of each subunit and the relative distribution of these channels are likely influencing their function. HCN channels were first



discovered in the rabbit sinoatrial node (SAN) (D. DiFrancesco, 1993) where they are highly expressed and initiate action potentials. They are also found in neurons where they regulate neuronal firing rates (Wahl-Schott & Biel, 2009). Although HCN4 has been determined as the principal HCN isoform in the heart (Herrmann et al., 2011; Ishii et al., 1999; Marionneau et al., 2005), a distinct expression of HCN1 and also a confined expression of HCN2 in murine sinoatrial cells at the protein level has been detected (Herrmann et al., 2011). This indicates that the expression of these three subunits together contribute to the I_f current in these cells (Herrmann et al., 2015). In addition, while HCN3 also plays a functional role in ventricular myocytes (Fenske et al., 2011), the basic biophysical and pharmacological properties of HCN3 channels, in comparison to the other isoforms of HCN channels, are less known because the functional expression of HCN3 proves to be difficult to detect (Stieber et al., 2005). Indeed, all four isoforms of the HCN channels have been expressed in the heart, with a highly different expression pattern depending on the heart region, heart health status, and species (Robinson & Siegelbaum, 2003). Overall it occurs that the human HCN4 is the most expressed isoform in the heart and contributes to 80% of the I_f current in SAN (Sartiani et al., 2017). Because of its prevalence in the heart the human HCN4 also represents an excellent, unique, and widely used marker for detection of cardiac pace-making cells (Herrmann et al., 2012).

HCN channels are also strongly expressed in the Central and Peripheral Nervous Systems (CNS, PNS) with distinct subunit-specific patterns (Novella Romanelli et al., 2016). In the CNS, HCN1 shows high expression within neurons of the neocortex, hippocampus, and cerebellar cortex (Santoro et al., 2000). HCN2 has a wide distribution in the CNS but is particularly abundant in hippocampus and neocortex (Notomi & Shigemoto, 2004). HCN4 is expressed strongly in the CNS in a limited number of areas such as the olfactory bulb and the thalamus (Novella Romanelli et al., 2016). Moreover, the expression of HCN channels in cells outside of the nervous system and heart such as the retina (Fyk-Kolodziej & Pourcho, 2007), kidney (Bolívar et al., 2008) pancreas (El-Kholy et al., 2007), and bladder (He et al., 2012) is demonstrated. In addition, unusual neuronal activity like epilepsy and environmental stimuli decrease the expression of HCN channels (Jung et al., 2010).

1.2.2 Functional role of HCN channels in nervous and cardiac tissues

The HCN channels possess biophysical properties which are essential for neuronal and cardiac physiology. In neuronal function, HCN channels control the excitability and electrical responsiveness of cells. The heart's HCN channels, which predominantly exist in the form of HCN4, generate the normal heart impulses that originate from SAN in the right atrial endocardium. In SAN, the HCN channels coordinate together with the ryanodine receptor spontaneous electrical activity (Wahl-Schott et al., 2014). In the atrioventricular node, the essential role of HCN channels has also been demonstrated to sustain the generation of spontaneous electrical activity and the conduction of stimuli from atria to ventricles (Verrier et al., 2014). In the heart and many neurons of the central nervous system, the HCN channels are constitutively open at the resting membrane potential. The consequent depolarizing inward I_f current maintains the membrane potential near the resting membrane potential and close to the firing threshold (Biel et al., 2009; Burke et al., 2013). In addition, constitutively open HCN channels also lower the membrane resistance and stabilize the resting membrane potential by opposing the hyperpolarizing or depolarizing inputs (Biel et al., 2009). This property of HCN channels results from its permeability to sodium and potassium; this mixed cation current counteracts both membrane hyperpolarization and depolarization. Thus, the HCN channels serve as a feedback mechanism-constantly opposing fluctuations of the membrane potential by generating depolarizing inward current or by facilitating hyperpolarization (Burke et al., 2013; Wahl-Schott & Biel, 2009).

In distal dendrites of several neurons, HCN1 has an important role in regulating dendritic integration, which is a crucial process in signal processing in most neurons (Burke et al., 2013), neuronal pace-making, and establishing action potential threshold (Tanguay et al., 2019). A lot of studies show the role of HCN2 in neuropathic pain, peripheral neuronal sensitization, the development of chronic pain, and in regulating the acute phase of neuronal hypersensitivity (Emery et al., 2011; Herrmann et al., 2015; Young et al., 2014).

1.2.3 Dysfunction of HCN channels

Given the importance of HCN channels in the nervous system and the heart, their malfunction plays a role in the genesis of human diseases such as cardiac arrhythmias,

epilepsy, neuropathic pain (Baruscotti et al., 2010; Biel et al., 2009) and depression-related behavior (Liston, 2019).

1.2.3.1 HCN1 and disease

Even though all four HCN isoforms are expressed in the brain, their expression profiles are heterogeneous with HCN1 being the predominant subtype in the cortex (Moosmang et al., 1999). Among HCN subtypes, HCN1 shows the most positive threshold for activation, the fastest activation kinetics, and the lowest sensitivity to cAMP (Chen et al., 2001; Marini et al., 2018). Interestingly, both long-term up- and downregulation of HCN channels, due to abnormal expression or cellular distribution that affect neuronal firing patterns, have been associated with epilepsy (Noam et al., 2011). Epilepsy is a group of neurological disorders in which hypersynchronous network activity drives the occurrence of recurrent spontaneous seizures (Reid et al., 2012). From a molecular point of view, a striking correlation between the epileptic phenotype observed in patients and the localization of epilepsy-causing mutations on the HCN1 gene has not yet been reported. In fact, studies on the characterization of HCN1 variants have shown that both HCN1 gain-of-function and loss-of-function mutations can lead to similar phenotypes which might be due to HCN's ability to counteract equally well both excitatory and inhibitory inputs in the brain (Porro et al., 2021). Because epilepsy-related mutations characterization in different expression systems has led to contrasting results, finding a homogeneous expression system to fully understand how HCN channel dysfunctions contribute to epilepsy is promptly needed. Since a specific and selective treatment for patients suffering from HCN1-related seizures is still missing, a benefit of being corroborated a human epilepsy gene would validate HCN1 as a good antiepileptic drug target (Reid et al., 2012).

1.2.3.2 HCN2 and disease

Other human diseases that have been linked to HCN channels mis-regulation, are inflammatory and neuropathic pain. In both causes patients have a continuous pain sensation and are hypersensitiv to normal stimuli. In the case inflammatory pain these sensations are transient, while neuropathic pain does not resolve with time. The insurgence of pain begins when a potentially harmful input opens ion channels in the sensory terminals of nociceptors

causing membrane depolarization and a consequent firing of action potentials; in this case the firing rate increases with the strength of the stimulus. Increasing evidence suggests HCN channels activity as one of the main players in the modulation of firing of these action potentials (Emery et al., 2011). Nociceptors mediate a slow and cAMP-sensitive current mainly carried by the HCN2 channel; an upregulation of I_f leads to increased cell excitability which in turn promotes the generation of ectopic neuronal firing (Wahl-Schott & Biel, 2009). Available treatments for pain are frequently ineffective and cause a substantial subset of side effects. The currently most used pain treatments include antidepressants, anticonvulsants, opioids, and cannabinoids. The possibility of employing ivabradine for the treatment of pain in humans has not been explored yet. But given the molecule's inability to discriminate between HCN subtypes, the concentration that can be used must be lower than those causing unwanted bradycardic side effects; such side effects could be elicited by blocking HCN4 in the heart. A better alternative for future applications could be an isoform specific targeting of the HCN2 channels. Such an isoform specific targeting of HCN channels which are crucial for both inflammatory and neuropathic pain could provide a common starting point for the development of a shared treatment in the future (Emery et al., 2011).

1.2.3.3 HCN4 and disease

It is long known that the generation and control of pacemaker activity in the heart is associated with HCN-mediated currents; it is therefore no surprise that mutations in the heart's predominant isoform, HCN4, have been linked to several rhythm disorders such as sinus bradycardia, atrial fibrillation, and other more complex arrhythmias (Difrancesco, 2013). HCN4 mutations have been frequently associated with cardiac arrhythmias and predispose humans to inherited sick sinus syndrome (SSS) and long QT syndrome; the latter is associated with bradycardia (Ueda et al., 2009). However, the alteration of HCN4 function can also be involved in human epilepsy. This can be mediated a loss-of-channel function and the consequent increases in neuronal excitability (Campostrini et al., 2018). It has been reported that increased I_f densities ectopically raise the tendency of cardiac myocytes to develop pacemaker action potentials, and therefore contribute to arrhythmias and sudden death (Wahl-Schott & Biel, 2009). Most mutations associated with HCN4-related cardiac phenotypes are heterozygous, dominant-negative and involve point mutations or truncations

in the C-linker/CNBD region. This region is known to be involved in linking structural rearrangements of the C-terminus to gating (Di Francesco, 2015). Pathological shifts in voltage dependency of I_f has been correlated with both gain-of-function and loss-of-function mutations causing different kinds of cardiovascular phenotypes; mutations that shift HCN4 activation curve towards more hyperpolarized potentials for example cause an effect similar to that induced by the inhibition of cAMP synthesis. Both lead to a decrease in the slope of diastolic depolarization with a consequent decrease of the heart rate (Difrancesco, 2013). Other loss-of-function mutations are caused by a lower density of channels in the membrane with a consequent reduction of the total current density. This phenomenon is generally associated with defects of channel synthesis and trafficking (Di Francesco, 2015). On the other hand, gain-of-function mutations are related to a positive shift of I_f activation. This property mimics the functional effect of β -adrenergic stimulation, which results from a hyper cAMP sensitivity. This kind of mutations is generally associated with tachycardia (Baruscotti et al., 2017).

It has been mentioned above that HCN channels have a key role in controlling cardiac pacemaker activity and that they are important regulators of neuronal excitability. With these key functions the HCN channels represent interesting drug targets for the treatment of neurological and cardiac disorders.

Currently Ivabradine, is the only available drug for HCN channels. It has been approved as a bradycardic agent for the treatment of stable angina, by the European Medicines Agency and by the US Food and Drug Administration (Santoro & Shah, 2020). Ivabradine specifically targets the I_f current in the sinoatrial node, which is mostly formed by the HCN4 subtype. Because of its lack of isoform specificity, it also affects other HCN subtypes in diverse tissues. Typical side effects of Ivabradine are phosphines, which are most probably caused by the block of HCN1 in retinal photoreceptors (Cervetto et al., 2007). Thus, selective HCN blockers for treating neurological and neuropsychiatric conditions are required, particularly for the treatment of chronic pain including neuropathy and inflammation, where HCN2 play a major role (Emery et al., 2012).

1.2.4 Structural features of HCN channels

1.2.4.1 Architecture of HCN1 channels

Using cryo-EM (single-particle electron cryo-microscopy), the full-length three-dimensional structure of a human HCN1 isoform in the absence and presence of cAMP was resolved at 3.5 Å resolution (Lee & MacKinnon, 2017). As expected from previous studies (Wahl-Schott & Biel, 2009), the overall structure is composed of four identical subunits. In the three-dimensional structures of hHCN1 each of the four subunits contributes identically to the formation of the pore that conducts the ion flow across the membrane. Each HCN subunit is comprised of highly preserved structural motifs: a transmembrane voltage-sensing domain (VSD: S1–S4), a transmembrane pore domain (PD: S5–S6), a cytosolic C-linker, and the cyclic nucleotide-binding domain (CNBD) (Figure 1). The hHCN1 structures confirm some previously described features of HCN channels and address three unique properties of HCN channels: First, in contrast to many K_v channels, in which the VSD contacts the PD of a neighboring subunit in a so called domain-swapped architecture (Holmgren et al., 1998; Wynia-Smith et al., 2008), the VSD of HCN1 contacts the PD of the same subunit. This results in a non-domain-swapped organization of the transmembrane core. Second, hHCN1 channels have an unusually long S4 helix compared to other voltage-gated channels and lack a covalent link between the VSD and the PD. Third, hHCN1 channels have a unique cytosolic domain, now termed HCN domain (HCND), that stabilizes the closed pore in the setting of a depolarized voltage sensor (Figure 1.2) (Lee & MacKinnon, 2017).

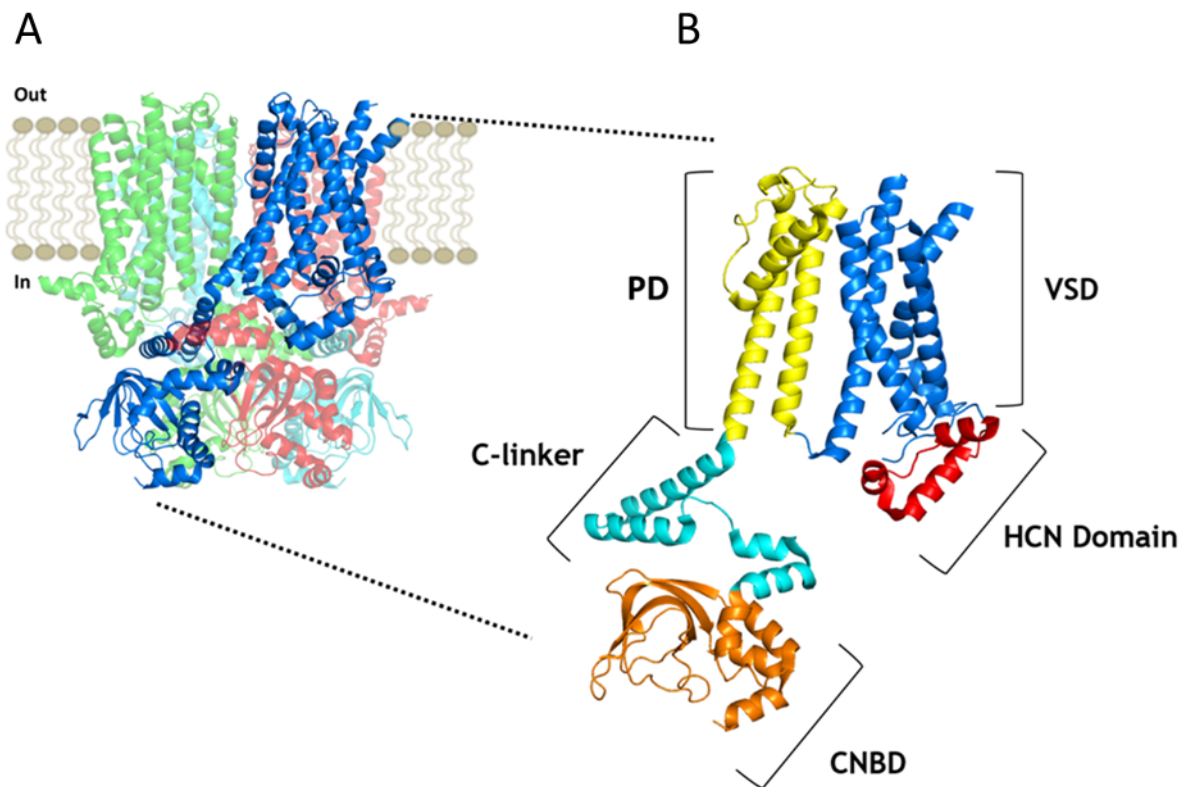


Figure 1.2 Ribbon representation of hHCN1 channel structures (PDB: 5U60). **A.** Side view of the four subunits, each in a different color, of the hHCN1 channel. **B.** Side view of one subunit with the transmembrane spanning segment, including the voltage sensor (VSD) the pore domain (PD), and cytosolic segment including C-linker, CNBD, and HCND (Lee & MacKinnon, 2017).

A recent study revealed that HCND mediated the contact between VSD and C-linker domain by bypassing the pore (Porro et al., 2019). Mutational studies have shown that this mechanical link is important for the translation of the conformational changes from the C-linker, which are generated by the binding of cAMP to CNBD, to the VSD (Porro et al., 2019).


Although the hHCN1 structures have addressed important structure/functional correlates in HCN channels at the molecular level, the functional role of each of these features is not completely known. Notably, the two structures of hHCN1 in the presence and absence of bound cAMP display the pore domain in a closed conformation (Lee & MacKinnon, 2017), even when the hyperpolarized conformation of S4 was imposed on the VSD by chemical crosslinking (Lee & MacKinnon, 2019). Hence, the characterization of dynamic conformational

changes that occur when the channel is open, as well as the mechanism of ion permeation, remains unexplained. Moreover, the hHCN1 structures lack insight into the mechanism of cAMP modulation of gating. While the goal of obtaining a structure of HCN channels in the closed and open configuration of the pore, seemed out of reach due to the strict voltage dependency of the channel, dissection of the cAMP pathway could be more easily pursued. In our opinion this could be achieved by studying alternative HCN subtype namely HCN4.- The latter exhibits a much large response to cAMP than HCN1. To this end we set up the protein purification of HCN4 and prepared the sample with and without ligand for subsequent cryo-electron microscopy (cryo-EM) single particle studies.

1.2.5 So similar, so different: The cAMP sensitivity

Different HCN isotypes display different sensitivities to cAMP: HCN1 is showing a modest response to cAMP, while HCN2 and HCN4 exhibit a very large response; HCN3 in contrast is not at all responding to cAMP (Chen et al., 2001; Moroni et al., 2000; Wainger et al., 2001; William N. Zagotta et al., 2003). Several studies have shown that the isoform specific sensitivity to cAMP lies mainly in the cytosolic region, and its interaction with the transmembrane domain of the channel (Alvarez-Baron et al., 2018; Lolicato et al., 2011; Momin et al., 2008). In line with this critical role of the cytosolic region, several disease-associated mutations affecting HCN channel gating and cAMP sensitivity have been identified in this region (Baruscotti et al., 2017; J. C. DiFrancesco et al., 2011). To strengthen the concept, the existent differences in the cytosolic domain of HCN channels led to the identification of a molecule, biphenyl urea (BPU), which binds to an isoform specific pocket in the C-linker of HCN4, and fully prevents cAMP modulation (Lolicato et al., 2014). To date this is the only example of an isoform specific drug for HCN channels.

Strikingly, the differences observed in the sensitivity and response to cAMP across HCN channels can hardly be tracked back to their primary sequence. In fact, HCN isoforms possess 80-90% sequence identity of their structural elements: HCN domains, core transmembrane regions (VSD and pore) and Clinker/CNBDs (Biel et al., 2009; Robinson & Siegelbaum, 2003).



Notwithstanding the extensive number of studies aimed at characterization of the intra-molecular pathway behind cAMP stimulation of HCN channels activation (Gross et al., 2018; Kusch et al., 2012; Lolicato et al., 2011; Porro et al., 2019; Saponaro et al., 2014; Wainger et al., 2001; Weißgraeber et al., 2017; William N. Zagotta et al., 2003) an exhaustive structural description remains elusive, while the primary protein sequence gives no insights into the differences between the HCNs.

These findings strongly suggest that only a structural comparison of HCN structures, especially in the cytosolic region and in its interaction with the transmembrane region, could lead to the identification of the molecular bases for the isoform specific sensitivity to cAMP.

This structural approach has been confirmed by our recent publication of the 3D structures of HCN4 and of its comparison with the ones of the HCN1 sub-type (Saponaro, Bauer, et al., 2021). From this work, it became, indeed, clear that the local differences observed in the cytosolic domains and in its connection to the transmembrane region translate into functional differences among isoforms (such as high cAMP-sensitivity of HCN4), despite the high sequence conservation between HCN1 and HCN4. A detailed description of this work constitutes the first chapter of the present thesis.



PART I

2.1 Materials and methods (part I and II)

2.1.1 Constructs

The cDNA encoding rabbit HCN4 (GenBank: NM_001082707) carrying an internal deletion (from residues 783 to 1064), hereafter HCN4 Δ C, was cloned into a modified pEG BacMam vector (Goehring et al., 2014) (hereafter pEGA) for large-scale protein purification from mammalian cells. The internal deletion eliminates a poorly conserved region in the C-terminal portion of the HCN channel protein, but preserves the extreme C-terminal SNL tripeptide sequence responsible for binding the auxiliary subunit TRIP8b (Santoro et al., 2004, 2011). The pEGA vector allows expression of the protein of interest with both eGFP and decahistidine tags at its N terminus. The tags can be cleaved using TEV enzyme, due to the presence of a TEV cleavage site between the tags and the protein of interest. For co-expression of HCN4 protein in the presence of TRIP8b, the cDNA encoding full-length mouse TRIP8b (splice variant 1a4) (GenBank: NM_001163516) was cloned into the pEGA vector and the HCN4 Δ C cDNA into pCI vector (Promega Corporation). For whole-cell patch clamp analysis, the human HCN1 cDNA, the rabbit HCN4 cDNA and the mouse HCN2 cDNA were cloned into the pCDNA3.1 and in the pCI vector, respectively, as reported in Saponaro et al., 2018. All mutations were generated by site-directed mutagenesis (QuikChange site-directed mutagenesis kit; Agilent Technologies) and confirmed by sequencing.

2.1.2 Protein expression and membrane isolation

Freestyle HEK293-F cell cultures (Thermo Fisher) were transiently transfected with pEGA: HCN4 Δ C (1mg per ml) at a cell density of 2×10^6 cells per ml using polyethyleneimine (PEI) (Polysciences). The transfected cells were harvested by centrifugation after 48 hours of growth in shaker flasks at 37°C, 5% CO₂. Cell pellets were resuspended in low salt buffer (10 mM KCl, 10 mM MgCl₂, 10 mM HEPES pH 7.5, 0.5 mM PMSF, EDTA-free complete protease inhibitor cocktail (Roche) (1:1000), 20 mg/mL DNase (Roche), and 10 mg/mL RNase (Sigma-Aldrich)) and lysed by gentle homogenization in a glass homogenizer. Membranes were isolated by ultracentrifugation (40 min at 17000 xg), resuspended by homogenization and washed two times with high salt buffer: 1 M NaCl, 10 mM KCl, 10 mM MgCl₂, 10 mM HEPES pH 7.5, 0.5 mM PMSF, EDTA-free complete protease inhibitor tablet, 20 mg/mL DNase, 10

mg/mL RNase. Isolated membranes were resuspended by homogenization in the storage buffer: 200 mM NaCl, 20 mM HEPES pH 7.5, 0.5 mM PMSF, EDTA-free complete protease inhibitor cocktail (1:1000) and stored at -80°C until use.

2.1.3 Protein purification in LMNG/CHS

The isolated membranes were thawed on ice and solubilized by the addition of a mixture of detergents (laurylmaltose neopentyl glycol (LMNG) with cholesteryl hemisuccinate (CHS) in a 5 to 1 ratio) to a final concentration of 1%(w/v), and gently agitated for 2 hours at 4°C. The solution was cleared by ultracentrifugation (40 min at 1700 xg). Pre-equilibrated Ni²⁺-NTA resin (QIAGEN) was added to the sample, together with 10 mM imidazole and the mixture allowed to gently rotate overnight at 4°C. After transferring the mixture to a column, the resin was washed in two steps: 1) 5 column volumes of buffer containing 50 mM imidazole; 2) 5 column volumes of buffer containing 75 mM imidazole. The proteins were eluted with 10 column volumes of the following buffer: 200 mM NaCl, 20 mM HEPES pH 7.5, 300 mM imidazole. The eluted protein was loaded on a Superose 6 increase 10/300 GL SEC column (GE Healthcare Life Sciences) pre-equilibrated with buffer containing 200 mM NaCl, 20 mM HEPES pH 7.0 and detergent (LMNG-CHS) at the concentration of 0.002% (w/v). For the protein sample used to solve the structure of HCN4 bound to cAMP, the ligand (Sigma-Aldrich) was kept at a concentration of 0.2 mM in all steps of membrane isolation and protein purification procedure described above. The decahistidine GFP tag at the N terminus of HCN4 protein was not removed. Final yield of purified protein was about 1mg per 1 L of cells.

2.1.4 Protein purification in amphipols

For purification in amphipols, HCN4 protein was obtained following co-expression and co-purification with the auxiliary subunit TRIP8b. This approach was chosen to prevent any cellular cAMP from occupying the CNBD (Lolicato et al., 2011) due to the antagonistic nature of TRIP8b/cAMP binding (Bankston et al., 2017; Gross et al., 2018; Hu et al., 2013; Saponaro et al., 2018). Although we were unable to detect signal for the TRIP8b protein upon cryo-EM image analysis, potentially due to loss of TRIP8b during vitrification and/or variability in the number of TRIP8b subunits associated with the channel, this approach did yield a near atomic-

resolution structure of the HCN4 channel protein stabilized by amphipols in the cAMP-unbound conformation.

Following co-transfection of pCI: HCN4 Δ C and pEGA: TRIP8b, membranes were isolated and the protein complex affinity purified with a Ni²⁺-NTA resin as described in the section 2.1.3. Proteins were then desalted by using PD-10 desalting columns (GE Healthcare) and reconstituted into amphipol A8-35 (Anatrace) at a protein: amphipol ratio of 1: 10 by weight. The protein– amphipol mixture was incubated for 4 hours with gentle rotation at 4°C. After 4 hours of incubation with amphipol, the detergent was removed by the addition of Bio-Beads (Bio-Rad) overnight at 4°C. The reconstituted protein was then loaded on a Superose 6 increase 10/300 GL SEC column pre-equilibrated in a buffer composed by 200 mM NaCl and 20 mM HEPES pH 7.0 without detergent in order to remove the excess of free amphipol and residual detergents. Final yield of purified HCN4 Δ C in complex with GFP-TRIP8b was about 1mg per 1 l of cells. The purified complex was concentrated to 0.5 mg ml⁻¹, using a 100 kDa concentrator (Amicon) for Cryo-EM sample preparation.

2.1.5 Thermal denaturation assay

GFP-HCN4 Δ C protein was purified following the procedure described in the section 2.1.3. The purified protein was maintained for 48 h at 4°C before being used for thermal denaturation assay. Before proceeding with the assay, the protein sample was split into equal parts. They were used to prepare samples for the following experimental conditions: control and protein + ligand. For each experimental condition samples were subsequently transferred into 10 PCR tubes containing 5 μ g of GFP-HCN4 each and brought them at the final volume of 50 μ L (0.2 μ M tetrameric GFP-HCN4). The samples were incubated for 10 min at 20, 30, 40, 45, 50, 55, 60, 65, 70, and 80 °C using a Thermal Cycler (Bio-Rad). The heated samples were then pelleted at 18,000 x g for 30 mins at 4 °C. The supernatant was loaded on the Size-Exclusion column (SEC) (Yarra SEC-4000) pre-equilibrated with the pre-equilibration buffer (see the section 2.1.3). The column was connected to the HPLC system (Shimadzu) equipped with a fluorescence detector (Shimadzu) to allow the emission signal (509nm) of an excited GFP (488nm) fused at the N terminus of HCN4.

To measure the height of the FSEC peaks corresponding to soluble GFP-HCN4, each chromatogram was exported on the data analysis and graphing Originpro software (Originlab,

Northampton, MA, USA). The data was normalized by using the height of the FSEC peak of the sample incubated at 20 °C and fitted with the following sigmoidal dose-response equation:

$$Y = A1 + (A2 - A1) / (1 + 10^{-(\text{LOG}x0 - x) \cdot p})$$

where Y is the fluorescence emission in arbitrary units, A1 the minimal fluorescence (from the sample heated at 80°C), A2 the maximal fluorescence (from the sample heated at 20 °C), LOGx0 the melting temperature (T_m), x a given temperature, and p is the Hill slope.

2.1.6 Thermal shift of GFP-HCN4 Holo following Mg²⁺ removal assay

GFP-HCN4ΔC protein was purified following the procedure described in the section 2.1.3. The buffer in which the protein was eluted from the SEC column contained 0.2 mM cAMP and 0.002% (w/v) LMNG-CHS which were kept present in all incubation buffers. The purified protein (3 μM) was maintained for 48 h at 4°C before being used for thermal denaturation assay. For Mg²⁺ removal assay, GFP-HCN4ΔC was incubated 1h with 10 mM Ethylenediaminetetraacetic acid (EDTA, Sigma-Aldrich) pH 7. The buffer with EDTA was replaced by using PD-G25 desalting columns (GE Healthcare) with a buffer without EDTA +10 mM MgCl₂. The denaturation curve of protein was obtained as mentioned in section 2.1.5. The assay was repeated for GFP-HCN4ΔC (HAHA) mutant in the same way.

2.1.7 Setting of a fast screening system for ligand binding to purified GFP-HCN4

In this screening assay the protein was heated at two temperatures only: (1) the starting temperature of the denaturing curve (in our case 20°C); (2) at a temperature corresponding to the T_m+5°C. The addition of 5°C to the T_m is to magnify any stabilizing (increase in fluorescence) and/or destabilizing (decrease in fluorescence) effects due to ligand binding. In our case, GFP-HCN4 has a T_m of 50°C and we used 55 °C. The protein samples were prepared according to the ligands to be screened in triplicate. As controls GFP-HCN4 protein samples without ligands heated for 10 min at 20°C and at 55°C. Protein samples heated at 55°C in the presence of 2mM cAMP (Sigma-Aldrich), 2mM cTMP (Sigma-Aldrich) or 5mM Ivabradine (Sigma-Aldrich). The height of each FSEC peak corresponding to soluble GFP-HCN4 was measured using the data analysis and graphing Originpro software (Originlab, Northampton, MA, USA). Data are analyzed as a change (in percentage) of the fluorescence at 55°C from the initial condition (20 °C).



2.1.8 Monitoring cyclic di-GMP binding to the GFP-HCN4 pacemaker channel using the thermal shift assay

The binding of c-di-GMP (BioLOG) to purified GFP-HCN4 Δ C or GFP-HCN4 Δ CR681E mutant was monitored using the fast screening system, as mentioned above (see section 2.1.7).

2.2 The cryo-EM structure determination of HCN4 with and without cAMP bound

The content of this chapter has been published in *Molecular Cell* (Saponaro, Bauer, et al., 2021). The figures reported here recapitulate my direct contribute to the published work as detailed below.

The first part of this project focused on studies of structure-function relations in the pacemaker HCN4 channel. I have there establishing the procedure for the transient heterologous expression of GFP-tagged HCN4 proteins, alone or in complex with their regulatory protein TRIP8b (Santoro et al., 2004), in HEK293F cells, a mammalian line able to grow in liquid (see methods of Saponaro, Bauer, et al., 2021). Moreover, I have set the protocol for the isolation of HCN4 from membranes and for its subsequent purification (see methods of Saponaro, Bauer, et al., 2021 and Figure 2.1).

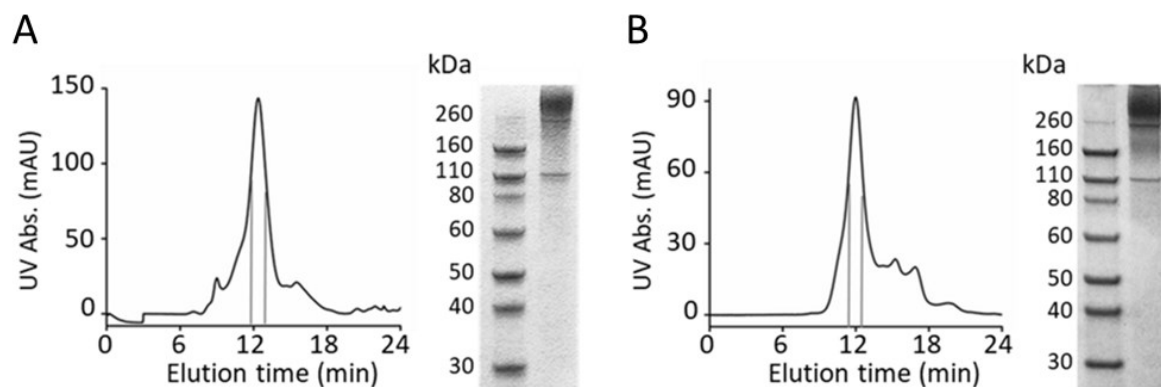


Figure 2.1 Purification of HCN4 protein for biochemistry and structural biology. **A.** Representative size-exclusion chromatography (SEC) of GFP-HCN4 Δ C (a mutant with an internal deletion that removes a poorly conserved region in the C terminus) following purification in LMNG/CHS detergent mixture. Peak fractions used for cryo-EM and fluorescent-based thermal denaturation (fSEC-TS) assay are delimited by the grey lines (left). SDS-PAGE gel of the pooled SEC fractions of HCN4, stained with Coomassie blue (right). **B.** Representative SEC of HCN4 Δ C – GFP-TRIP8b complex following purification and reconstitution in amphipols. Peak fractions used for cryo-EM are delimited by the grey lines (left). SDS-PAGE gel of the pooled SEC fractions of HCN4 Δ C – GFP-TRIP8b complex, stained with Coomassie blue (right). Note that the expected size of the HCN4 Δ C and GFP-TRIP8b proteins is the same. [adapted from (Saponaro, Bauer, et al., 2021) with permission].

The detergent purified HCN4 proteins were employed for obtaining their 3D structure by single particle cryo-EM (Saponaro, Bauer, et al., 2021). They were further employed for a biochemical experiment namely a thermostability assay based on fluorescence-detection size-exclusion chromatography (fSEC-TS). I have established the fSEC-TS assays in the laboratory and performed the measurements published in Saponaro, Bauer, et al., 2021. A detailed description of the method is part of the second part of the thesis and it is published (Saponaro, Sharifzadeh, et al., 2021).

HCN4 has unique functional features that distinguish it from other HCN subtypes, the most prominent being a larger response in the shift of the voltage dependency of channel activation to cAMP binding. Being interested in unravelling the atomistic details of the cAMP signal within HCN channel proteins, we focused our attention on this HCN isotype.

We determined three cryo-EM structures of the pacemaker HCN4 channel in the ligand-free and ligand-bound states in different environments (Saponaro, Bauer, et al., 2021). Two structures were solved in the detergent mix LMNG/CHS (HCN4 apo/LC, HCN4 holo/LC) and one with the membrane mimetic amphipols (HCN4 apo/AM). Our structures reveal specific features concerning the response of the HCN4 subtype to cAMP as well as general features of the HCN channels with respect to the pore and ion selectivity.

2.2.1 HCN4 response to cAMP: a structural view

Although the structure of human HCN1, solved in both the cAMP-free and bound, undoubtedly represent a milestone in the HCN research field (Lee & MacKinnon, 2017) no significant ligand-induced conformational changes were identified, beside the expected and already well characterized cAMP-dependent movements of the ligand binding domain (CNBD). This is most likely the case because of the HCN isotypes display different sensitivity to cAMP, with HCN1 showing only a modest response to cAMP. The response to cAMP binding is much larger in HCN2 and HCN4 (Stieber et al., 2005). This led us to focus our attention on HCN4 as a model to finally unravel the atomistic details of the propagation of the cAMP signal from the cytosolic region to the transmembrane one.

A detailed comparison of the structures of HCN4 in the presence and absence of cAMP uncovered indeed conformational changes induced in this protein by ligand binding (Saponaro, Bauer, et al., 2021).

HCN4 protein shows a large displacement of the cytosolic regulatory region (the Clinker/CNBD), which ultimately tilts the last two helices of the C-linker, called helix A' and B'. Therefore, in the cAMP bound structure, HCN4 HOLO, helix A' and B' are positioned just below the transmembrane region where they contact the S4-S5 linker (Figure 2.2A). The latter structural element physically connects the VSD to the pore domain of the channel. The S4-S5 linker and the underlying helix A' and B' build sort of a tetrahedral arrangement that we refer to as "tetrad". This is a unique structure of HCN4 channels, as it is not present in the HCN1 structures (Figure 2.2B). Because of the chemical nature of these residues and their organization, they can form a metal-ion coordination site which appears as an extra density map at the center of the tetrad. We assumed that the coordinated ion could be Mg^{2+} because Mg^{2+} is present at high concentration (10 mM) in our purification procedure.

By performing a fSEC-TS assay in the presence of the chelating agent EDTA, we could show: i) that indeed Mg^{2+} is involved in tetrad formation and ii) that the formation of the tetrad, promotes the stability of the HCN4 channel (Figure 2.2C and D). We performed the same experiments also on mutants in which residues that are form the tetrad were corrupted (Figure 2.2C and D). As previously mentioned, fSEC-TS were performed by me. The formation of tetrad was further evaluated by using electrophysical measurements of HCN4 function in presence and absence of cAMP (Saponaro, Bauer, et al., 2021). Notably, our data show that tetrad formation facilitates the transmission of the cAMP effect between C-linker and VSD. Moreover, we can confirm that the tetrad is an isotype-specific feature of the HCN4, as the corresponding mutations introduced in HCN1 or HCN2 had no effect on cAMP response in these subtypes.

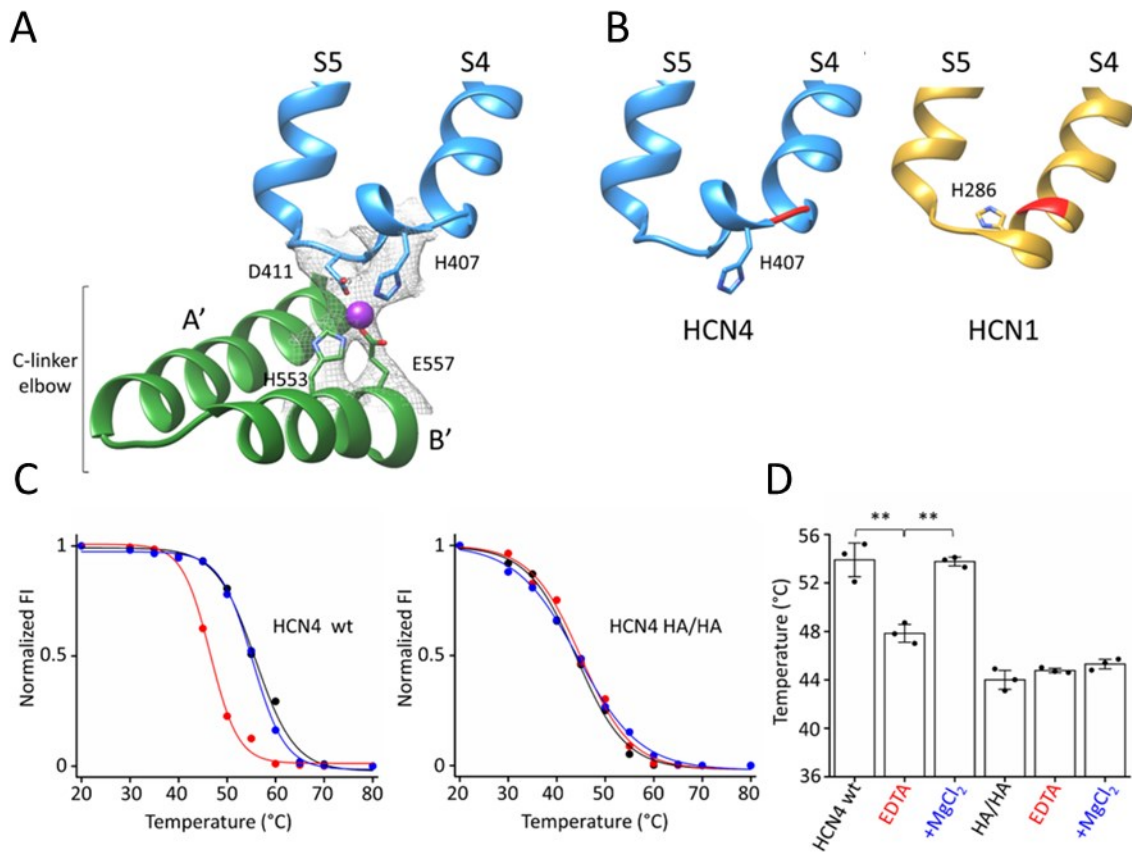


Figure 2.2 HCN4 specific mechanism of cAMP signal transduction from the cytosolic machinery to the transmembrane region. **A.** Ribbon representation of S4-S5 linker of one subunit (blue) and underlying C-linker “elbow” (A’–B’ helices) of adjacent subunit (green) of HCN4. Four residues forming the ion coordination site (tetrad) in HCN4 are shown as sticks and labeled (H407, D411, H553, E557). Ion coordinated by the tetrad is represented as a purple sphere. **B.** Comparison of the S4-S5 linker of HCN1 (yellow) and HCN4 (blue). Backbones of I405 in HCN4 and the corresponding I284 in HCN1 are shown in red. **C** and **D.** Thermostability assay based on fluorescence-detection size-exclusion chromatography (fSEC-TS) was employed to quantify the change in melting temperature of purified protein in absence or presence of Mg^{2+} . **C.** Representative melting curves for holo HCN4 protein purified in LMNG/CHS. Normalized fluorescence intensity (FI) plotted over pre-conditioning temperature. The protein was incubated without (black) or with 10 mM EDTA (red), or, after EDTA removal, with 10 mM $MgCl_2$ (blue). Wild-type protein (HCN4 WT) is shown on the left; double-mutant H407A/H553A (HCN4 HA/HA) is shown on the right. Data points are fitted with sigmoidal dose-response equation (see STAR Methods). **D.** Mean denaturation midpoint temperature (T_m) for HCN4 WT in control ($53.6C \pm 1.5C$), EDTA ($47.8C \pm 0.8C$), + Mg^{2+} ($53.7C \pm 0.4C$); for HCN4 HA/HA: control ($44C \pm 0.5C$), EDTA ($44.8C \pm 0.1C$), + Mg^{2+} ($45.3C \pm 0.3C$). Values are mean of $n = 3$ experiments \pm SEM.

Statistical analysis performed with one-way ANOVA, followed by Fisher's test (**p < 0.01). [adapted from Saponaro, Bauer, et al., 2021 with permission].

2.2.2 The closed and open pore structure of HCN4

A second important finding described in Saponaro, Bauer, et al., 2021 was that two of the three structures showed the pore in the open conformation (Figure 2.3). This was an unexpected finding because the cryo-EM data collections were performed at 0 mV, a condition which keeps HCN channels close.

In the cAMP-bound structure (HCN4 HOLO) several lipids surround the S4 and S5 and stabilize the HCN4 structure in the closed pore state (Figure 2.3A and C) as it happened in HCN1 (Figure 2.3B). In the apo structures (HCN4 APO/LC and AM), on the contrary, these lipids were not present (Figure 2.3D and E), and the pores were found in the open configuration (Figure 2.3F-H). Protein delipidation, that occurred in APO structures only for so far unknown reasons, dramatically influenced the conformation of the transmembrane helices, (S4-S6). Specifically, detachment of S4 helix (VSD) from S5 (pore), allows S5 to tilt (Figure 2.3D, inset). This induces the concomitant rotation of the S6 helix (pore) (Figure 2.3D, inset and F). This movements, occurring at the level of the TM helices, presumably mimic the voltage-activated state of the channel leading to the open pore configuration. Indeed, the detachment of S4 and S5 helices resembles the recently published structure of HCN1 in which the voltage sensor was kept by the biochemical cross-linker in a voltage-like activated state, capturing S4 of the VSD in its active state (Lee & MacKinnon, 2019) (Figure 2.3E).

The open conformation of the pore was further validated by MD simulations and docking experiments (please, see Figure 5A and B of Saponaro, Bauer, et al., 2021). MD showed that the cytosolic entrance of the pores of both HCN4 APO/LC and AM was fully solvated, and, most important, could detect passage of ions through the bundle crossing. Docking experiments were performed with Ivabradine, a pharmacologically well-known open pore blocker of HCN channels (please, see Figure 5C and D of Saponaro, Bauer, et al., 2021). The cytosolic entrance of both HCN4 APO/LC and AM offers free access of Ivabradine into the cavity. Strikingly, the docking experiments confirmed previous data on Ivabradine - HCN4 interaction obtained by functional and mutational analysis (Bucchi et al., 2013).

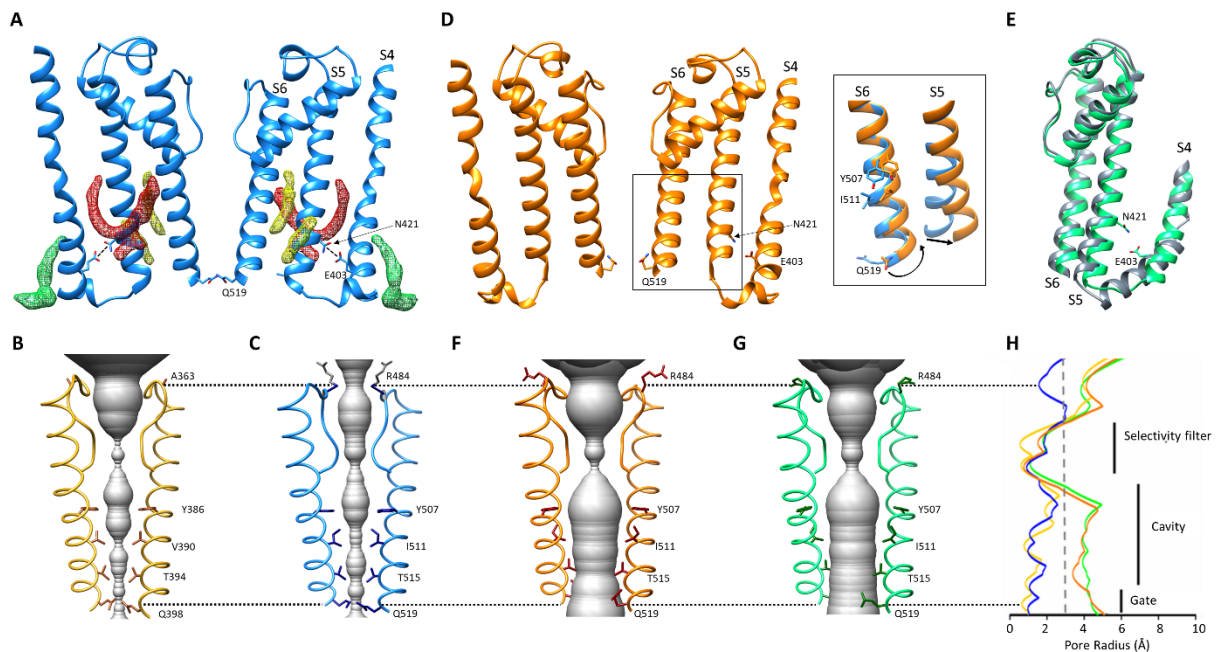



Figure 2.3. Molecular mechanism of pore opening in HCN4 channel. **A.** Ribbon representation of S4, S5, and S6 TM helices in HCN4 holo configuration (blue) in a cross-membrane view. For clarity, only two subunits are shown. Putative lipid densities contacting S4 (green mesh) and S5 (red and yellow mesh) are shown. Residues involved in polar interaction (dotted line) between S4 (E403) and S5 (N421) are shown as sticks and labelled on one subunit. TM helices S4, S5, and S6 are also labelled on one subunit. **B** and **C.** Ribbon representation of pore of HCN1 holo configuration (yellow, PDB: 5U6P) (**B**) and HCN4 holo configuration (blue) (**C**). For ease of view, only two opposite subunits in the assembled tetramer are shown. The pore diameter is shown as a grey surface. Residues facing pore inner cavity and residue of SF facing extracellular side (A363 in HCN1 and R484 in HCN4) are shown as sticks and labelled. The atoms of side chain of R484 whose density is not resolved are coloured in grey. **D.** Ribbon representation of S4, S5, and S6 TM helices in HCN4 apo/LC (orange) in a cross-membrane view. For clarity, only two subunits of tetramer are shown. Lipids are absent, and polar interaction between E403 and N421 is lost. Inset: in comparison with HCN4 holo configuration (blue), the apo/LC structure shows a tilting movement of S5 and rotation of S6, as shown by shift in the side chains of Y507, I511, and Q519. **E.** Superimposition of helices S4, S5, and S6 of HCN4 apo/AM (green) and HCN1 in hyperpolarized conformation (grey, PDB: 6UQF). In HCN4 apo/AM, the lipids are absent, and both the polar interaction E403-N421 and hydrophobic interactions between S4 and S5 are lost (see also Figure S10). **F** and **G.** Ribbon representation of pore of HCN4 apo/LC (orange) (**F**) and HCN4 apo/AM (green) (**G**). Labelling as in (**B**) and (**C**). Rotation in lower part of S6 relocates side chains of indicated residues away from cavity, widening solvent-accessible pathway (grey) from cytosolic side. **H.** Plot of pore radii,



color-coded as in (B), (C), (F), and (G). The dotted line marks the radius of hydrated K^+ . Corresponding portions of selectivity filter, cavity, and gate are indicated by black vertical bars. Dotted black lines encompassing (B), (C), and (F)–(H) indicate, respectively, R484 in HCN4, the corresponding A363 residue in HCN1, and glutamine residues at the cytosolic gate (Q519 in HCN4, Q398 in HCN1). [taken from Saponaro, Bauer, et al., 2021 with permission].

2.2.3 Selectivity and permeation in HCN

The process of a physiologically meaningful open state of HCN channel provided us with the unique opportunity to perform MD simulations and to acquire a detailed view on ion selectivity and permeation through an HCN pore.

The results of the MD simulation revealed two important features of the ion binding sites in the filter (please, see Figure 6 of Saponaro, Bauer, et al., 2021). First, the binding sites are partially formed by the atoms of the backbone of the filters and partially by water molecules. Thereby, the permeation of K^+ ions is associated with the passage of water molecules and ultimately based on the soft knock-on permeation mechanism in which ions are partially desolvated ions in the channels' selectivity filter (Kopec et al., 2018). Second, the selectivity filter can enlarge its dimensions to adapt to K^+ ions. This flexibility of the selectivity filter is a peculiar property of HCN channels and different from the filter in canonical K^+ channels. The dynamics in the filter of the HCN channel explains the mixed selectivity of these channels compared to the rigid filter of the typical purely selective potassium channels.

References

- Altomare, C., Terragni, B., Brioschi, C., Milanesi, R., Pagliuca, C., Viscomi, C., Moroni, A., Baruscotti, M., & DiFrancesco, D. (2003). Heteromeric HCN1-HCN4 channels: A comparison with native pacemaker channels from the rabbit sinoatrial node. *Journal of Physiology*, 549(2), 347–359. <https://doi.org/10.1113/jphysiol.2002.027698>
- Alvarez-Baron, C. P., Klenchin, V. A., & Chanda, B. (2018). Minimal molecular determinants of isoform-specific differences in efficacy in the HCN channel family. *Journal of General Physiology*, 150(8), 1203–1213. <https://doi.org/10.1085/jgp.201812031>
- Bankston, J. R., DeBerg, H. A., Stoll, S., & Zagotta, W. N. (2017). Mechanism for the inhibition of the cAMP dependence of HCN ion channels by the auxiliary subunit TRIP8b. *Journal of Biological Chemistry*, 292(43), 17794–17803.
- Baruscotti, M., Bottelli, G., Milanesi, R., DiFrancesco, J. C., & DiFrancesco, D. (2010). HCN-related channelopathies. *Pflugers Archiv European Journal of Physiology*, 460(2), 405–415. <https://doi.org/10.1007/s00424-010-0810-8>
- Baruscotti, M., Bucchi, A., Barbuti, A., & DiFrancesco, D. (2012). Funny current and cardiac rhythm: insights from HCN knockout and transgenic mouse models. *Frontiers in Physiology*, 3, 240.
- Baruscotti, M., Bucchi, A., Milanesi, R., Paina, M., Barbuti, A., Gneccchi-Ruscione, T., Bianco, E., Vitali-Serdoz, L., Cappato, R., & DiFrancesco, D. (2017). A gain-of-function mutation in the cardiac pacemaker HCN4 channel increasing cAMP sensitivity is associated with familial Inappropriate Sinus Tachycardia. *European Heart Journal*, 38(4), 280–288.
- Baruscotti, M., & DiFrancesco, D. (2004). Pacemaker channels. *Annals of the New York Academy of Sciences*, 1015(1), 111–121.
- Biel, M., Wahl-Schott, C., Michalakis, S., & Zong, X. (2009). Hyperpolarization-activated cation channels: From genes to function. *Physiological Reviews*, 89(3), 847–885. <https://doi.org/10.1152/physrev.00029.2008>
- Bolívar, J. J., Tapia, D., Arenas, G., Castanon-Arreola, M., Torres, H., & Galarraga, E. (2008). A hyperpolarization-activated, cyclic nucleotide-gated, (I_h-like) cationic current and HCN gene expression in renal inner medullary collecting duct cells. *American Journal of Physiology-Cell Physiology*, 294(4), C893–C906.
- Bucchi, A., Baruscotti, M., Nardini, M., Barbuti, A., Micheloni, S., Bolognesi, M., & DiFrancesco, D. (2013). Identification of the Molecular Site of Ivabradine Binding to HCN4 Channels. *PLoS ONE*, 8(1), 1–12. <https://doi.org/10.1371/journal.pone.0053132>
- Bucchi, A., Tognati, A., Milanesi, R., Baruscotti, M., & DiFrancesco, D. (2006). Properties of ivabradine-induced block of HCN1 and HCN4 pacemaker channels. *The Journal of Physiology*, 572(2), 335–346.
- Burke, D., Howells, J., & Tomlinson, S. E. (2013). Hcn channels: Function and clinical implications. *Neurology*, 81(5), 513–514. <https://doi.org/10.1212/01.wnl.0000433163.22224.2c>
- Camprostrini, G., DiFrancesco, J. C., Castellotti, B., Milanesi, R., Gneccchi-Ruscione, T., Bonzanni, M., Bucchi, A., Baruscotti, M., Ferrarese, C., Franceschetti, S., Canafoglia, L., Ragona, F., Freri, E., Labate, A., Gambardella, A., Costa, C., Gellera, C., Granata, T., Barbuti, A., & DiFrancesco, D. (2018). A loss-of-function HCN4 mutation associated with familial benign myoclonic epilepsy in infancy causes increased neuronal excitability. *Frontiers in Molecular Neuroscience*, 11(August), 1–15. <https://doi.org/10.3389/fnmol.2018.00269>

-
- Cervetto, L., Demontis, G. C., & Gargini, C. (2007). Cellular mechanisms underlying the pharmacological induction of phosphenes. *British Journal of Pharmacology*, 150(4), 383–390. <https://doi.org/10.1038/sj.bjp.0706998>
- Chen, S., Wang, J., & Siegelbaum, S. A. (2001). Properties of hyperpolarization-activated pacemaker current defined by coassembly of HCN1 and HCN2 subunits and basal modulation by cyclic nucleotide. *The Journal of General Physiology*, 117(5), 491–504.
- Di Francesco, D. (2015). HCN4, sinus bradycardia and atrial fibrillation. *Arrhythmia and Electrophysiology Review*, 4(1), 9–13. <https://doi.org/10.15420/aer.2015.4.1.9>
- DiFrancesco, D. (2013). Funny channel gene mutations associated with arrhythmias. *Journal of Physiology*, 591(17), 4117–4124. <https://doi.org/10.1113/jphysiol.2013.253765>
- DiFrancesco, D. (1993). Pacemaker mechanisms in cardiac tissue. *Annual Review of Physiology*, 55(1), 455–472.
- DiFrancesco, D. (2006). Funny channels in the control of cardiac rhythm and mode of action of selective blockers. *Pharmacological Research*, 53(5), 399–406.
- DiFrancesco, J. C., Barbuti, A., Milanesi, R., Coco, S., Bucchi, A., Bottelli, G., Ferrarese, C., Franceschetti, S., Terragni, B., Baruscotti, M., & DiFrancesco, D. (2011). Recessive loss-of-function mutation in the pacemaker HCN2 Channel causing increased neuronal excitability in a patient with idiopathic generalized epilepsy. *Journal of Neuroscience*, 31(48), 17327–17337. <https://doi.org/10.1523/JNEUROSCI.3727-11.2011>
- DiFrancesco, J. C., & DiFrancesco, D. (2015). Dysfunctional HCN ion channels in neurological diseases. *Frontiers in Cellular Neuroscience*, 9(March), 1–10. <https://doi.org/10.3389/fncel.2015.00071>
- El-Kholy, W., MacDonald, P. E., Fox, J. M., Bhattacharjee, A., Xue, T., Gao, X., Zhang, Y., Stieber, J., Li, R. A., & Tsushima, R. G. (2007). Hyperpolarization-activated cyclic nucleotide-gated channels in pancreatic β -cells. *Molecular Endocrinology*, 21(3), 753–764.
- Emery, E. C., Young, G. T., Berrocoso, E. M., Chen, L., & McNaughton, P. A. (2011). HCN2 ion channels play a central role in inflammatory and neuropathic pain. *Science*, 333(6048), 1462–1466.
- Emery, E. C., Young, G. T., & McNaughton, P. A. (2012). HCN2 ion channels: An emerging role as the pacemakers of pain. *Trends in Pharmacological Sciences*, 33(8), 456–463. <https://doi.org/10.1016/j.tips.2012.04.004>
- Fenske, S., Mader, R., Scharr, A., Pappas, C., Cao-Ehlker, X., Michalakis, S., Shaltiel, L., Weidinger, M., Stieber, J., & Feil, S. (2011). HCN3 contributes to the ventricular action potential waveform in the murine heart. *Circulation Research*, 109(9), 1015–1023.
- Flynn, G. E., & Zagotta, W. N. (2018). Insights into the molecular mechanism for hyperpolarization-dependent activation of HCN channels. *Proceedings of the National Academy of Sciences of the United States of America*, 115(34), E8086–E8095. <https://doi.org/10.1073/pnas.1805596115>
- Fürst, O., & D’Avanzo, N. (2015). Isoform dependent regulation of human HCN channels by cholesterol. *Scientific Reports*, 5, 1–12. <https://doi.org/10.1038/srep14270>
- Fyk-Kolodziej, B., & Pourcho, R. G. (2007). Differential distribution of hyperpolarization-activated and cyclic nucleotide-gated channels in cone bipolar cells of the rat retina. *Journal of Comparative Neurology*, 501(6), 891–903.
- Gareth, R., Physiological, T. H. E., Of, S., Firing, R., Role, T. H. E., Hcn, T. H. E., Family, G., Patterns, E., The, O. F., Genes, H. C. N., Molecular, P., For, B., Low, T. H. E., Selectivity, I.

-
- O. N., Nucleotide, C., & Of, M. (2005). The HCN Gene Family : Molecular Basis of the Hyperpolarization-Activated ABSTRACT : AND THE ROLE OF I h. 868, 1–23.
- Goehring, A., Lee, C.-H., Wang, K. H., Michel, J. C., Claxton, D. P., Bacongus, I., Althoff, T., Fischer, S., Garcia, K. C., & Gouaux, E. (2014). Screening and large-scale expression of membrane proteins in mammalian cells for structural studies. *Nature Protocols*, 9(11), 2574–2585.
- Gross, C., Saponaro, A., Santoro, B., Moroni, A., Thiel, G., & Hamacher, K. (2018). Mechanical transduction of cytoplasmic-to-transmembrane-domain movements in a hyperpolarization-activated cyclic nucleotide-gated cation channel. *Journal of Biological Chemistry*, 293(33), 12908–12918. <https://doi.org/10.1074/jbc.RA118.002139>
- Hattori, M., Hibbs, R. E., & Gouaux, E. (2012). A fluorescence-detection size-exclusion chromatography-based thermostability assay for membrane protein precrystallization screening. *Structure*, 20(8), 1293–1299.
- Hayoz, S., Tiwari, P. B., Piszczek, G., Üren, A., & Brelidze, T. I. (2017). Investigating cyclic nucleotide and cyclic dinucleotide binding to HCN channels by surface plasmon resonance. *PLoS ONE*, 12(9), 1–20. <https://doi.org/10.1371/journal.pone.0185359>
- He, P., Deng, J., Zhong, X., Zhou, Z., Song, B., & Li, L. (2012). Identification of a hyperpolarization-activated cyclic nucleotide-gated channel and its subtypes in the urinary bladder of the rat. *Urology*, 79(6), 1411-e7.
- Herrmann, S., Hofmann, F., Stieber, J., & Ludwig, A. (2012). HCN channels in the heart: Lessons from mouse mutants. *British Journal of Pharmacology*, 166(2), 501–509. <https://doi.org/10.1111/j.1476-5381.2011.01798.x>
- Herrmann, S., Layh, B., & Ludwig, A. (2011). Novel insights into the distribution of cardiac HCN channels: an expression study in the mouse heart. *Journal of Molecular and Cellular Cardiology*, 51(6), 997–1006.
- Herrmann, S., Schnorr, S., & Ludwig, A. (2015). Hcn channels—modulators of cardiac and neuronal excitability. *International Journal of Molecular Sciences*, 16(1), 1429–1447. <https://doi.org/10.3390/ijms16011429>
- Holmgren, M., Shin, K. S., & Yellen, G. (1998). The activation gate of a voltage-gated K⁺ channel can be trapped in the open state by an intersubunit metal bridge. *Neuron*, 21(3), 617–621.
- Hu, L., Santoro, B., Saponaro, A., Liu, H., Moroni, A., & Siegelbaum, S. (2013). Binding of the auxiliary subunit TRIP8b to HCN channels shifts the mode of action of cAMP. *Journal of General Physiology*, 142(6), 599–612.
- Ishii, T. M., Takano, M., Xie, L.-H., Noma, A., & Ohmori, H. (1999). Molecular characterization of the hyperpolarization-activated cation channel in rabbit heart sinoatrial node. *Journal of Biological Chemistry*, 274(18), 12835–12839.
- Jung, S., Bullis, J. B., Lau, I. H., Jones, T. D., Warner, L. N., & Poolos, N. P. (2010). Downregulation of dendritic HCN channel gating in epilepsy is mediated by altered phosphorylation signaling. *Journal of Neuroscience*, 30(19), 6678–6688. <https://doi.org/10.1523/JNEUROSCI.1290-10.2010>
- Kopec, W., Köpfer, D. A., Vickery, O. N., Bondarenko, A. S., Jansen, T. L. C., De Groot, B. L., & Zachariae, U. (2018). Direct knock-on of desolvated ions governs strict ion selectivity in K⁺ channels. *Nature Chemistry*, 10(8), 813–820.
- Kusch, J., Thon, S., Schulz, E., Biskup, C., Nache, V., Zimmer, T., Seifert, R., Schwede, F., &

-
- Benndorf, K. (2012). How subunits cooperate in cAMP-induced activation of homotetrameric HCN2 channels. *Nature Chemical Biology*, 8(2), 162–169.
- Lee, C. H., & MacKinnon, R. (2017). Structures of the Human HCN1 Hyperpolarization-Activated Channel. *Cell*, 168(1–2), 111–120.e11. <https://doi.org/10.1016/j.cell.2016.12.023>
- Lee, C. H., & MacKinnon, R. (2019). Voltage Sensor Movements during Hyperpolarization in the HCN Channel. *Cell*, 179(7), 1582–1589.e7. <https://doi.org/10.1016/j.cell.2019.11.006>
- Liston, C. (2019). Targeting pacemaker channels in depression. *Science Translational Medicine*, 11(477), eaaw5318.
- Lolicato, M., Bucchi, A., Arrigoni, C., Zucca, S., Nardini, M., Schroeder, I., Simmons, K., Aquila, M., DiFrancesco, D., Bolognesi, M., Schwede, F., Kashin, D., Fishwick, C. W. G., Johnson, A. P., Thiel, G., & Moroni, A. (2014). Cyclic dinucleotides bind the C-linker of HCN4 to control channel cAMP responsiveness. *Nature Chemical Biology*, 10(6), 457–462. <https://doi.org/10.1038/nchembio.1521>
- Lolicato, M., Nardini, M., Gazzarrini, S., Möller, S., Bertinetti, D., Herberg, F. W., Bolognesi, M., Martin, H., Fasolini, M., Bertrand, J. A., Arrigoni, C., Thiel, G., & Moroni, A. (2011). Tetramerization dynamics of C-terminal domain underlies isoform-specific cAMP gating in hyperpolarization-activated cyclic nucleotide-gated channels. *Journal of Biological Chemistry*, 286(52), 44811–44820. <https://doi.org/10.1074/jbc.M111.297606>
- Marini, C., Porro, A., Rastetter, A., Dalle, C., Rivolta, I., Bauer, D., Oegema, R., Nava, C., Parrini, E., Mei, D., Mercer, C., Dhamija, R., Chambers, C., Coubes, C., Thévenon, J., Kuentz, P., Julia, S., Pasquier, L., Dubourg, C., ... Depienne, C. (2018). HCN1 mutation spectrum: From neonatal epileptic encephalopathy to benign generalized epilepsy and beyond. *Brain*, 141(11), 3160–3178. <https://doi.org/10.1093/brain/awy263>
- Marionneau, C., Couette, B., Liu, J., Li, H., Mangoni, M. E., Nargeot, J., Lei, M., Escande, D., & Demolombe, S. (2005). Specific pattern of ionic channel gene expression associated with pacemaker activity in the mouse heart. *Journal of Physiology*, 562(1), 223–234. <https://doi.org/10.1113/jphysiol.2004.074047>
- Möller, S., Alfieri, A., Bertinetti, D., Aquila, M., Schwede, F., Lolicato, M., Rehmann, H., Moroni, A., & Herberg, F. W. (2014). Cyclic nucleotide mapping of hyperpolarization-activated cyclic nucleotide-gated (HCN) channels. *ACS Chemical Biology*, 9(5), 1128–1137. <https://doi.org/10.1021/cb400904s>
- Momin, A., Cadiou, H., Mason, A., & McNaughton, P. A. (2008). Role of the hyperpolarization-activated current I_h in somatosensory neurons. *Journal of Physiology*, 586(24), 5911–5929. <https://doi.org/10.1113/jphysiol.2008.163154>
- Moosmang, S., Biel, M., Hofmann, F., & Ludwig, A. (1999). Differential distribution of four hyperpolarization-activated cation channels in mouse brain.
- Moroni, A., Barbuti, A., Altomare, C., Viscomi, C., Morgan, J., Baruscotti, M., & DiFrancesco, D. (2000). Kinetic and ionic properties of the human HCN2 pacemaker channel. *Pflügers Archiv European Journal of Physiology*, 439(5), 618–626. <https://doi.org/10.1007/s004240050985>
- Nji, E., Chatzikyriakidou, Y., Landreh, M., & Drew, D. (2018). An engineered thermal-shift screen reveals specific lipid preferences of eukaryotic and prokaryotic membrane proteins. *Nature Communications*, 9(1). <https://doi.org/10.1038/s41467-018-06702-3>
- Noam, Y., Bernard, C., & Baram, T. Z. (2011). Towards an integrated view of HCN channel role

-
- in epilepsy. *Current Opinion in Neurobiology*, 21(6), 873–879.
- Notomi, T., & Shigemoto, R. (2004). Immunohistochemical localization of Ih channel subunits, HCN1–4, in the rat brain. *Journal of Comparative Neurology*, 471(3), 241–276.
- Novella Romanelli, M., Sartiani, L., Masi, A., Mannaioni, G., Manetti, D., Mugelli, A., & Cerbai, E. (2016). HCN Channels Modulators: The Need for Selectivity. *Current Topics in Medicinal Chemistry*, 16(16). <https://doi.org/10.2174/1568026616999160315130832>
- Pape, H.-C., & McCormick, D. A. (1989). Noradrenaline and serotonin selectively modulate thalamic burst firing by enhancing a hyperpolarization-activated cation current. *Nature*, 340(6236), 715–718.
- Porro, A., Abbandonato, G., Veronesi, V., Russo, A., Binda, A., Antolini, L., Granata, T., Castellotti, B., Marini, C., Moroni, A., DiFrancesco, J. C., & Rivolta, I. (2021). Do the functional properties of HCN1 mutants correlate with the clinical features in epileptic patients? *Progress in Biophysics and Molecular Biology*, 166, 147–155. <https://doi.org/10.1016/j.pbiomolbio.2021.07.008>
- Porro, A., Saponaro, A., Gasparri, F., Bauer, D., Gross, C., Pisoni, M., Abbandonato, G., Hamacher, K., Santoro, B., Thiel, G., & Moroni, A. (2019). The HCN domain couples voltage gating and cAMP response in hyperpolarization-activated cyclic nucleotide-gated channels. *ELife*, 8, 1–23. <https://doi.org/10.7554/eLife.49672>
- Porro, A., Thiel, G., Moroni, A., & Saponaro, A. (2020). cyclic AMP Regulation and Its Command in the Pacemaker Channel HCN4. *Frontiers in Physiology*, 11, 771. <https://doi.org/10.3389/fphys.2020.00771>
- Reid, C. A., Phillips, A. M., & Petrou, S. (2012). HCN channelopathies: Pathophysiology in genetic epilepsy and therapeutic implications. *British Journal of Pharmacology*, 165(1), 49–56. <https://doi.org/10.1111/j.1476-5381.2011.01507.x>
- Robinson, R. B., & Siegelbaum, S. A. (2003). Hyperpolarization-Activated Cation Currents: From Molecules to Physiological Function. *Annual Review of Physiology*, 65(4), 453–480. <https://doi.org/10.1146/annurev.physiol.65.092101.142734>
- Santoro, B., Chen, S., Lüthi, A., Pavlidis, P., Shumyatsky, G. P., Tibbs, G. R., & Siegelbaum, S. A. (2000). Molecular and functional heterogeneity of hyperpolarization-activated pacemaker channels in the mouse CNS. *Journal of Neuroscience*, 20(14), 5264–5275. <https://doi.org/10.1523/jneurosci.20-14-05264.2000>
- Santoro, B., Hu, L., Liu, H., Saponaro, A., Pian, P., Piskorowski, R. A., Moroni, A., & Siegelbaum, S. A. (2011). TRIP8b regulates HCN1 channel trafficking and gating through two distinct C-terminal interaction sites. *Journal of Neuroscience*, 31(11), 4074–4086.
- Santoro, B., Liu, D. T., Yao, H., Bartsch, D., Kandel, E. R., Siegelbaum, S. A., & Tibbs, G. R. (1998). Identification of a gene encoding a hyperpolarization-activated pacemaker channel of brain. *Cell*, 93(5), 717–729.
- Santoro, B., & Shah, M. M. (2020). Hyperpolarization-Activated Cyclic Nucleotide-Gated Channels as Drug Targets for Neurological Disorders.
- Santoro, B., Wainger, B. J., & Siegelbaum, S. A. (2004). Regulation of HCN channel surface expression by a novel C-terminal protein-protein interaction. *Journal of Neuroscience*, 24(47), 10750–10762. <https://doi.org/10.1523/JNEUROSCI.3300-04.2004>
- Saponaro, A., Bauer, D., Giese, M. H., Swuec, P., Porro, A., Gasparri, F., Sharifzadeh, A. S., Chaves-Sanjuan, A., Alberio, L., Parisi, G., Cerutti, G., Clarke, O. B., Hamacher, K., Colecraft, H. M., Mancina, F., Hendrickson, W. A., Siegelbaum, S. A., DiFrancesco, D.,

-
- Bolognesi, M., ... Moroni, A. (2021). Gating movements and ion permeation in HCN4 pacemaker channels. *Molecular Cell*, 81(14), 2929-2943.e6. <https://doi.org/10.1016/j.molcel.2021.05.033>
- Saponaro, A., Cantini, F., Porro, A., Bucchi, A., Difrancesco, D., Maione, V., Donadoni, C., Introini, B., Mesirca, P., Mangoni, M. E., Thiel, G., Banci, L., Santoro, B., & Moroni, A. (2018). A synthetic peptide that prevents camp regulation in mammalian hyperpolarization-activated cyclic nucleotide-gated (HCN) channels. *ELife*, 7, 1–22. <https://doi.org/10.7554/eLife.35753>
- Saponaro, A., Pauleta, S. R., Cantini, F., Matzapetakis, M., & Hammann, C. (2014). Structural basis for the mutual antagonism of cAMP and TRIP8b in regulating HCN channel function. *PNAS*, 111(40), 14577–14582. <https://doi.org/10.1073/pnas.1410389111>
- Saponaro, A., Sharifzadeh, A. S., & Moroni, A. (2021). Detection of ligand binding to purified HCN channels using fluorescence-based size exclusion chromatography. In *Ion Channels Part A* (1st ed., Vol. 652). Elsevier Inc. <https://doi.org/10.1016/bs.mie.2021.01.043>
- Sartiani, L., Mannaioni, G., Masi, A., Romanelli, M. N., & Cerbai, E. (2017). The hyperpolarization-activated cyclic nucleotide-gated channels: from biophysics to pharmacology of a unique family of ion channels. *Pharmacological Reviews*, 69(4), 354–395.
- Stieber, J., Stöckl, G., Herrmann, S., Hassfurth, B., & Hofmann, F. (2005). Functional expression of the human HCN3 channel. *Journal of Biological Chemistry*, 280(41), 34635–34643. <https://doi.org/10.1074/jbc.M502508200>
- Tanguay, J., Callahan, K. M., & D’Avanzo, N. (2019). Characterization of drug binding within the HCN1 channel pore. *Scientific Reports*, 9(1), 1–14. <https://doi.org/10.1038/s41598-018-37116-2>
- Ueda, K., Hirano, Y., Higashiuesato, Y., Aizawa, Y., Hayashi, T., Inagaki, N., Tana, T., Ohya, Y., Takishita, S., Muratani, H., Hiraoka, M., & Kimura, A. (2009). Role of HCN4 channel in preventing ventricular arrhythmia. *Journal of Human Genetics*, 54(2), 115–121. <https://doi.org/10.1038/jhg.2008.16>
- Verrier, R. L., Bonatti, R., Silva, A. F. G., Batatinha, J. A. P., Nearing, B. D., Liu, G., Rajamani, S., Zeng, D., & Belardinelli, L. (2014). If inhibition in the atrioventricular node by ivabradine causes rate-dependent slowing of conduction and reduces ventricular rate during atrial fibrillation. *Heart Rhythm*, 11(12), 2288–2296.
- Wahl-Schott, C., & Biel, M. (2009). HCN channels: Structure, cellular regulation and physiological function. *Cellular and Molecular Life Sciences*, 66(3), 470–494. <https://doi.org/10.1007/s00018-008-8525-0>
- Wahl-Schott, C., Fenske, S., & Biel, M. (2014). HCN channels: new roles in sinoatrial node function. *Current Opinion in Pharmacology*, 15, 83–90.
- Wainger, B. J., DeGennaro, M., Santoro, B., Siegelbaum, S. A., & Tibbs, G. R. (2001). Molecular mechanism of cAMP modulation of HCN pacemaker channels. *Nature*, 411(6839), 805–810.
- Weißgraeber, S., Saponaro, A., Thiel, G., & Hamacher, K. (2017). A reduced mechanical model for cAMP-modulated gating in HCN channels. *Scientific Reports*, 7(January), 1–9. <https://doi.org/10.1038/srep40168>
- William N. Zagotta, Nelson B. Olivier, Kevin D. Black, Edgar C. Young, Rich Olson2, & Eric Gouaux. (2003). Structural basis for modulation and agonist specificity of HCN pacemaker

-
- channels. *Nature*, 425(6954), 196–200. <https://doi.org/10.1038/nature01932.1>.
- Wu, J., Sun, L., Chen, X., Du, F., Shi, H., Chen, C., & Chen, Z. J. (2013). Cyclic GMP-AMP is an endogenous second messenger in innate immune signaling by cytosolic DNA. *Science (New York, N.Y.)*, 339(6121), 826–830. <https://doi.org/10.1126/science.1229963>
- Wynia-Smith, S. L., Gillian-Daniel, A. L., Satyshur, K. A., & Robertson, G. A. (2008). hERG gating microdomains defined by S6 mutagenesis and molecular modeling. *The Journal of General Physiology*, 132(5), 507–520.
- Young, G. T., Emery, E. C., Mooney, E. R., Tsantoulas, C., & McNaughton, P. A. (2014). Inflammatory and neuropathic pain are rapidly suppressed by peripheral block of hyperpolarisation-activated cyclic nucleotide-gated ion channels. *PAIN®*, 155(9), 1708–1719.



PART II

3. Monitoring ligand binding to purified HCN4 channels

The following content has been published in *Methods in Enzymology* as a chapter of the book entitled: "Ion Channels: Channel Biochemistry, Reconstitution, and Function" (Saponaro, Sharifzadeh, et al., 2021). The figures reported in this part of the thesis are related to my direct contribute to the published work as detailed below.

This part of the project describes the methodological approach that I have established and used for detecting ligand binding to purified HCN4 proteins.

Biochemical measurements of ligand binding to purified eukaryotic membrane proteins are challenging because of their low yield of expression and purification. Starting from an existing assay, which consists on a thermostability assay based on fluorescence-detection size-exclusion chromatography (fSEC-TS) (Nji et al., 2018), I set the protocol for detecting cAMP binding to purified HCN4 channel proteins. The assay is based on the possibility to monitor the stabilizing effect of ligand binding on the thermal denaturation curve of the protein. Changes in the melting temperature of the protein provide a quantitative value for estimating ligand/protein interaction. What makes this assay suitable for low expressing proteins is the fact that it is based on the fluorescence detection of the GFP tag fused to the target protein, in our case HCN4. This ensures a significant increase in the sensitivity compared to UV (280nm) absorbance. This assay was further used to detect the binding of Ivabradine, a pharmacologically well-known HCN channel blockers.

Moreover, this technique requires very low amounts (nanograms) of protein compared to traditional methods employed to measure protein/ligand interaction, which need large amount of protein. This method opens up the possibility of detecting the binding of pharmacologically relevant drugs to HCN channels.

FSEC-TS uses analytical size exclusion chromatography to detect the temperature-dependent unfolding of a protein by monitoring the progressive disappearance of a given protein peak (Figure 3.1A, black arrow). Size exclusion chromatography is also necessary to discriminate the fluorescence signal of the protein peak from that of the aggregate (Figure 3.1A). Indeed, due to the very high thermostability of (Bokman & Ward, 1981; Hattori et al., 2012; Ward, 1981), also the aggregate still emits fluorescence. We then measured the heights of individual protein peaks (Figure 3.1A, black arrow) and normalized them to the height of

the peak from protein incubated at a reference temperature of 20 °C. The normalized data were finally plotted as a function of the temperature (Figure 3.1B). By fitting the values with a sigmoidal dose-response equation we obtained the thermal denaturing curve of purified GFP-HCN4. The melting temperature (T_m) of the protein is defined as the temperature value at which half of the protein is denaturated. This value corresponds to the inflection point of the sigmoidal curve (black dotted lines in Figure 3.1B).

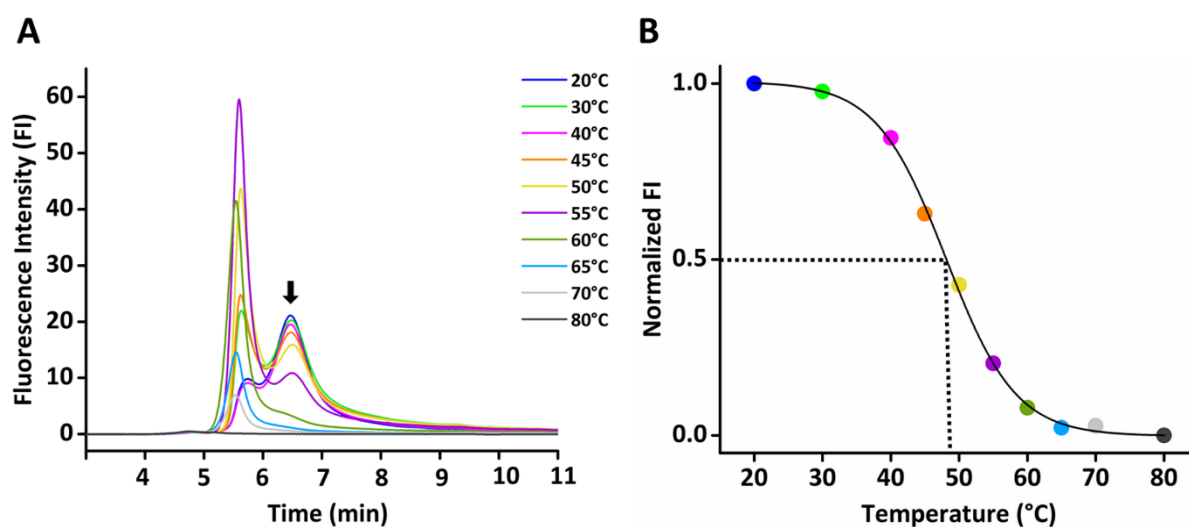


Figure 3.1. Fluorescence-SEC-based thermostability (FSEC-TS) of purified GFP-HCN4. A. Superimposition of the FSEC chromatograms of GFP-HCN4 following purification in LMNG/CHS and 10 min incubation at 20, 30, 40, 45, 50, 55, 60, 65, 70 and 80 °C. The traces are color-coded as described in the inset. The chromatograms display two peaks: the first one corresponds to the aggregated state of GFP-HCN4, while the second one to soluble GFP-HCN4. The peak corresponding to the aggregated protein progressively increases with temperature, while that of the soluble GFP-HCN4 decreases. The black arrow indicates the peak values used to obtain the denaturing curve of GFP-HCN4. **B.** Denaturing curve of the GFP-HCN4 protein shown in (A). The height of the peaks of the soluble GFP-HCN4, normalized to the height of the peak of the same sample treated at 20 °C, is plotted as a function of the pre-conditioning temperature (°C). Dots are color-coded as in (A). Data are fitted with a sigmoidal dose-response equation (see Material and Methods section 2.1.5 for details) and shown as solid black line. T_m value obtained from the fitting is indicated by the black dotted lines; in this example the T_m value is 48.1 °C. [taken from Saponaro, Sharifzadeh, et al., 2021 with permission].

Once identified, the T_m of the target protein can be used to establish a much faster but still accurate screening system in which molecule binding is evaluated as a change in fluorescence from the control (=reference) value (no ligand) relative to one temperature point in response to a treatment (Hattori et al., 2012; Nji et al., 2018). This procedure is much faster because it does not require the acquisition of the whole data set, usually ten temperatures (see Figure 3.1). This procedure also allows the simultaneous comparison of several molecules. For the choice of the respective temperature setting the literature suggests to use a value corresponding to $T_m + 5^\circ\text{C}$ (Hattori et al., 2012; Nji et al., 2018). Indeed, the additional 5°C above the melting temperature magnifies any stabilizing (increase in fluorescence) and/or destabilizing (decrease in fluorescence) effects due to ligand binding to the target protein.

Given that GFP-HCN4 has a T_m of about 50°C (see Fig. 3.1B), we used 55°C as reference temperature. In this screening system data are normalized and expressed as a change (in percentage) of the fluorescence at 55°C from the initial control condition (20°C). As a proof of concept for using the FSEC-TS-dependent screening system of ligand binding to GFP-HCN4 we employed cAMP as a positive control. cTMP was used as a negative control since this molecule is not able to bind to the CNBD of HCN channels and should hence not affect the thermostability of the protein (Möller et al., 2014). Finally, we also used Ivabradine, a commercially well-known open pore blocker of HCN4 channels (Bucchi et al., 2006). The latter was selected because we are able to purify HCN4 with the pore in the open state (see the first chapter of the thesis and the related publication Saponaro, Bauer, et al., 2021). As shown in Figure 3.2, the percentage of fluorescence of the samples heated at 55°C and pre-incubated with cAMP and with Ivabradine is significantly higher than the one of GFP-HCN4 heated at 55°C without ligands. The results of these experiments are compatible with a binding of both ligands to HCN and a consequent thermostabilization. This interpretation is furthermore supported by the finding that cTMP, a known non-binder to HCN channels, has no effect on the fluorescence signal (Fig. 3.2).

Strikingly, the thermal stabilization induced by Ivabradine is important for two reasons: i) it is the first biochemical evidence of a drug binding to the purified full-length HCN4 protein, and it opens the possibility of using this binding assay for other molecules, as reported at the

end of this chapter; ii) it conclusively validates the structural and computational data, which suggest that the pore of the HCN channel is in an open conductive state (see the first chapter of the thesis and the related publication Saponaro, Bauer, et al., 2021).

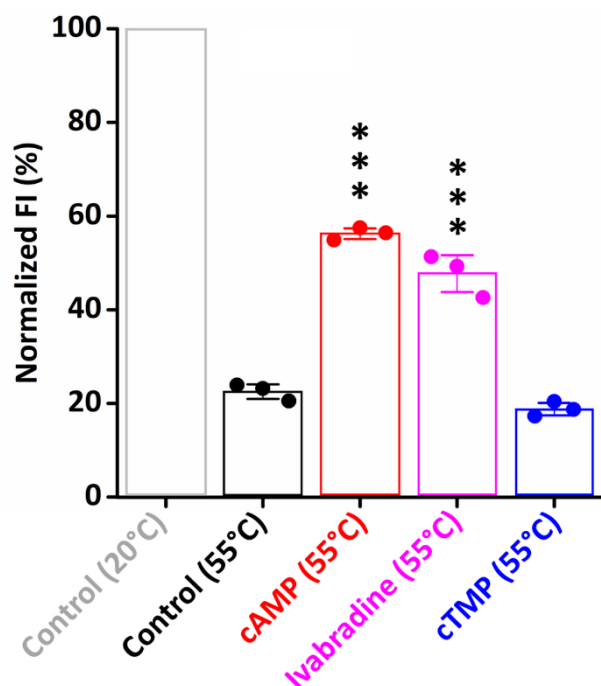


Figure 3.2. Fast screening system for the identification of interactors of HCN4. Graph bar showing the normalized fluorescence intensity (FI) from control: GFP-HCN4 protein samples heated for 10 min at 20 °C (gray, 100%) and at 55 °C (black, 22.5 ± 1%); + cyclic nucleotides: protein samples heated at 55 °C in the presence of 2 mM cAMP (red, 56.3 ± 0.8%), or 2 mM cTMP (blue, 18.8 ± 0.9%); + Ivabradine: protein samples heated at 55 °C in the presence of 0.5 mM Ivabradine (magenta, 47.7 ± 2.6%). The fluorescence intensities were normalized to that from the sample at 20 °C without ligands. Normalized FI values are mean of $n = 3 \pm \text{SEM}$. Statistical analysis performed with one-way ANOVA, followed by Fisher's test (***) $P < 0.001$. [taken from Saponaro, Bauer, et al., 2021 with permission].

At the end of this second part, I have added a chapter in which I describe, in addition to the data above reported, yet unpublished data concerning the binding of cyclic dinucleotides, a new class of second messengers, which regulate the activity of HCN4.

3.1 Detection of cyclic di-GMP binding to the HCN4 pacemaker channel

It was previously shown (Lolicato et al., 2014) that HCN4 channels are regulated by cyclic di-GMP (c-di-GMP, see Figure 3.1A) and more in general by cyclic dinucleotides, an emerging class of regulatory molecules. These molecules were originally identified in bacteria but more recently their function as second messengers was also discovered in mammals in the context of the immune system (Wu et al., 2013). Further electrophysiological and structural studies showed that the function of cyclic dinucleotides is not limited to regulation of immune reactions; it was shown that c-di-GMP also antagonizes specifically the cAMP regulation of the pacemaker HCN4 channels (Lolicato et al., 2014).

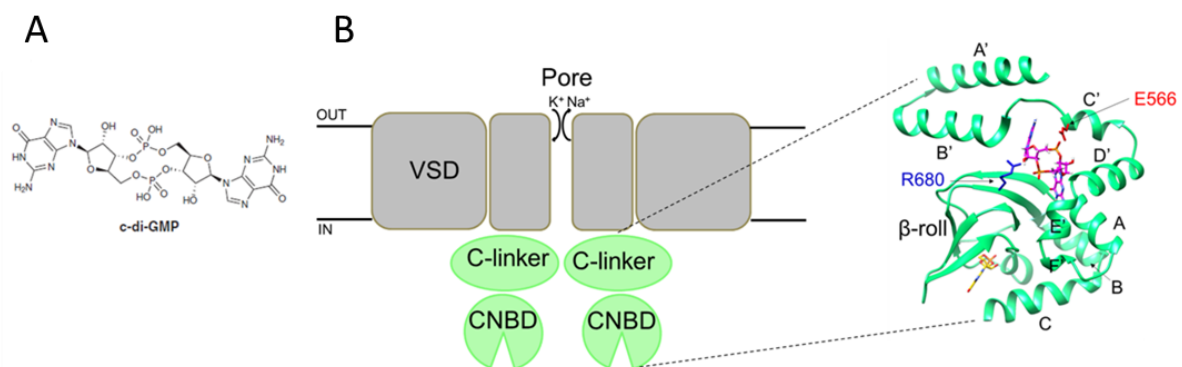



Figure 3.1 Putative binding site of c-di-GMP in the Clinker/CNBD of HCN4. **A.** Chemical structure of c-di-GMP. **B.** Cartoon representation of two of the four subunits forming HCN channels. The principal domains are labelled: voltage sensor domain (VSD, grey); Pore (grey); C-linker (light green) and cyclic nucleotide binding domain (CNBD, light green). Right inset: Docking simulation of c-di-GMP (magenta sticks) by using the X-ray structure of the HCN4 Clinker/CNBD fragment in complex with cGMP (orange sticks) (PDB_ID: 4KL1). The crucial residues involved in the interaction with c-di-GMP (magenta sticks) are shown, labeled and colored based on their chemical nature: blue for the positive residue and red for the negative residue. The figures of panel B are adapted from (Porro et al., 2020).

The interest for this finding is therefore two folded: 1) cyclic di nucleotides constitute a new class of second messengers, which have now been identified also in humans (Wu et al., 2013), and 2), very important for this work, their regulation of HCN channels is subtype-




specific. Indeed, they are so far the only known HCN4-specific modulator. In general terms they are off to date the only example for an isotype specific drug for HCN channels.

c-di-GMP binding to HCN4 was serendipitously discovered in relation to work on the X-ray structure of the cytosolic fragment of the protein, that includes the C-linker and the CNBD only (Lolicato et al., 2011, 2014). When the C-linker/CNBD fragment of HCN4 was crystallized in the presence of the agonist cyclic GMP (cGMP), the ligand was found not only in its canonical ligand binding site in the CNBD (Figure 3.1B, cGMP colored in orange) but also in a second pocket at the interface between the CNBD and the C-linker, defined as the C-linker pocket (CLP). Subsequent *in silico* docking performed in the CLP by using the X-ray structure of the HCN4 C-linker/CNBD identified c-di-GMP (Figure 3.1B, cGMP colored in magenta) as potential binder of the CLP (Lolicato et al., 2014). This prediction was confirmed by experiments which showed that c-di-GMP is an effective and isoform specific regulator of HCN4 gating. Up to now the ability of c-di-GMP to HNC4 is only based on indirect evidence namely molecular docking and electrophysiological recordings of HCN4 function (Lolicato et al., 2014). Biochemical attempts to detect c-di-GMP binding to the HCN4 failed (Hayoz et al., 2017). This may suggest the involvement of other domains of HCN channels in the interaction with c-di-GMP, beside the C-linker/CNBD previously indicated by the docking analysis.

After establishing the fluorescence size exclusion chromatography-based thermostability assay (FSEC-TS) to monitor ligand binding to purify GFP-tagged HCN4 pacemaker channels (Saponaro, Sharifzadeh, et al., 2021), we decided to use it to detect c-di-GMP interaction with the full-length channel protein.

As we have demonstrated in our publication (Saponaro, Sharifzadeh, et al., 2021), the same assay can be used in a much faster way once the melting temperature (T_m) of the target protein is identified. By comparing the stability of a protein under different conditions (e.g., \pm ligand) at a given temperature in the dynamic range of the melting curve, provides an accurate and fast screening system in which molecule binding can be evaluated from a change in fluorescence under the test condition compared to the control (no ligand) at one point only ($T_m + 5$ °C). This procedure is much faster because it does not require the acquisition of the whole data set, usually ten temperatures, and allows the simultaneous comparison of several molecules instead (Saponaro, Sharifzadeh, et al., 2021).



As shown in Figure 3.2A, we found that c-di-GMP increases the thermal stability of HCN4 as much as cAMP (positive control). To further validate our result, we repeated the same FSEC-TS assay with a single point mutant of HCN4 (R681E), which is known to abolish the effect of c-di-GMP. This residue is located in the CNBD (Figure 3.1B). We were choosing this mutation for two reasons: i) We consider it most clearly associated with a direct impairment of c-di-GMP binding to HCN4 because this mutation causes no significant alterations in the biophysical properties of the channel; it only abolishes the c-di-GMP mediated inhibition on the cAMP effect on channel gating (Lolicato et al., 2014); ii) Among the residues of the CLP previously tested by electrophysiology (Lolicato et al., 2014), the R681 residue is pointing in the cryo-EM structures of HCN4 (Saponaro, Bauer, et al., 2021) towards the HCND domain and the adjacent S4-S5 linker. Both these two structural elements were recently shown as key players in the propagation of the cAMP signal in HCN channels (Porro et al., 2019; Saponaro, Bauer, et al., 2021). Moreover, in both structural elements we found specific features which are present in HCN4 but not in HCN1 and which could eventually account for the isotype specificity of c-di-GMP (Saponaro, Bauer, et al., 2021).

Figure 3.2B shows that the addition of c-di-GMP to the HCN4 R681E mutant does not increase the thermal stability of the protein as much as cAMP. This result not only confirms that we detected c-di-GMP binding to HCN4, but also highlights the key role of R681 in the interaction with the ligand. Overall, this is the first biochemical evidence of c-di-GMP binding to HCN4 channels.

Based on these promising results, we collected single particle cryo-EM data of HCN4 bound to c-di-GMP and we are currently analyzing the dataset to obtain the high-resolution EM density map of the complex. This will allow to conclusively establish the binding area of c-di-GMP, thus visualizing the eventual involvement of the HCN domain and/or of the S4-S5 linker in the interaction with the ligand.

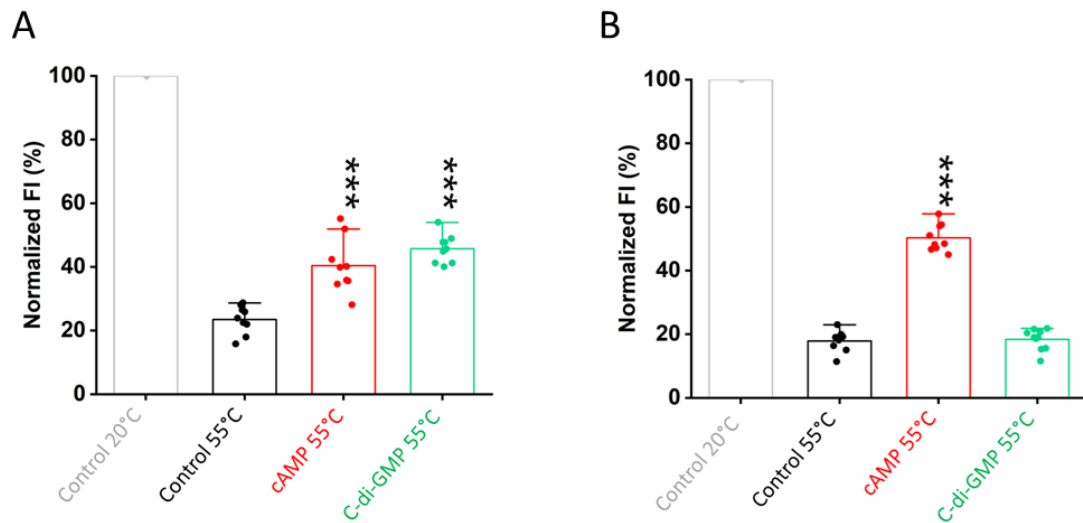


Figure 3.2 Measurements of c-di-GMP binding to purified GFP-HCN4 by using FSEC-TS. A. Graph bar showing the normalized fluorescence intensity (FI) from control: Protein samples heated for 10 min at 20°C (gray, 100%), at 55°C (black, 23.5 ± 1.4%); + ligands: Protein samples heated at 55 °C in the presence of 2mM cAMP (red, 41.1± 2.8%, positive control); or 2 mM c-di-GMP (green, 46 ± 1.4%). The fluorescence intensities were normalized to that from the sample at 20°C without ligands. c-di-GMP stabilizes GFP-HCN4 as the known ligand cAMP. **B.** To further validate our result, we performed FSEC-TS with a single point mutant of HCN4 (R681E). Graph bar as in panel A: control at 20°C (gray, 100%) and at 55°C (black, 15 ± 1.7%); +2 mM cAMP (red, 45.1± 1.7%); and +2 mM cdi-GMP (green, 16.1% ± 1.1%). R681E mutation fully abolishes the c-di-GMP-dependent thermal stabilization of GFP-HCN4. Normalized FI values are mean of n =9 ± SEM. Statistical analysis performed with one-way ANOVA, followed by Fisher's test (***P <0.001).

References

- Altomare, C., Terragni, B., Brioschi, C., Milanesi, R., Pagliuca, C., Viscomi, C., Moroni, A., Baruscotti, M., & DiFrancesco, D. (2003). Heteromeric HCN1-HCN4 channels: A comparison with native pacemaker channels from the rabbit sinoatrial node. *Journal of Physiology*, 549(2), 347–359. <https://doi.org/10.1113/jphysiol.2002.027698>
- Alvarez-Baron, C. P., Klenchin, V. A., & Chanda, B. (2018). Minimal molecular determinants of isoform-specific differences in efficacy in the HCN channel family. *Journal of General Physiology*, 150(8), 1203–1213. <https://doi.org/10.1085/jgp.201812031>
- Bankston, J. R., DeBerg, H. A., Stoll, S., & Zagotta, W. N. (2017). Mechanism for the inhibition of the cAMP dependence of HCN ion channels by the auxiliary subunit TRIP8b. *Journal of Biological Chemistry*, 292(43), 17794–17803.
- Baruscotti, M., Bottelli, G., Milanesi, R., DiFrancesco, J. C., & DiFrancesco, D. (2010). HCN-related channelopathies. *Pflügers Archiv European Journal of Physiology*, 460(2), 405–415. <https://doi.org/10.1007/s00424-010-0810-8>
- Baruscotti, M., Bucchi, A., Barbuti, A., & DiFrancesco, D. (2012). Funny current and cardiac rhythm: insights from HCN knockout and transgenic mouse models. *Frontiers in Physiology*, 3, 240.
- Baruscotti, M., Bucchi, A., Milanesi, R., Paina, M., Barbuti, A., Gneccchi-Ruscione, T., Bianco, E., Vitali-Serdoz, L., Cappato, R., & DiFrancesco, D. (2017). A gain-of-function mutation in the cardiac pacemaker HCN4 channel increasing cAMP sensitivity is associated with familial Inappropriate Sinus Tachycardia. *European Heart Journal*, 38(4), 280–288.
- Baruscotti, M., & DiFrancesco, D. (2004). Pacemaker channels. *Annals of the New York Academy of Sciences*, 1015(1), 111–121.
- Biel, M., Wahl-Schott, C., Michalakis, S., & Zong, X. (2009). Hyperpolarization-activated cation channels: From genes to function. *Physiological Reviews*, 89(3), 847–885. <https://doi.org/10.1152/physrev.00029.2008>
- Bolívar, J. J., Tapia, D., Arenas, G., Castanon-Arreola, M., Torres, H., & Galarraga, E. (2008). A hyperpolarization-activated, cyclic nucleotide-gated, (I_h-like) cationic current and HCN gene expression in renal inner medullary collecting duct cells. *American Journal of Physiology-Cell Physiology*, 294(4), C893–C906.
- Bucchi, A., Baruscotti, M., Nardini, M., Barbuti, A., Micheloni, S., Bolognesi, M., & DiFrancesco, D. (2013). Identification of the Molecular Site of Ivabradine Binding to HCN4 Channels. *PLoS ONE*, 8(1), 1–12. <https://doi.org/10.1371/journal.pone.0053132>
- Bucchi, A., Tognati, A., Milanesi, R., Baruscotti, M., & DiFrancesco, D. (2006). Properties of ivabradine-induced block of HCN1 and HCN4 pacemaker channels. *The Journal of Physiology*, 572(2), 335–346.
- Burke, D., Howells, J., & Tomlinson, S. E. (2013). Hcn channels: Function and clinical implications. *Neurology*, 81(5), 513–514. <https://doi.org/10.1212/01.wnl.0000433163.22224.2c>
- Camprostrini, G., DiFrancesco, J. C., Castellotti, B., Milanesi, R., Gneccchi-Ruscione, T., Bonzanni, M., Bucchi, A., Baruscotti, M., Ferrarese, C., Franceschetti, S., Canafoglia, L., Ragona, F., Freri, E., Labate, A., Gambardella, A., Costa, C., Gellera, C., Granata, T., Barbuti, A., & DiFrancesco, D. (2018). A loss-of-function HCN4 mutation associated with familial benign myoclonic epilepsy in infancy causes increased neuronal excitability. *Frontiers in Molecular Neuroscience*, 11(August), 1–15. <https://doi.org/10.3389/fnmol.2018.00269>

-
- Cervetto, L., Demontis, G. C., & Gargini, C. (2007). Cellular mechanisms underlying the pharmacological induction of phosphenes. *British Journal of Pharmacology*, 150(4), 383–390. <https://doi.org/10.1038/sj.bjp.0706998>
- Chen, S., Wang, J., & Siegelbaum, S. A. (2001). Properties of hyperpolarization-activated pacemaker current defined by coassembly of HCN1 and HCN2 subunits and basal modulation by cyclic nucleotide. *The Journal of General Physiology*, 117(5), 491–504.
- Di Francesco, D. (2015). HCN4, sinus bradycardia and atrial fibrillation. *Arrhythmia and Electrophysiology Review*, 4(1), 9–13. <https://doi.org/10.15420/aer.2015.4.1.9>
- DiFrancesco, D. (2013). Funny channel gene mutations associated with arrhythmias. *Journal of Physiology*, 591(17), 4117–4124. <https://doi.org/10.1113/jphysiol.2013.253765>
- DiFrancesco, D. (1993). Pacemaker mechanisms in cardiac tissue. *Annual Review of Physiology*, 55(1), 455–472.
- DiFrancesco, D. (2006). Funny channels in the control of cardiac rhythm and mode of action of selective blockers. *Pharmacological Research*, 53(5), 399–406.
- DiFrancesco, J. C., Barbuti, A., Milanesi, R., Coco, S., Bucchi, A., Bottelli, G., Ferrarese, C., Franceschetti, S., Terragni, B., Baruscotti, M., & DiFrancesco, D. (2011). Recessive loss-of-function mutation in the pacemaker HCN2 Channel causing increased neuronal excitability in a patient with idiopathic generalized epilepsy. *Journal of Neuroscience*, 31(48), 17327–17337. <https://doi.org/10.1523/JNEUROSCI.3727-11.2011>
- DiFrancesco, J. C., & DiFrancesco, D. (2015). Dysfunctional HCN ion channels in neurological diseases. *Frontiers in Cellular Neuroscience*, 9(March), 1–10. <https://doi.org/10.3389/fncel.2015.00071>
- El-Kholy, W., MacDonald, P. E., Fox, J. M., Bhattacharjee, A., Xue, T., Gao, X., Zhang, Y., Stieber, J., Li, R. A., & Tsushima, R. G. (2007). Hyperpolarization-activated cyclic nucleotide-gated channels in pancreatic β -cells. *Molecular Endocrinology*, 21(3), 753–764.
- Emery, E. C., Young, G. T., Berrocoso, E. M., Chen, L., & McNaughton, P. A. (2011). HCN2 ion channels play a central role in inflammatory and neuropathic pain. *Science*, 333(6048), 1462–1466.
- Emery, E. C., Young, G. T., & McNaughton, P. A. (2012). HCN2 ion channels: An emerging role as the pacemakers of pain. *Trends in Pharmacological Sciences*, 33(8), 456–463. <https://doi.org/10.1016/j.tips.2012.04.004>
- Fenske, S., Mader, R., Scharr, A., Pappazios, C., Cao-Ehlker, X., Michalakis, S., Shaltiel, L., Weidinger, M., Stieber, J., & Feil, S. (2011). HCN3 contributes to the ventricular action potential waveform in the murine heart. *Circulation Research*, 109(9), 1015–1023.
- Flynn, G. E., & Zagotta, W. N. (2018). Insights into the molecular mechanism for hyperpolarization-dependent activation of HCN channels. *Proceedings of the National Academy of Sciences of the United States of America*, 115(34), E8086–E8095. <https://doi.org/10.1073/pnas.1805596115>
- Fürst, O., & D’Avanzo, N. (2015). Isoform dependent regulation of human HCN channels by cholesterol. *Scientific Reports*, 5, 1–12. <https://doi.org/10.1038/srep14270>
- Fyk-Kolodziej, B., & Pourcho, R. G. (2007). Differential distribution of hyperpolarization-activated and cyclic nucleotide-gated channels in cone bipolar cells of the rat retina. *Journal of Comparative Neurology*, 501(6), 891–903.
- Gareth, R., Physiological, T. H. E., Of, S., Firing, R., Role, T. H. E., Hcn, T. H. E., Family, G., Patterns, E., The, O. F., Genes, H. C. N., Molecular, P., For, B., Low, T. H. E., Selectivity, I.

-
- O. N., Nucleotide, C., & Of, M. (2005). The HCN Gene Family : Molecular Basis of the Hyperpolarization-Activated ABSTRACT : AND THE ROLE OF I h. 868, 1–23.
- Goehring, A., Lee, C.-H., Wang, K. H., Michel, J. C., Claxton, D. P., Bacongus, I., Althoff, T., Fischer, S., Garcia, K. C., & Gouaux, E. (2014). Screening and large-scale expression of membrane proteins in mammalian cells for structural studies. *Nature Protocols*, 9(11), 2574–2585.
- Gross, C., Saponaro, A., Santoro, B., Moroni, A., Thiel, G., & Hamacher, K. (2018). Mechanical transduction of cytoplasmic-to-transmembrane-domain movements in a hyperpolarization-activated cyclic nucleotide-gated cation channel. *Journal of Biological Chemistry*, 293(33), 12908–12918. <https://doi.org/10.1074/jbc.RA118.002139>
- Hattori, M., Hibbs, R. E., & Gouaux, E. (2012). A fluorescence-detection size-exclusion chromatography-based thermostability assay for membrane protein precrystallization screening. *Structure*, 20(8), 1293–1299.
- Hayoz, S., Tiwari, P. B., Piszczek, G., Üren, A., & Brelidze, T. I. (2017). Investigating cyclic nucleotide and cyclic dinucleotide binding to HCN channels by surface plasmon resonance. *PLoS ONE*, 12(9), 1–20. <https://doi.org/10.1371/journal.pone.0185359>
- He, P., Deng, J., Zhong, X., Zhou, Z., Song, B., & Li, L. (2012). Identification of a hyperpolarization-activated cyclic nucleotide-gated channel and its subtypes in the urinary bladder of the rat. *Urology*, 79(6), 1411-e7.
- Herrmann, S., Hofmann, F., Stieber, J., & Ludwig, A. (2012). HCN channels in the heart: Lessons from mouse mutants. *British Journal of Pharmacology*, 166(2), 501–509. <https://doi.org/10.1111/j.1476-5381.2011.01798.x>
- Herrmann, S., Layh, B., & Ludwig, A. (2011). Novel insights into the distribution of cardiac HCN channels: an expression study in the mouse heart. *Journal of Molecular and Cellular Cardiology*, 51(6), 997–1006.
- Herrmann, S., Schnorr, S., & Ludwig, A. (2015). Hcn channels—modulators of cardiac and neuronal excitability. *International Journal of Molecular Sciences*, 16(1), 1429–1447. <https://doi.org/10.3390/ijms16011429>
- Holmgren, M., Shin, K. S., & Yellen, G. (1998). The activation gate of a voltage-gated K⁺ channel can be trapped in the open state by an intersubunit metal bridge. *Neuron*, 21(3), 617–621.
- Hu, L., Santoro, B., Saponaro, A., Liu, H., Moroni, A., & Siegelbaum, S. (2013). Binding of the auxiliary subunit TRIP8b to HCN channels shifts the mode of action of cAMP. *Journal of General Physiology*, 142(6), 599–612.
- Ishii, T. M., Takano, M., Xie, L.-H., Noma, A., & Ohmori, H. (1999). Molecular characterization of the hyperpolarization-activated cation channel in rabbit heart sinoatrial node. *Journal of Biological Chemistry*, 274(18), 12835–12839.
- Jung, S., Bullis, J. B., Lau, I. H., Jones, T. D., Warner, L. N., & Poolos, N. P. (2010). Downregulation of dendritic HCN channel gating in epilepsy is mediated by altered phosphorylation signaling. *Journal of Neuroscience*, 30(19), 6678–6688. <https://doi.org/10.1523/JNEUROSCI.1290-10.2010>
- Kopec, W., Köpfer, D. A., Vickery, O. N., Bondarenko, A. S., Jansen, T. L. C., De Groot, B. L., & Zachariae, U. (2018). Direct knock-on of desolvated ions governs strict ion selectivity in K⁺ channels. *Nature Chemistry*, 10(8), 813–820.
- Kusch, J., Thon, S., Schulz, E., Biskup, C., Nache, V., Zimmer, T., Seifert, R., Schwede, F., &

-
- Benndorf, K. (2012). How subunits cooperate in cAMP-induced activation of homotetrameric HCN2 channels. *Nature Chemical Biology*, 8(2), 162–169.
- Lee, C. H., & MacKinnon, R. (2017). Structures of the Human HCN1 Hyperpolarization-Activated Channel. *Cell*, 168(1–2), 111–120.e11. <https://doi.org/10.1016/j.cell.2016.12.023>
- Lee, C. H., & MacKinnon, R. (2019). Voltage Sensor Movements during Hyperpolarization in the HCN Channel. *Cell*, 179(7), 1582–1589.e7. <https://doi.org/10.1016/j.cell.2019.11.006>
- Liston, C. (2019). Targeting pacemaker channels in depression. *Science Translational Medicine*, 11(477), eaaw5318.
- Lolicato, M., Bucchi, A., Arrigoni, C., Zucca, S., Nardini, M., Schroeder, I., Simmons, K., Aquila, M., DiFrancesco, D., Bolognesi, M., Schwede, F., Kashin, D., Fishwick, C. W. G., Johnson, A. P., Thiel, G., & Moroni, A. (2014). Cyclic dinucleotides bind the C-linker of HCN4 to control channel cAMP responsiveness. *Nature Chemical Biology*, 10(6), 457–462. <https://doi.org/10.1038/nchembio.1521>
- Lolicato, M., Nardini, M., Gazzarrini, S., Möller, S., Bertinetti, D., Herberg, F. W., Bolognesi, M., Martin, H., Fasolini, M., Bertrand, J. A., Arrigoni, C., Thiel, G., & Moroni, A. (2011). Tetramerization dynamics of C-terminal domain underlies isoform-specific cAMP gating in hyperpolarization-activated cyclic nucleotide-gated channels. *Journal of Biological Chemistry*, 286(52), 44811–44820. <https://doi.org/10.1074/jbc.M111.297606>
- Marini, C., Porro, A., Rastetter, A., Dalle, C., Rivolta, I., Bauer, D., Oegema, R., Nava, C., Parrini, E., Mei, D., Mercer, C., Dhamija, R., Chambers, C., Coubes, C., Thévenon, J., Kuentz, P., Julia, S., Pasquier, L., Dubourg, C., ... Depienne, C. (2018). HCN1 mutation spectrum: From neonatal epileptic encephalopathy to benign generalized epilepsy and beyond. *Brain*, 141(11), 3160–3178. <https://doi.org/10.1093/brain/awy263>
- Marionneau, C., Couette, B., Liu, J., Li, H., Mangoni, M. E., Nargeot, J., Lei, M., Escande, D., & Demolombe, S. (2005). Specific pattern of ionic channel gene expression associated with pacemaker activity in the mouse heart. *Journal of Physiology*, 562(1), 223–234. <https://doi.org/10.1113/jphysiol.2004.074047>
- Möller, S., Alfieri, A., Bertinetti, D., Aquila, M., Schwede, F., Lolicato, M., Rehmann, H., Moroni, A., & Herberg, F. W. (2014). Cyclic nucleotide mapping of hyperpolarization-activated cyclic nucleotide-gated (HCN) channels. *ACS Chemical Biology*, 9(5), 1128–1137. <https://doi.org/10.1021/cb400904s>
- Momin, A., Cadiou, H., Mason, A., & Mcnaughton, P. A. (2008). Role of the hyperpolarization-activated current I_h in somatosensory neurons. *Journal of Physiology*, 586(24), 5911–5929. <https://doi.org/10.1113/jphysiol.2008.163154>
- Moosmang, S., Biel, M., Hofmann, F., & Ludwig, A. (1999). Differential distribution of four hyperpolarization-activated cation channels in mouse brain.
- Moroni, A., Barbuti, A., Altomare, C., Viscomi, C., Morgan, J., Baruscotti, M., & DiFrancesco, D. (2000). Kinetic and ionic properties of the human HCN2 pacemaker channel. *Pflügers Archiv European Journal of Physiology*, 439(5), 618–626. <https://doi.org/10.1007/s004240050985>
- Nji, E., Chatzikyriakidou, Y., Landreh, M., & Drew, D. (2018). An engineered thermal-shift screen reveals specific lipid preferences of eukaryotic and prokaryotic membrane proteins. *Nature Communications*, 9(1). <https://doi.org/10.1038/s41467-018-06702-3>
- Noam, Y., Bernard, C., & Baram, T. Z. (2011). Towards an integrated view of HCN channel role

-
- in epilepsy. *Current Opinion in Neurobiology*, 21(6), 873–879.
- Notomi, T., & Shigemoto, R. (2004). Immunohistochemical localization of Ih channel subunits, HCN1–4, in the rat brain. *Journal of Comparative Neurology*, 471(3), 241–276.
- Novella Romanelli, M., Sartiani, L., Masi, A., Mannaioni, G., Manetti, D., Mugelli, A., & Cerbai, E. (2016). HCN Channels Modulators: The Need for Selectivity. *Current Topics in Medicinal Chemistry*, 16(16). <https://doi.org/10.2174/1568026616999160315130832>
- Pape, H.-C., & McCormick, D. A. (1989). Noradrenaline and serotonin selectively modulate thalamic burst firing by enhancing a hyperpolarization-activated cation current. *Nature*, 340(6236), 715–718.
- Porro, A., Abbandonato, G., Veronesi, V., Russo, A., Binda, A., Antolini, L., Granata, T., Castellotti, B., Marini, C., Moroni, A., DiFrancesco, J. C., & Rivolta, I. (2021). Do the functional properties of HCN1 mutants correlate with the clinical features in epileptic patients? *Progress in Biophysics and Molecular Biology*, 166, 147–155. <https://doi.org/10.1016/j.pbiomolbio.2021.07.008>
- Porro, A., Saponaro, A., Gasparri, F., Bauer, D., Gross, C., Pisoni, M., Abbandonato, G., Hamacher, K., Santoro, B., Thiel, G., & Moroni, A. (2019). The HCN domain couples voltage gating and cAMP response in hyperpolarization-activated cyclic nucleotide-gated channels. *ELife*, 8, 1–23. <https://doi.org/10.7554/eLife.49672>
- Porro, A., Thiel, G., Moroni, A., & Saponaro, A. (2020). cyclic AMP Regulation and Its Command in the Pacemaker Channel HCN4. *Frontiers in Physiology*, 11, 771. <https://doi.org/10.3389/fphys.2020.00771>
- Reid, C. A., Phillips, A. M., & Petrou, S. (2012). HCN channelopathies: Pathophysiology in genetic epilepsy and therapeutic implications. *British Journal of Pharmacology*, 165(1), 49–56. <https://doi.org/10.1111/j.1476-5381.2011.01507.x>
- Robinson, R. B., & Siegelbaum, S. A. (2003). Hyperpolarization-Activated Cation Currents: From Molecules to Physiological Function. *Annual Review of Physiology*, 65(4), 453–480. <https://doi.org/10.1146/annurev.physiol.65.092101.142734>
- Santoro, B., Chen, S., Lüthi, A., Pavlidis, P., Shumyatsky, G. P., Tibbs, G. R., & Siegelbaum, S. A. (2000). Molecular and functional heterogeneity of hyperpolarization-activated pacemaker channels in the mouse CNS. *Journal of Neuroscience*, 20(14), 5264–5275. <https://doi.org/10.1523/jneurosci.20-14-05264.2000>
- Santoro, B., Hu, L., Liu, H., Saponaro, A., Pian, P., Piskorowski, R. A., Moroni, A., & Siegelbaum, S. A. (2011). TRIP8b regulates HCN1 channel trafficking and gating through two distinct C-terminal interaction sites. *Journal of Neuroscience*, 31(11), 4074–4086.
- Santoro, B., Liu, D. T., Yao, H., Bartsch, D., Kandel, E. R., Siegelbaum, S. A., & Tibbs, G. R. (1998). Identification of a gene encoding a hyperpolarization-activated pacemaker channel of brain. *Cell*, 93(5), 717–729.
- Santoro, B., & Shah, M. M. (2020). Hyperpolarization-Activated Cyclic Nucleotide-Gated Channels as Drug Targets for Neurological Disorders.
- Santoro, B., Wainger, B. J., & Siegelbaum, S. A. (2004). Regulation of HCN channel surface expression by a novel C-terminal protein-protein interaction. *Journal of Neuroscience*, 24(47), 10750–10762. <https://doi.org/10.1523/JNEUROSCI.3300-04.2004>
- Saponaro, A., Bauer, D., Giese, M. H., Swuec, P., Porro, A., Gasparri, F., Sharifzadeh, A. S., Chaves-Sanjuan, A., Alberio, L., Parisi, G., Cerutti, G., Clarke, O. B., Hamacher, K., Colecraft, H. M., Mancina, F., Hendrickson, W. A., Siegelbaum, S. A., DiFrancesco, D.,

-
- Bolognesi, M., ... Moroni, A. (2021). Gating movements and ion permeation in HCN4 pacemaker channels. *Molecular Cell*, 81(14), 2929-2943.e6. <https://doi.org/10.1016/j.molcel.2021.05.033>
- Saponaro, A., Cantini, F., Porro, A., Bucchi, A., Difrancesco, D., Maione, V., Donadoni, C., Introini, B., Mesirca, P., Mangoni, M. E., Thiel, G., Banci, L., Santoro, B., & Moroni, A. (2018). A synthetic peptide that prevents camp regulation in mammalian hyperpolarization-activated cyclic nucleotide-gated (HCN) channels. *ELife*, 7, 1–22. <https://doi.org/10.7554/eLife.35753>
- Saponaro, A., Pauleta, S. R., Cantini, F., Matzapetakis, M., & Hammann, C. (2014). Structural basis for the mutual antagonism of cAMP and TRIP8b in regulating HCN channel function. *PNAS*, 111(40), 14577–14582. <https://doi.org/10.1073/pnas.1410389111>
- Saponaro, A., Sharifzadeh, A. S., & Moroni, A. (2021). Detection of ligand binding to purified HCN channels using fluorescence-based size exclusion chromatography. In *Ion Channels Part A* (1st ed., Vol. 652). Elsevier Inc. <https://doi.org/10.1016/bs.mie.2021.01.043>
- Sartiani, L., Mannaioni, G., Masi, A., Romanelli, M. N., & Cerbai, E. (2017). The hyperpolarization-activated cyclic nucleotide-gated channels: from biophysics to pharmacology of a unique family of ion channels. *Pharmacological Reviews*, 69(4), 354–395.
- Stieber, J., Stöckl, G., Herrmann, S., Hassfurth, B., & Hofmann, F. (2005). Functional expression of the human HCN3 channel. *Journal of Biological Chemistry*, 280(41), 34635–34643. <https://doi.org/10.1074/jbc.M502508200>
- Tanguay, J., Callahan, K. M., & D’Avanzo, N. (2019). Characterization of drug binding within the HCN1 channel pore. *Scientific Reports*, 9(1), 1–14. <https://doi.org/10.1038/s41598-018-37116-2>
- Ueda, K., Hirano, Y., Higashiuesato, Y., Aizawa, Y., Hayashi, T., Inagaki, N., Tana, T., Ohya, Y., Takishita, S., Muratani, H., Hiraoka, M., & Kimura, A. (2009). Role of HCN4 channel in preventing ventricular arrhythmia. *Journal of Human Genetics*, 54(2), 115–121. <https://doi.org/10.1038/jhg.2008.16>
- Verrier, R. L., Bonatti, R., Silva, A. F. G., Batatinha, J. A. P., Nearing, B. D., Liu, G., Rajamani, S., Zeng, D., & Belardinelli, L. (2014). If inhibition in the atrioventricular node by ivabradine causes rate-dependent slowing of conduction and reduces ventricular rate during atrial fibrillation. *Heart Rhythm*, 11(12), 2288–2296.
- Wahl-Schott, C., & Biel, M. (2009). HCN channels: Structure, cellular regulation and physiological function. *Cellular and Molecular Life Sciences*, 66(3), 470–494. <https://doi.org/10.1007/s00018-008-8525-0>
- Wahl-Schott, C., Fenske, S., & Biel, M. (2014). HCN channels: new roles in sinoatrial node function. *Current Opinion in Pharmacology*, 15, 83–90.
- Wainger, B. J., DeGennaro, M., Santoro, B., Siegelbaum, S. A., & Tibbs, G. R. (2001). Molecular mechanism of cAMP modulation of HCN pacemaker channels. *Nature*, 411(6839), 805–810.
- Weißgraeber, S., Saponaro, A., Thiel, G., & Hamacher, K. (2017). A reduced mechanical model for cAMP-modulated gating in HCN channels. *Scientific Reports*, 7(January), 1–9. <https://doi.org/10.1038/srep40168>
- William N. Zagotta, Nelson B. Olivier, Kevin D. Black, Edgar C. Young, Rich Olson2, & Eric Gouaux. (2003). Structural basis for modulation and agonist specificity of HCN pacemaker

-
- channels. *Nature*, 425(6954), 196–200. <https://doi.org/10.1038/nature01932.1>.
- Wu, J., Sun, L., Chen, X., Du, F., Shi, H., Chen, C., & Chen, Z. J. (2013). Cyclic GMP-AMP is an endogenous second messenger in innate immune signaling by cytosolic DNA. *Science (New York, N.Y.)*, 339(6121), 826–830. <https://doi.org/10.1126/science.1229963>
- Wynia-Smith, S. L., Gillian-Daniel, A. L., Satyshur, K. A., & Robertson, G. A. (2008). hERG gating microdomains defined by S6 mutagenesis and molecular modeling. *The Journal of General Physiology*, 132(5), 507–520.
- Young, G. T., Emery, E. C., Mooney, E. R., Tsantoulas, C., & McNaughton, P. A. (2014). Inflammatory and neuropathic pain are rapidly suppressed by peripheral block of hyperpolarisation-activated cyclic nucleotide-gated ion channels. *PAIN®*, 155(9), 1708–1719.



PART III

4. Isolation of state-dependent nanobodies against HCN4 channels using a yeast surface display platform

Abstract

Dysfunction of HCN channels, typically gain of function mutations, have been linked to different cardiac and neurological disorders. Since Ivabradine, the only commercially available blocker of HCN channels, does not sufficiently discriminate between different HCN isoforms, we setup a screening strategy to find subtype-specific drugs. In this approach, purified HCN4 protein, which we can obtain with the closed and open pore, is used as antigen to screen an available yeast-display library of synthetic nanobodies by combining magnetic and fluorescence activated cell sorting for the rapid identification of conformationally selective nanobodies.

Following this procedure, we isolated ten candidate hits that were further tested on HCN4 currents in patch clamp recordings. Seven nanobodies gave a measurable effect on the current, inducing a facilitating effect on HCN4 gating in form of a right shift in the activation curve. Three NBs were not specific for HCN4, as their effect was similarly visible on HCN1 current, but not in the cognate channel hERG. Three NBs did not show any measurable effect. Of the seven functional NBs in total, six acted from the extracellular side and one from the cytosolic side. None of them acted as a pore blocker or reduced/inhibited the channel current. Of the HCN4 specific binders, one displays a high affinity for the target protein, in the range of sub-micromolar. This nanobody will be tested in the future to counteract, and possibly revert, the effect of HCN4 loss-of-function mutations. Furthermore, Fluorescence activated cell sorting (FACS) assays on mammalian cells expressing HCN4 allowed us to verify that all three NBs with no measurable effect on channel currents do bind to HCN4 from the extracellular side. Attractive practical application would see these nanobodies as carriers for proteins or small molecules targeting HCN channels for their modulation. Taken together, these results demonstrate that our protocol successfully isolated nanobodies in an isotype-specific manner with potential use in research and therapy.

4.1 Introduction

4.1.1 Nanobodies

Single-domain antibodies, also referred to as nanobodies (Nbs), are antigen-binding proteins that bind to their targets through a single variable domain called VHH. Unlike conventional antibodies which are made of two heavy chains and two light chains, nanobodies are derived from heavy chain only antibodies present in camelids and cartilaginous fish (Flajnik et al., 2011; Hamers-Casterman et al., 1993) (Figure 4.1 A). Nanobodies (Nbs) are small proteins (12-15 kDa) that have been shown to be functionally equivalent to traditional antibodies in recognizing target antigens (Liu & Yang, 2022). The structural architecture of Nbs comprises two β -sheets with three antigen-binding loops in between them; these are hypervariable regions (complementarity determining regions, CDR1-3) responsible for recognition and binding. CDR3 is the main contributor, which, by being long and flexible provides nanobodies with more diverse paratopes that can potentially bind target proteins; CDR1 and CDR2 assist the binding process (Liu & Yang, 2022) (Figure 4.1 B).

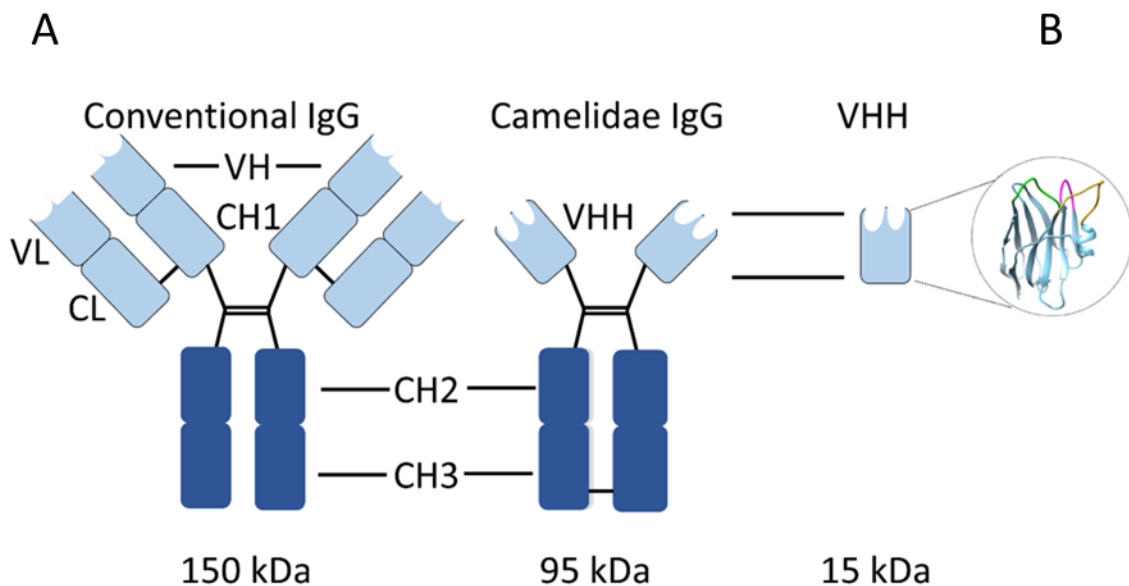



Figure 4.1 Comparison between conventional antibodies and nanobodies. A. Conventional antibodies (left) are composed of two heavy chains and two light chains, while the Camelidae variants

(center) possess two heavy chains only (C = constant domain, V = variable domain, H = heavy chain, L = light chain). The single variable region of Camelidae antibodies, called VHH, can be cloned and expressed independently (right). This is termed nanobody. **B.** Ribbon representation of the 3D structure of a nanobody. The structural architecture of a nanobody includes two antiparallel β -sheets forming a β -roll. Complementarity-determining loops, CDR1, 2, 3, which form the antigen binding site, are highlighted in green, purple, and yellow, respectively.

Development of drugs targeting ion channels has always been challenging; poor selectivity, toxicity and suboptimal efficacy are the main obstacles that need to be faced in this process. The lack of success in targeting the ion-conducting pore of ion channels with small molecules, has inspired the research of new strategies to overcome these issues. Given their high specificity and solubility, as well as their propensity to recognize small clefts within proteins, nanobodies offer an attractive strategy in the development of selective approaches to target ion channels (Stortelers et al., 2018). Nanobodies for therapeutic use need to be engineered to extend their half-life, which otherwise is only in the range of an hour because of their passage through the renal filtration barrier. But depending on the affinity for their targets, the duration of functional ion channel blockade can be much longer than their serum half-life (Stortelers et al., 2018).

Being a relatively new approach, there are not many examples for an employment of nanobody in the modulation of ion channels. One example are alpaca-derived nanobodies which have been identified to specifically bind with high affinity the human ASIC1a, the proton-gated Na^+ channel involved in pain modulation. In this case it was shown that the Nbs was able to discern between isoforms (Y. Wu et al., 2021). Similarly, a subtype-specific nanobody has been found to fully block ATP-induced Ca^{++} influx in human cells expressing the P2X7 ligand-gated channel (Danquah et al., 2016). Another group has selected, from a synthetic nanobody library, a nanobody selective against CFTR (Cl^- channel) channels. But in this case binding did not affect the physiological channel function (Kanner et al., 2020). Recently, a study has been published on the isolation of nanobodies that specifically target voltage-gated sodium channels (NaVs), but no data on possible effects of these Nbs on channel function have so far been reported (Srinivasan et al., 2022). Therefore, there are no data on the ability of nanobodies to selectively bind voltage-gated channels and modulate



their voltage dependency. Nonetheless the above-mentioned encouraging results seem to be a promising starting point for the identification, isolation, and characterization of nanobodies that specifically target HCN channels.

HCN channel mutations are often correlated with alterations of I_f currents; although treatment for constitutively closed pores or trafficking deficient mutants is harder to achieve; it is reasonable to think that gain-of-function phenotypes can be reverted by the administration of pore blocking drugs. Such a new strategy in blocking HCN channels seems even more important considering the fact that gain-of-function point mutations in the HCN1 pore domain have been shown to respond to channel blocking compounds to a lesser extent than the wild-type protein. Hence an alternative strategy to treat such mutations could be a nanobody-induced block of the ion-conducting pore.

Finding pore-blocking nanobodies with the characteristics of being isoform-specific and conformationally selective is of great interest in the search for an alternative to ivabradine, the only commercially available HCN channel blocker (Postea & Biel, 2011). Nanobodies directed towards HCN4 potentially offer an isoform-specific block of the pore, or a modulatory effect of the channel's voltage dependency. To this end, by taking advantage of our ability to purify HCN4 channel in the open and closed pore conformations (Saponaro, Bauer, et al., 2021), we have used the protein in these two states as positive and negative antigens, respectively for the identification of conformationally selective nanobodies.

Direct immunization of animals for the isolation of nanobodies carries some limitations such as a hefty cost and the need for an antigen with more than optimal purification yield, which unfortunately is not the case for the HCN4 protein. For this reason, we used a yeast nanobody library surface-display approach to circumvent these problems and to identify HCN4 selective binders. This synthetic library was created by Conor McMahon and co workers (McMahon et al., 2018) starting from a consensus framework derived from llama genes combined with random mutagenesis of the three CDR sequences that comprise the antigen-binding interface of nanobodies. To display the nanobody on the surface of *Saccharomyces cerevisiae* cell wall, the former is fused to the cell wall glycoprotein, *a*-agglutinin, which consists of two subunits referred to as Aga1p and Aga2p, linked by disulfide

bridges. The nanobody is fused to Aga2p in order to be displayed on the yeast cell surface (Figure 4.2).

Starting from 10^8 unique nanobody clones displayed on the surface of *Saccharomyces cerevisiae* yeast cells exposed to the HCN4 open channel antigen, ten unique binders were isolated after an iterative process of selection and enrichment through FACS and MACS (Fluorescent- and Magnetic- Activated Cell Sorting). These ten binders were subsequently screened and functionally characterized in this work by means of patch clamp experiments performed on HEK293T cells expressing the HCN4 channel.

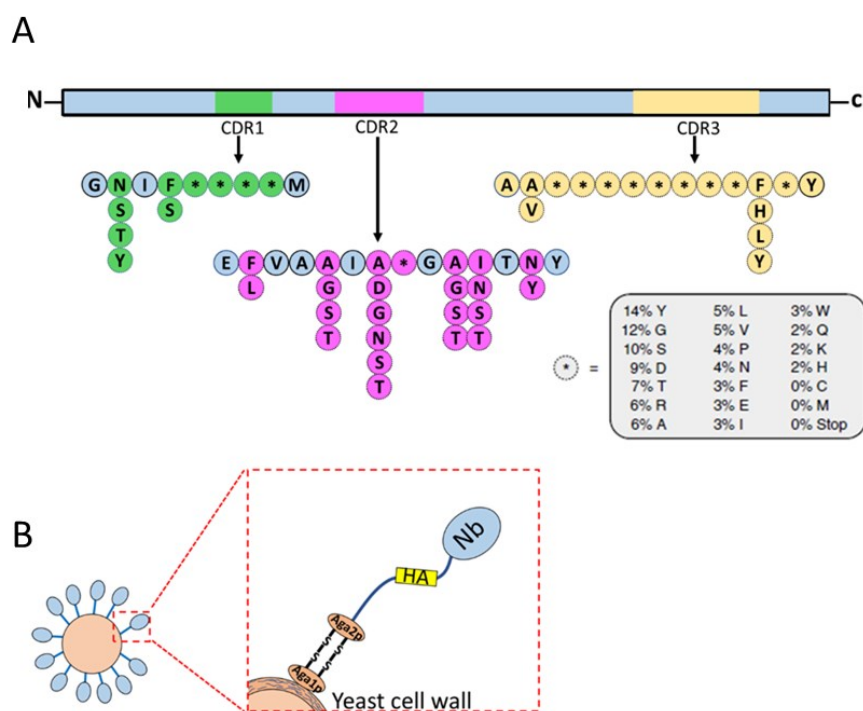


Figure 4.2. The synthetic nanobody library. A. Construction of synthetic nanobody library; framework regions were fixed in sequence are shown in gray, while the variable regions are shown in green, purple, and yellow for CDR1, CDR2, and CDR3, respectively. This panel is modified from McMahon et al (McMahon et al., 2018). **B.** Schematic representation of synthetic nanobody displayed on the yeast cell wall. In the red inlet, nanobody (light blue) is shown with an HA tag (yellow) inserted at its C-terminus, followed by a long flexible stalk which covalently tethers the nanobody to the yeast cell wall Aga2p - Aga1p complex.

4.2 Materials and Methods

4.2.1 Constructs

We used the nanobody DNA library pool which was created by Conor McMahon and coworkers (McMahon et al., 2018) in which the nanobody gene was cloned into the engineered surface display vector, pYDS649, (Pen-Strep') downstream of a Gal promoter. In this way, the system allowed the expression of nanobodies only under controlled conditions, i.e. by the addition of galactose (McMahon et al., 2018).

The rabbit HCN4 gene used in this work for the expression and purification of GFP-HCN4_{CLOSED} and GFP-HCN4_{OPEN} proteins. For the details of this construct see section 2.1.1.

4.2.2 Preparation of antigens

The GFP-HCN4_{CLOSED} and GFP-HCN4_{OPEN} proteins were prepared as described in section 2.1.3.

The GFP protein was prepared as follow: pEGA vector carrying GFP-His_{x10}-TEV gene was transfected into 500mL of HEK 293F cells as described before (Saponaro, Bauer, et al., 2021; Saponaro, Sharifzadeh, et al., 2021). Cells were harvested at 48 hr post-transfection and resuspended in 10mL of low salt buffer (10 mM KCl, 10 mM MgCl₂, 10 mM HEPES pH 7.5, 0.5 mM PMSF, EDTA-free complete protease inhibitor cocktail (Roche) (1:1000), 20 µg/mL DNase, and 10 µg/mL RNase) and lysed by gentle homogenization in a glass homogenizer. The solution was cleared by ultracentrifugation (40min at 17000 x g). The supernatant was applied to a pre-equilibrated Ni²⁺-NTA resin (QIAGEN), supplemented with 10mM imidazole and the mixture allowed to gently rotate overnight at 4°C. After transferring the mixture to a column, the resin was washed using 10 column volumes of PBS 1X buffer containing 60mM imidazole. The protein was eluted using PBS 1X containing 300mM imidazole. The eluted protein was loaded on a Superose 6 increase 10/300 GL SEC column (GE Healthcare Life Sciences) pre-equilibrated with PBS 1X buffer. Final yield of purified protein was about 4mg per 1L of cells.

4.2.3 Naïve yeast library growth and induction of protein expression

An aliquot of the nanobody naïve yeast library (McMahon et al., 2018) was inoculated into 100 mL of growing medium: -Trp drop-out medium (3.8 g/L -Trp drop-out medium supplement (Sigma), 6.7 g/L yeast nitrogen base (sigma), 10 mL/L Pen-Strep (10,000 units/mL

stock, sigma)) supplemented with 2% glucose at 30 °C with shaking (220 rpm, Excella E25 NewBrunswick) for 24h. To induce cells, the cells were pelleted at 3500 × g for 3 min at 4 °C. The supernatant was removed, and the cells were resuspended into 100 mL inducing medium: –Trp drop-out medium supplemented with 2% galactose at 30 °C with shaking (200 rpm, Excella E25 NewBrunswick) for 48h.

4.2.4 Nanobody expression test

The nanobody expression was tested before any enrichment step. First, the cell density of induced nanobody naïve yeast library was measured by quantifying the optical density at 600 nm (OD_{600}). An OD_{600} of 1 corresponds to approximately 1.5×10^7 cells per 1mL (McMahon et al., 2018). 500µl of selection buffer (20mM HEPES pH 7.5, 200mM NaCl, 0.1% (w/v) BSA, 5mM Maltose) was added to two microcentrifuge tubes. According to the measured OD_{600} , approximately 7×10^6 induced yeast cells were added into the one tube. The same amount of non-induced cells was added to the second tube, as a control. Both tubes were centrifuged at 4 °C for 1 min at 3500 × g. The pellet was resuspended in 100µl selection buffer. In both tubes 0.5 µg of anti-HA antibody conjugated with AlexaFluor647 (Thermofisher) was added and were incubated on ice for 15 minutes. At the end of this time, both tubes were spun down as before. To remove the excess of dye, the pellet was resuspended in 500 µL of selection buffer and centrifuged as before. The washing was repeated one more time and the pellet was resuspended in 500 µL of selection buffer. The nanobody expression level was assessed by FACS.

4.2.5 Procedure of selection using MACS and FACS

To isolate the nanobody binders to HCN4_{OPEN}, we performed 7 rounds of selections, in which we have repeated two times the following scheme: two consecutive MACS selections, followed by a FACS run. The first and last rounds of selection began with preclearing step. The procedure was as follow: the first round of MACS selection began with a preclearing step using the negative selection to deplete the naïve library from eventual binders to the GFP tag, antibodies, and iron-beads. For the preclearing step, 5×10^9 induced yeast cells were pelleted at 4 °C for 3 min at 3500 × g, resuspended in 5 mL of selection buffer (see section 4.2.4) containing 0.5 µM purified GFP protein and anti-GFP- Alexa Fluor 647 conjugated antibody

(Thermofisher, 1:200) followed by the gently rotation for 1 hour at 4°C. The cells were spun as above, and the pellet was incubated with 4.5 mL of selection buffer together with 500µL of anti-Alexa Fluor 647 microbeads (Miltenyi) for 40 min at 4°C. At the end of this time, the cells were pelleted and resuspended in 5 mL of selection buffer. The resuspended cells were passed through an LD column (Miltenyi), pre-equilibrated with 5mL of selection buffer. The remaining yeast cells from the flow-through were resuspended in 5 mL of growing medium (see section 4.2.3) at 30 °C with shaking (250 rpm) for 24h to recover. The expression of nanobody was performed as mentioned in the section 4.2.3. For the first round of selection, 5×10^9 induced yeast cells were pelleted and resuspended in 5 mL of selection buffer (see section 4.2.4) supplemented with 0.002% LMG-CHS, containing 0.250 µM purified HCN4_{OPEN} antigen and anti-GFP- Alexa Fluor 647 conjugated antibody (1:200) followed by gently rotation for 1 hour at 4°C. The cells then were spun and resuspended in 4.5 mL of selection buffer. The 500 µL of anti-Alexa Fluor 647 microbeads was added to the resuspended cells and incubated for 1 hour at 4°C. To remove the unbound microbeads, at the end of incubation time, the cells were spun, and the pelleted cells were resuspended in 5 mL of selection buffer. The resuspended cells were passed through an LS column (Miltenyi), pre-equilibrated with 5 mL of selection buffer. The weak binders were washed from the column by passing 8 mL of selection buffer through the column. Finally, the cells associated to HCN4_{OPEN} molecules were eluted from the column by removing the magnetic field. The cells eluted from the LS column were pelleted as mentioned before and resuspended in 5 mL of growing medium (see section 4.2.3) at 30 °C with shaking (250 rpm) for 24h to recover. The expression of nanobodies were induced as mentioned in 4.2.3. The round 2 used MACS (positive selection) again, but by taking 3×10^7 induced yeast cells for this round and also for the consequent rounds. Therefore, the induced yeast cells were incubated with 250 µL of selection buffer containing 0.250 µM HCN4_{OPEN} and anti-GFP- Alexa Fluor 647 conjugated antibody (1:200). The selection procedure using the magnetic microbeads was performed as mentioned for the round 1. In round 3, the yeast induced cells were incubated with 250 µL selection buffer containing HCN4_{OPEN} protein for 15 min at 4°C. The cells were pelleted and washed two times using 1 mL of selection buffer to remove the excess of antigen. The yeast cells were resuspended in 2 mL of selection buffer and sorted by the FACS. The round 4 was started with the counterselection

against HCN4_{CLOSED} to deplete nanobody clones that bind conformationally invariant epitopes. To this end, 3×10^7 induced cells were resuspended in selection buffer containing $0.250 \mu\text{M}$ purified HCN4_{CLOSED} protein and anti-GFP- Alexa Fluor 647 conjugated antibody (Thermofisher, 1:200) and processed as detailed above for the initial preclearing step using the LD column. The flow-through from the LD column was used for the positive selection using MACS as mentioned for round 2. For round 5, the conformational selection procedure (counterselection + positive selection) was repeated as in round 4. Yeast displaying selectivity for the HCN4_{OPEN}, after round 5, were collected expanded in growth media, induced, and subjected to the second round of FACS (round 6). Finally, the last round of selection (round 7) was started with depletion of cells interacting with GFP tag, antibodies, and iron-beads as performed at the beginning of the selection procedure. The process ended with a positive selection performed with MACS.

Of note, to monitor the enrichment of specific binders of HCN4_{OPEN} we performed analytical FACS of the key steps of the selection (naïve library, GFP-depleted library, post round 6 and post round 7). The analytical FACS performed using 7×10^6 of induced cells following the procedure was mentioned for the FACS in round 3 and 6, but this time without sorting.

The isolated yeast cells displaying affinity for the HCN4_{OPEN} were recovered in growing medium (see section 4.2.3). We plated different dilutions (100, 200, 400 and 800) of the cells on –Trp plates to obtain single clones and could obtain 100 colonies from a plate in which 800 cells were initially seeded. Nanobody plasmids of individual clones were extracted from the yeast cells (zymoresearch) and transformed into DH5 α E. coli strain to obtain a suitable and pure amount for the sequencing.

4.2.6 Fast-screening method for identifying the sequences over-represented

The first sequence results of the selected population (15 clones over 100 clones) revealed that there are two sequences (Nb1 and Nb5) highly over-represented. To identify and remove these two sequences before sequencing the remaining 85 clones, we performed PCR based on primers designed to anneal to the variable regions of CDR1 and CDR3 of the Nb1 sequence which was over-represented. The forward and reverse primers were 24 and 23

bp long with a melting temperature (T_m) of 60°C and 61°C, respectively, which are listed below:

FW: 5'-CGGCACTATTTCTTACCTGAACGG-3'
REV: 5'-GTAAGAACGCGGGATAGAAGCCG-3'

The string PCR condition: The annealing temperature was set at the T_m (60°C) and the time of primer annealing was set at 10 seconds. In this way we could avoid nonspecific binding and increase the specificity of the screening.

The final DNA fragments were separated electrophoretically in an 2% (w/v) agarose gel. The band corresponding to the DNA fragment of interest was detected at 235 bp.

The non-identical clones to the Nb1 were chosen for the second PCR using following primers designed to anneal to the variable regions of CDR1 and CDR3 of the Nb5.

FW: 5'-GGCACTATTTTTCTGCCGCG-3'
REV: 5'-GGCACTATTTTTCTGCCGCG-3'

The designed primers were 20 bp long with a melting temperature (T_m) of 60°C and 59°C, respectively. The string PCR condition was the same as mentioned above.

The final DNA fragments were separated electrophoretically in an 2% (w/v) agarose gel, as mentioned above.

Using this approach, the non-identical clones to the over-represented nanobodies (Nb1 and Nb5) were detected and selected for the sequencing.

4.2.7 Cloning the isolated nanobody genes into bacterial vector

Isolated nanobody genes were cloned into the linearized bacterial periplasmic expression vector pET-27b(+). The pET-27b(+) vector carries an N-terminal pelB signal sequence for the localization of the protein in the bacterial periplasm, plus C-terminal HSV epitope tag for the visualization using immunochemical methods, and His-Tag sequences for the affinity purification. Firstly, the pET-27b(+) vector was linearized by PCR amplification using a pair of primers. This allowed the cloning of the fragment downstream to the N-terminal pelB signal and upstream to the HSV and hexa-histidine tags. The forward and reverse primers were 27 and 22 bp long with a T_m of 60°C and 61°C, respectively:

FW: 5'-CAGCCAGAACTCGCCCCGGAAGACCCC-3'
REV: 5'-GGCCATCGCCGGCTGGGCAGCG-3'

Then, the DNA fragment encoding nanobody was amplified using following primers in order to add at each end overlapping sequences that are complementary to the linearized pET-27b(+) vector. The vector sequences are shown in bold to distinguish from the nanobody sequences:

FW: 5'-**GCTGCTCCTCGCTGCCAGCCGGCGATGGCC**CAGGTGCAGCTGCAGGAAAGCGG-3'
REV: 5'-**CGGGGTCTCCGGGGCGAGTTCTGGCTGGCTGCTCACGGTCACCTGGG**-3'

The PCR products were purified using the clean-up PCR kit (GeneAll), following the manufacturer's instructions. The presence of desired fragments was analyzed on a gel to verify the expected size (425 bp). At the end, the double-stranded DNA fragment of nanobody was inserted into the linearized vector using Gibson cloning which is a single-reaction of three enzymes: 5' exonuclease, a DNA polymerase and a DNA ligase, that allows the seamless joining of multiple overlapping fragments (Gibson et al., 2009). The final nanobody construct was sequenced to verify the proper insertion.

4.2.8 Expression and purification of isolated nanobodies in E.coli

The pET-27b(+) plasmid containing the nanobody genes was transformed into and expressed from Rosetta E.coli cells. For each nanobody, E. coli cells were grown in 500 mL Terrific Broth medium (Research Products International) with shaking (280 RPM, Excella E25 NewBrunswick) at 37°C. The cells were induced after reaching OD₆₀₀ 0.6–0.8 with 1 mM IPTG (SIGMA) with shaking (240 RPM, Excella E25 NewBrunswick) at 25°C for about 15 h. Induced cells were pelleted and resuspended in 25 mL of lysis Buffer (200mM Tris pH 8, 500mM Sucrose, 500μM EDTA) at room temperature. The resuspended cells osmotically were shocked by adding 50mL of cold water containing 5mM MgCl₂ and 1μL benzonase nuclease (SIGMA) with 1h stirring. This process allows the releasing of periplasmic nanobody. The lysate was centrifuged at 14000 x g for 30 min at 4°C. The supernatant was brought to a concentration of 100mM NaCl with stirring for 15 min at room temperature and applied to a prepacked Nickel column 5 mL (GE Healthcare), pre-equilibrated with 5CV of high salt wash buffer (20mM HEPES pH 7.5, 500 mM NaCl, 20mM Imidazole). The resin was washed with 10 CV of a high-salt buffer and then washed with a low-salt buffer (20mM HEPES pH 7.5, 150mM NaCl, 20mM Imidazole). The nanobodies were eluted with elution buffer (20mM HEPES pH 7.5, 150mM NaCl, 400mM imidazole) and successively injected to a HiLoad 16/600 Superdex

200 Prep Grade column (GE Healthcare), pre-equilibrated with buffer containing 150mM NaCl, 20mM HEPES pH 7.5, 10% Glycerol.

The final protein concentration was determined based on the measured absorbance at 280 nm using the calculated molecular absorbance coefficient $37,485 \text{ M}^{-1} \text{ cm}^{-1}$.

4.2.9 SDS-PAGE and Western Blot analysis

Purified protein samples together with the samples were collected from each step of purification were separated in SDS- polyacrylamide gels (NuPAGE™ 4 to 12%, Bis-Tris, Invitrogen) and Novex Sharp Prestained Protein Standards (Invitrogen) were used as size references. Samples were successively stained with Coomassie blue (Sigma-Aldrich). The same aliquot of samples was separated in the SDS- polyacrylamide gels for the Western Blot technique. For the immunological detection of proteins, the gels were blotted onto a PVDF Transfer Membrane (Invitrogen) and incubated with the primary monoclonal anti-polyHistidine (mouse IgG2a) antibody (Sigma-Aldrich) that is able to detect the histidine-tag positioned at the C-terminus of each nanobody construct. The secondary antibody anti-mouse IgG conjugated to alkaline phosphatase (Sigma-Aldrich) allowed the detection of the bands relative to the histidine-tagged proteins upon addition of the enzyme's substrate (SIGMAFAST™ BCIP®/NBT, Sigma-Aldrich).

4.2.10 Nanobody Labelling

The optimal condition of labelling was identified by calculating the KD of Red-His-NTA dye for Nb5 according to the manufacturer's instructions (Nanotemper). After finding the best condition for the labelling, the Nb5 was labelled using Red-Tris dye performed according to the manufacturer's instructions (Nanotemper). The excess of dye was removed after the labelling reaction using a PD Minitrap™ G-25 desalting column, following the manufacturer's instructions (Sigma-Aldrich).

4.2.11 Analysis the interaction affinity and the dissociation constant (KD) using Microscale Thermophoresis (MST)

Microscale thermophoresis (MST) experiments were performed according to the manufacturer's instructions (NanoTemper), using a Monolith NT.115. In brief, 100nM of labelled Nb5 was incubated for 5 min, in the presence of a serial dilution of the purified GFP-

HCN4_{OPEN} with the maximum concentration of 2 μ M. In this way the concentration of labelled nanobody reached to 50 nM while the initial concentration of GFP-HCN4_{OPEN} in the serial dilution reached to 1 μ M. Samples were filled into capillaries (NanoTemper) and placed in a capillary tray Monolith NT.115. All the measurements were performed at a constant temperature of 22 °C, with an LED excitation power of 40% and an MST laser power of 40%. The changes in the thermophoretic movement were depicted using MO.Control software (NanoTemper). The fluorescence ratio before and after heating was normalized (ΔF_{norm} [%]) and plotted as a function of the ligand concentration and fitted using the KD model by the MO.Analysis software (NanoTemper).

4.2.12 Binding check assay

For each nanobody two samples were prepared: 100nM of the fluorescently labelled nanobody alone and in the presence of an excess of 2 μ M purified GFP-HCN4_{OPEN}. In this way the final concentration of labelled nanobody and GFP-HCN4_{OPEN} reached to 50 nM and 1 μ M, respectively. Samples filled into capillaries (NanoTemper) and placed in a capillary tray Monolith NT.115. All the measurements were performed at a constant temperature of 22 °C, with an LED excitation power of 40% and an MST laser power of 40% using MO.Control and MO.Analysis softwares (NanoTemper).

4.2.13 Monitoring the interaction of Nb19, 34 and 68 with the HEK cells expressing GFPHCN4 using the analytical FACS

The Red-Tris dye was diluted in PBS to use for the labelling of Nb 19, Nb 34 and Nb 68 according to the manufacturer's instructions (Nano temper).

100 mL of HEK293F cells were transiently transfected with plasmids encoding either for GFP-HCN4 or for GFP as mentioned before (Saponaro, Bauer, et al., 2021; Saponaro, Sharifzadeh, et al., 2021). 100mL of HEK293F cells was remained non-transfected. 48 hour later, 6 x10⁶ of either transfected or non-transfected cells were collected and washed in 1m PBS supplemented with 2% of Bovine Serum Albumin (BSA, Sigma). The cells were centrifuged at 4°C for 5 minutes at 0.9 RCF. The washing step was repeated for another time. After the second wash, the cells were incubated with 100 μ L of labelled nanobody for 15 minutes. At

the end of this time, the cells were centrifuged as mentioned above and washed 3 times using 1 mL of PBS supplemented with 2% of BSA and analyzed in the FACS.

4.2.14 Electrophysiology

HEK293-T cells (Invitrogen) were cultured as described (Porro et al., 2019, 2020) and transiently transfected either with HCN4, or HCN1 wild-type or mutant channels (1mg per transfection) using Turbofect transfection reagent (ThermoFisher) according to the manufacturer recommended protocol. When needed, GFP (cloned in pMAX vector) was cotransfected to identify successfully transfected cells. All the experiments were performed at room temperature (about 25C). Currents were recorded in whole-cell configuration with an Axopatch 200B amplifier (Molecular Devices, CA, USA) or with an ePatch amplifier (Elements, Cesena, Italy); data acquired with the Axopatch 200B amplifier were digitized with an Axon Digidata 1550B (Molecular Devices, CA, USA) converter. All data were analyzed offline with Axon pClamp 10.7. Data acquisition and analysis follow the procedures detailed in (Porro et al., 2019, 2020).

4.3 Results

4.3.1 Checking the quality of nanobodies' expression on the surface of yeast

The proper expression of nanobodies on the surface of yeast is crucial to ensure a good yield of variability of the library. Based on the work of the creators of the library, expression of nanobodies ranging between 15-25% results in a good representation of the library diversity (McMahon et al., 2018). Therefore, every step of the selection was preceded by a test of the nanobody expression on the surface of yeasts. To do so, a small fraction of the yeast population grown in the inducible medium (for details, see mat and methods, section 4.2.4) was subjected to analytical FACS by taking advantage of the HA epitope inserted between the engineered cell wall protein Aga2p and the nanobody (see Figure 4.2B). Indeed, prior to FACS analysis, cells were labelled with an anti-HA tag antibody conjugated with a Alexa 647 fluorophore. the immunodecorated cells were analyzed via FACS to visualize the percentage of cells expressing the nanobody on their surface. Figure 4.3A presents the results from an analytical FACS performed on the naïve library. As stated above, we performed this analysis for all the steps of the nanobody selection to ensure a good representation of the library diversity during the entire process. The analytical FACS assays showed a percentage of nanobody expression ranging between 18 (Figure 4.3A) to 24%. This range matches the one reported by the creators of the library (McMahon et al., 2018), thus indicating that we performed all the steps of the selection with a well-represented nanobody library.

It is worth noting that cells may have autofluorescence due to cellular compounds. In yeast riboflavin is the major contributor for both green and red autofluorescence and it can significantly differ between stains (Maslanka et al., 2018). Therefore, as a control of the analytical FACS performed on the naïve library (the starting point of the selection), we tested the eventual green and red auto-fluorescence of the yeast strain. These are the two wavelength that we examined in FACS assays. As shown in Figure 4.3B, the strain does not show autofluorescence at both red (647 nm) and green (509 nm) wavelengths.

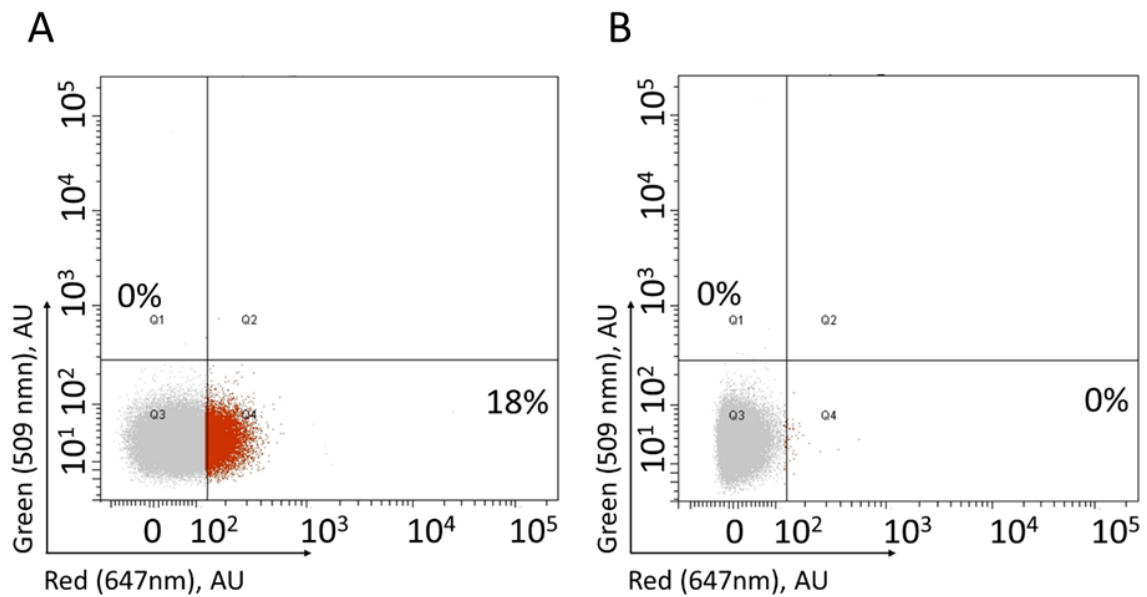



Figure 4.3. FACS analysis of the expression level of Nbs displayed by yeasts. **A.** FACS contour plot showing double gate signals (red in the x axis – 647 nm and green in the y axis – 509 nm) for yeast cells expressing Nbs on their cell wall. 18% of cells are red positive because they are displaying Nbs. Indeed, the red signal (647 nm) comes from the Alexa 647 dye conjugated to the anti-HA tag antibody used to decorate Nbs expressing yeast (see Figure 4.2B). The absence of green positive cells indicates that this yeast cells do not have autofluorescence in the green range of light (509 nm) under our experimental conditions. **B** FACS contour plot showing double gate signals (red and green) for yeast cells non-expressing nanobodies. The absence of double red and green positive cells confirms that the yeast strain employed does not show autofluorescence at both 647 and 509 and nm wavelengths under our experimental conditions. In both Panel A and B the fluorescence is expressed in arbitrary units (AU).

4.3.2 Selection procedure using iterative MACS and FACS

Nanobodies able to bind HCN4, possibly in a state dependent manner, i.e., open pore binders, were identified by combining two selection systems: Magnetic- and Fluorescent-Activated Cell Sorting (MACS and FACS respectively) (Figure 4.4). To do so, yeast cells expressing nanobodies on their surface were alternatively preincubated with detergent purified HCN4 molecules having the pore in the open state (hereafter HCN4_{OPEN}, positive selection) and with the closed pore (hereafter HCN4_{CLOSED}, negative selection). The latter



selection was performed by using MACS only. This was done because MACS is an iron bead-based low-cost cell separation technique (Miltenyi et al., 1990) that works with two different types of magnetic columns allowing for positive, but also for a very efficient negative selection. The two columns differ in shape and matrix, which define the flow rate of cells. For both positive and negative selections performed with MACS, the antigens were coated by iron-beads. It is worth noting that to label the antigens with the iron beads, it was necessary to use a double decoration (see the blue inlet of Figure 4.4). Antigens were first labelled with an antibody anti GFP conjugated with Alexa fluor 647. This was done because GFP is fused at the N-terminus of HCN4. The first antibody allows to decorate HCN4 with iron beads, since these are coated with anti-Alexa fluor 647 antibodies. In the positive selection, which was done with MACS, once the magnetic field was removed, the cells associated to HCN4_{OPEN} molecules elute from the column. On the contrary, the column for the negative selection was done in such a way that the flow rate of cells was significantly slowed down. This allows to retain with high efficiency also weakly labeled cells. Thus, all cells interacting with HCN4_{CLOSED} will be retained in the column. In this way these unwanted yeasts can be removed from the pool of cells interacting with HCN4_{OPEN}. In the negative selection the latter cells come out in the flowthrough of the column. It is worth noting that, given the complexity of the decoration with the iron beads, the purity/specificity of the selection of nanobodies is guaranteed by the application, at the beginning and at the end of the process, of negative selections performed with the following antigens: i) GFP tag; ii) a mix of iron beads and antibodies anti GFP conjugated with Alexa fluor 647.

For what concerns selection with FACS (only positive), the procedure was simpler. Indeed, we simply exposed the yeast cells to HCN4_{OPEN} and then sorted them by following the light emitted by the excited GFP fused to the channel.

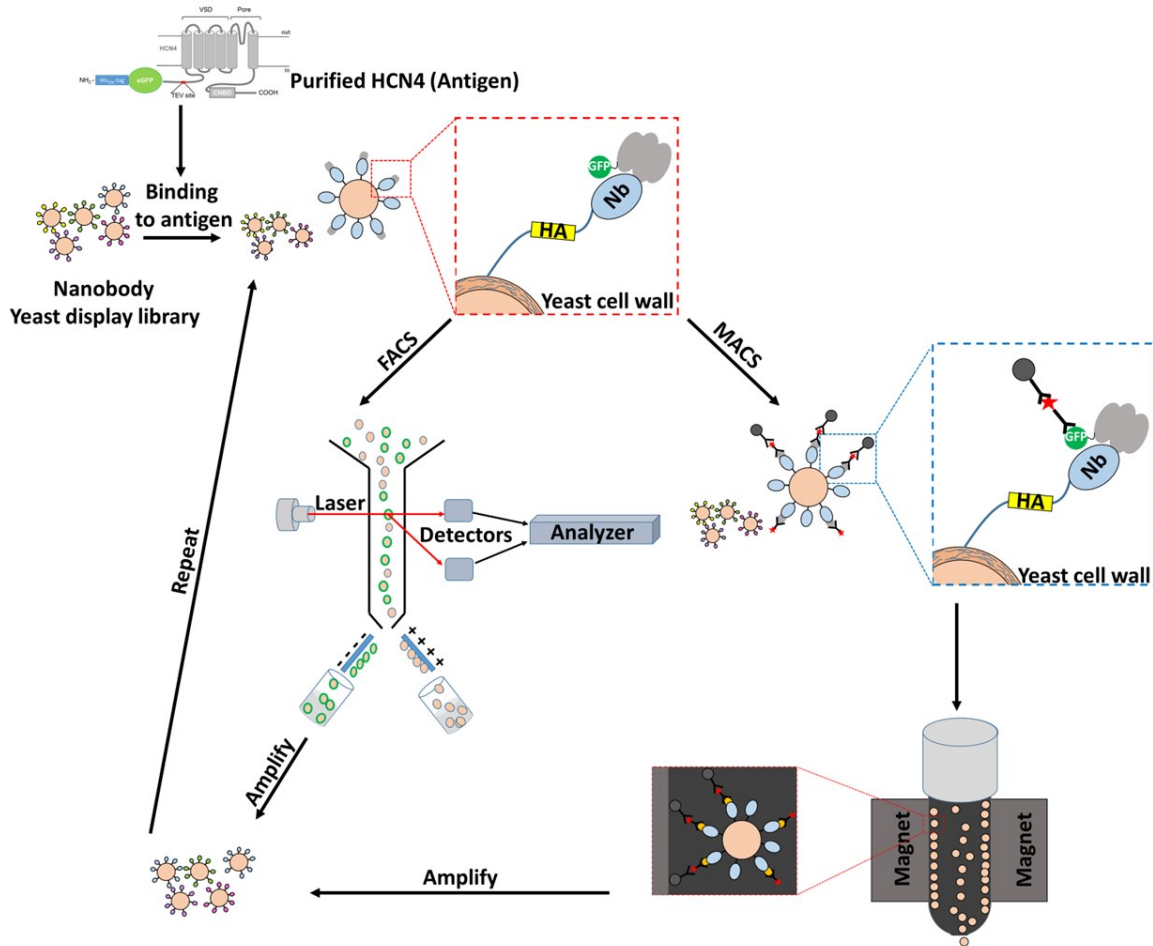



Figure 4.4. Schematic drawing of the nanobody selection process. The Yeast display nanobody library is exposed to the purified GFP-HCN4, used as antigen. In the red inlet GFP-HCN4 interacts with Nb expressed on the surface of yeast. Magnetic-Activated Cell Sorting (MACS) and Fluorescence-Activated Cell Sorting (FACS) are alternatively used to select the Nb binders to HCN4. The blue inlet is schematized the double immunodecoration need to perform MACS: 1) anti-GFP antibody conjugated with Alexa 647; 2) anti- Alexa 647 antibody conjugated with a magnetic microbead.

Figure 4.5 shows all steps of the process of nanobody selection described above. In summary, we have repeated two times the following scheme: Three steps of positive selection composed of two consecutive runs of MACS and one FACS (Figure 4.5A, red inlet, round 1 to 3). In the second repetition (two MACS + one FACS) the positive selections of MACS



was preceded by negative selection step (Figure 4.5A, blue inlet, round 4 to 6). As above stated, because of the double immunodecoration of HCN4 molecules for MACS, the process of nanobody selection was preceded and followed by the depletion of cells interacting with GFP tag, antibodies, and iron-beads (Figure 4.5A, green brackets). The process ended with a positive selection performed with MACS (round 7).

To monitor the enrichment of specific binders of HCN4_{OPEN} we performed analytical FACS of the key steps of the procedure of selection (Figure 4.5B). The naïve library displays a quite high percentage of cells able to interact with HCN4_{OPEN} (15%). This can be explained by the presence of a large GFP tag fused to the antigen. Also, the fact that HCN4 possesses large soluble N and C termini may add to this unspecific interaction. In agreement with the idea that multiple interactions contribute to this unspecific effect, the percentage of cells positive for HCN4 significantly decreases to 5%, but not to zero, after the depletion of binders of the GFP tag. The success of the enrichment of specific binders of HCN4_{OPEN} is demonstrated by the four-fold increase (19%) in the cells able to bind to HCN4_{OPEN} after the two runs of selection (two MACS + a FACS). Finally, the last positive selection (MACS, round 7 of Figure 4.5) almost duplicated (37%) the percentage of yeasts expressing nanobodies able to interact with HCN4_{OPEN}.

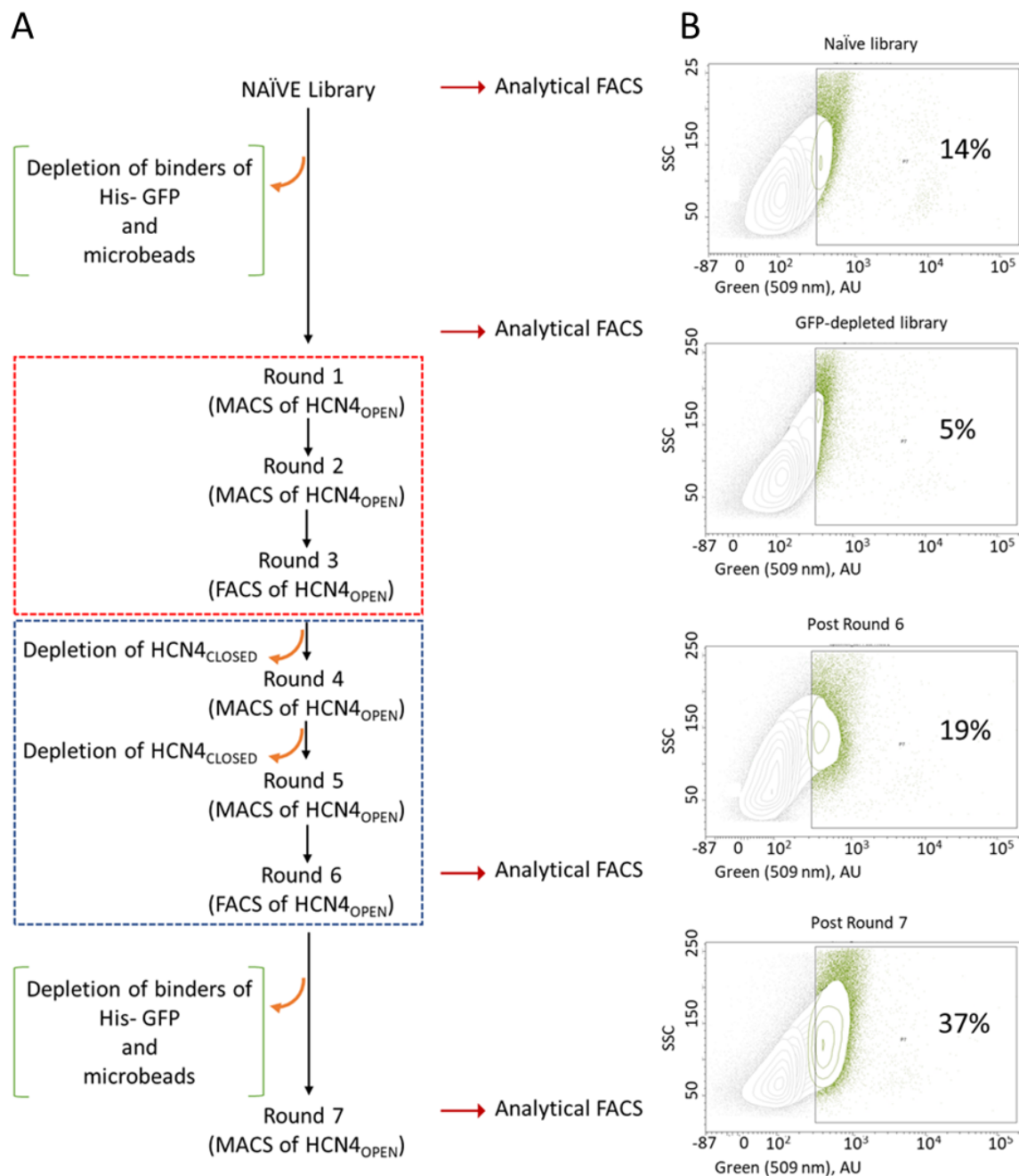



Figure 4.5. Summary of the selection procedure. **A.** The workflow of the selection for the isolation of conformationally state-dependent nanobodies. The naïve library is depleted from Nbs binding to GFP and microbeads prior to start with the selection (green brackets). The procedure of selection is formed by the double repetition of the following scheme: Three steps of positive selection composed by two consecutive MACS and a FACS (red inlet, round 1 to 3). In the second repetition (blue inlet, round 4 to 6) we preceded the positive selections of MACS with negative ones. Positive selections were

performed with purified HCN4 having the pore in the open state, while negative selections with purified HCN4 with the closed pore. Prior to conclude the entire procedure with a last positive selection (round 7), a second depletion of Nbs binding to GFP and microbeads was performed (green brackets). **B.** Analytical FACS to monitor the enrichment of the library. In the X axis there is side scatter (SSC) signal, while in the y axis the green fluorescence (509 nm) in arbitrary units (AU). Green positive cells are highlighted by a black square and colored in green. The first analytical FACS shows that 15% of the naïve library were able to interact with HCN4_{OPEN}. This fraction of cells was decreased to 5% after depleting the library from GFP and microbead binders. After six rounds of positive and negative selections the number of HCN4_{OPEN} binders increased by around four-fold (19%). After the last positive selection (round 7) this value almost duplicates (37%).

4.3.3 Isolation of clones

Following the last round of nanobody selection (see Figure 4.5), we proceeded with the sequencing of the isolated binders. To this end, we first seeded the yeast cells onto plates to obtain single colonies (for details, see mat and methods, section 4.2.5). Following the literature (Kanner et al., 2020; McMahon et al., 2018), we analyzed the plasmid DNA extracted from 100 clones. DNAs were first isolated from yeast and then amplified in *E. coli* to obtain it in a suitable and pure amount for sequencing (for details, see mat and methods, section 4.2.5). As reported in the literature (Xu et al., 2022) in an enriched library some clones are highly represented. Therefore, we sequenced 15 DNAs out of the 100 isolated to identify the ones over-represented. The sequencing results of the selected population (15% of the total one) indicated two sequences occurring with a frequency of 50% and 28.5%, respectively. The other clones were unique sequences. Based on these results, we developed a two-step fast-screening method to identify and consequently remove the two over-represented sequences. To do so, we performed two consecutive PCRs. The first with primers designed to anneal to the CDR1 and CDR3 variable regions of the sequence occurring with a frequency of 50%. All non-positive clones were subjected to a second round of PCR with primers specific for CDR1 and CDR3 variable regions of the sequence occurring with 28.5% frequency. In order to significantly increase the specificity of the screening, we identified stringent conditions for both PCRs (for details, see mat and methods, section 4.2.6). PCR results were analyzed by agarose gel electrophoresis to detect the presence of the band of interest (see Figure 4.6A as



an example). In agreement with the percentage of occurrence of the clones in the small screening (15% of the entire population), 42% and 25% sequences were identical to the over-represented ones and thus discarded. The sequencing of the remaining candidates revealed that we were able to isolate ten unique nanobodies (hereafter Nb), most likely able to bind to HCN4_{OPEN}: Nb1, Nb3, Nb5, Nb6, Nb11, Nb19, Nb34, Nb60, Nb66, Nb68. Figure 4.6B reports the sequence alignment of the ten unique Nbs. As expected, they share four conserved framework regions (highlighted in blue) and differ in complementarity-determining loops (CDR1-3), both in length and residue identity. The highest degree of variability is located in CDR1 and CDR3. Table 4.1 shows the percentage of occurrence of the ten Nbs.

Each Nb was expressed in *E. coli*, from which the protein was purified and resuspended in a saline buffer for electrophysiological experiments.

Nanobodies	Representativeness (%)
Nb 1	42
Nb 5	25
Nb 3	15
Nb 11	5
Nb 68	4
Nb 60	3
Nb 6	2
Nb 34	2
Nb 19	1
Nb 66	1

Table 4.1. The ten unique Nbs ordered based on their representativeness.

4.3.4 Expression and purification of nanobodies for functional studies

The ultimate goal of the present work is the identification of Nbs targeting HCN4 with the potentiality of isolating an isotype-specific block of the pore, or to find Nbs which modulate the channel's voltage dependency. To test whether the ten nanobodies selected possess these features, we set a procedure for their expression in bacteria, and subsequent purification with the goal of employing the isolated Nbs in electrophysiological assays.

To this end, each of the ten unique cDNAs encoding for the selected Nbs was inserted into a vector for their expression in the periplasm of bacteria (for details, see material and methods, 4.2.7). This is important for the correct folding of Nb, as they have a disulfide bond whose formation is crucial (Billen et al., 2017; Kariuki & Magez, 2021). Indeed, the periplasm possesses an oxidizing environment, which favor the formation of the disulfide bond.

The extraction of the proteins from the periplasm was performed according to the protocol described in the material and methods, section 4.2.8. Subsequently, taking advantage of a hexa-histidine tag fused at the C-terminus of the Nbs (for details, see material and methods, section 4.2.7), we performed an affinity chromatography using a nickel resin (Figure 4.7A). Nbs eluted from the nickel resin were further subjected to a second purification step, the size exclusion chromatography (SEC), which allows separation of proteins based on the size of particles. The latter purification was performed to monitor the stability of the

purified protein. Unstable proteins tend to aggregate, and the occurrence of this phenomenon can be visualized in SEC. Indeed, aggregated proteins form the large macromolecular complexes, which elute in the void volume of the SEC column (for the purification details, see material and methods, section 4.2.8). Figure 4.7B shows a representative SEC profile of a nickel-purified Nb. None of the ten Nbs purified display aggregation; all of them exhibit a rather single monodisperse peak eluting at a volume consistent with the expected molecular weight (MW) of a folded protein (17 KDa). It should be mentioned that the assignment of a MW to the elution peak was possible because molecular weight markers were previously run to calibrate the SEC column. Coomassie-stained denaturing gels (SDS-PAGE) of the pooled fractions of the peak and related western blots performed with an antibody anti His tag further validate the purity of the samples (Figure 4.7C). Seven Nbs out of the ten purified Nbs show a mean yield of 6 mg per liter of bacterial culture, while three of them displayed a significantly lower yield. The ca. four-fold reduced yield was due to a significant lower expression of these three candidates.

Finally, we tested whether the purified Nbs could sustain a freezing/thawing procedure consisting of a freezing step at -80°C and subsequent de-freezing at room temperature. This test was performed to establish whether we could store the purified Nbs, a step which could favor their use in electrophysiology. Altogether this would allow to parallelize the process of production/purification with various functional assays. It is worth noting that the Nbs' solution contains glycerol, a known cryo-protectant which favors the stability of purified protein. To test Nb stability, after the de-freezing step from -80°C we ran equal amounts of freshly purified and thawed protein on an analytical SEC. Figure 4.8 shows a representative example of the stability test. The black line corresponds to a SEC chromatogram of a freshly purified Nb, while the red line represents the SEC chromatogram from the same amount of de-frozen protein. Since for all purified Nbs the two SEC profiles were identical, we concluded that the ten proteins can sustain without damage a freezing (-80°C)/thawing cycle.

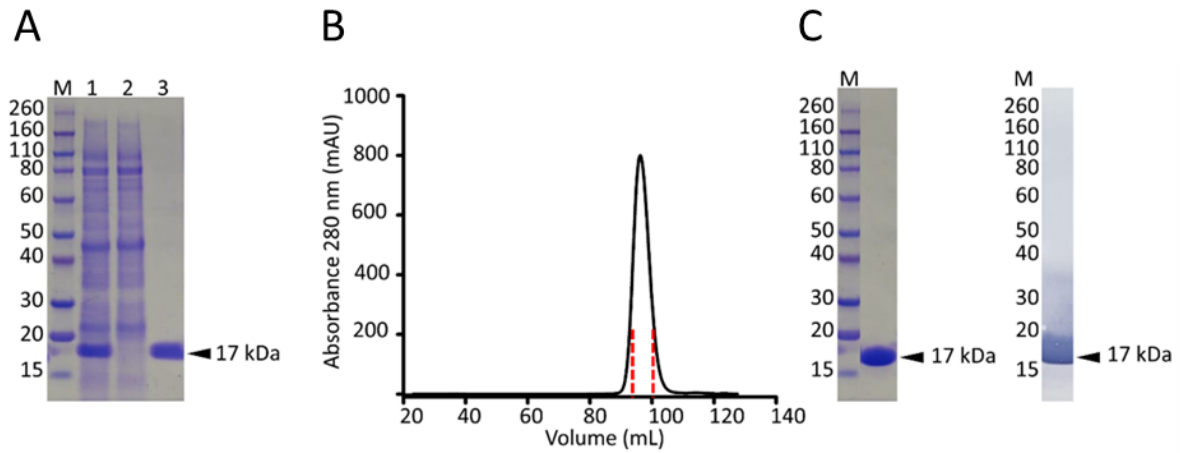


Figure 4.7. Purification of Nb. **A.** A representative coomassie-stained SDS-PAGE gel summarizing all steps of the affinity chromatography (Ni^{2+} -column) used to isolate Nbs from the *E. coli* lysate thanks to the His-tag fused at their C-terminus: Markers (M), clarified *E. coli* lysate before the incubation with the Ni^{2+} -resin (lane 1), flow through (lane 2), and elution of the Ni^{2+} -resin (lane 3). **B.** Representative size exclusion chromatography (SEC) of a Nb following affinity chromatography. The pooled peak fractions are delimited by the red lines. **C.** Left, a representative coomassie-stained SDS-PAGE gel of the pooled SEC fractions (Panel B), and (right) the related western blot performed by using the anti His-tag antibody as a primary antibody.

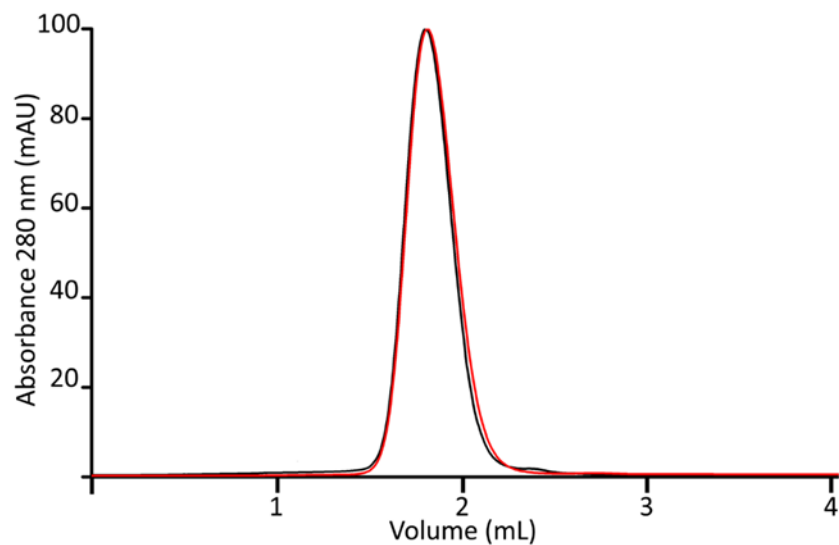


Figure 4.8. Stability test of the purified Nbs. Superimposition of the analytical SEC chromatograms of a freshly purified Nb (black), and the same amount of the de-frozen one (red).

4.3.5 Functional characterization of nanobodies in HEK293T cells

4.3.5.1 Effect of nanobodies from the extracellular side

The ten purified Nbs were tested in electrophysiological assays. Briefly, cDNA encoding for either of the three channels HCN4, HCN1, or hERG (the latter channel was used as a control of the specificity of Nbs for HCN channels) was co-transfected with GFP in HEK293T cells. Patch clamp experiments in the whole cell mode were performed 24 hours after transfection on GFP-positive cells according to the protocol previously published (Porro et al., 2019; Saponaro et al., 2018; Saponaro, Bauer, et al., 2021). We performed two consecutive electrophysiological screenings with HCN4-expressing cells. In the first assay channel currents were recorded and Nbs added during the measurements to the extracellular solution. This allowed us to select Nbs acting from the extracellular side. The Nbs not displaying effects in this assay on HCN4 currents were further subjected to a second screening. In this case they were added via the pipette to the intracellular solution.

It is worth noting that a desirable Nb with very high affinity should have a low nanomolar or even picomolar equilibrium dissociation constant (K_D). An acceptable affinity range for future in vivo applications should be in the low micromolar to nanomolar concentration window (Debie et al., 2020). Nonetheless, for the initial screening of Nb candidates, we decided to use a quite high concentration (20 μ M) because we were interested in highlighting any eventual effects on HCN4 currents.

Although our initial purpose was to find Nbs which are able to block HCN4 currents, we realized that our isolated proteins were not reducing the current. Instead, they were either having no effect (Nb19, Nb34, Nb68) or they altered the voltage dependency of the HCN4 channel (Nb1, Nb3, Nb5, Nb6, Nb11, Nb60, Nb66). Figure 4.9 shows a representative recording of HCN4 currents in the absence (panel A, left) and the presence of Nb5 in the external medium (panel A, right). The individual examples as well as the detailed analysis of a large number of cells shows that the Nb5 causes a significant right shift of the channel activation curve without any appreciable impact on the steepness of the curve (Panel B). The voltage for half maximal activation shifts after addition of the Nb from -104.8 ± 0.8 mV to -95.7 ± 0.9 mV (Panel C).

The same assay and analysis were performed for all candidate NBs and Table 4.2 summarizes the electrophysiological effects observed. When applied to the extracellular solution, Nb3, Nb5, Nb6, Nb11, Nb60 and Nb66 affected the voltage dependency of HCN4 by shifting the activation curve toward more positive potentials. The extent of the shift is reported in Table 4.2, and it is measured as a difference between the half activation potential ($V_{1/2}$) values as in Figure 4.9 from currents recorded in the presence and in the absence of Nbs, respectively. Based on these results, we can conclude that these Nbs act as agonists of the HCN4 channel because they increase the voltage-dependent gating of this channel.

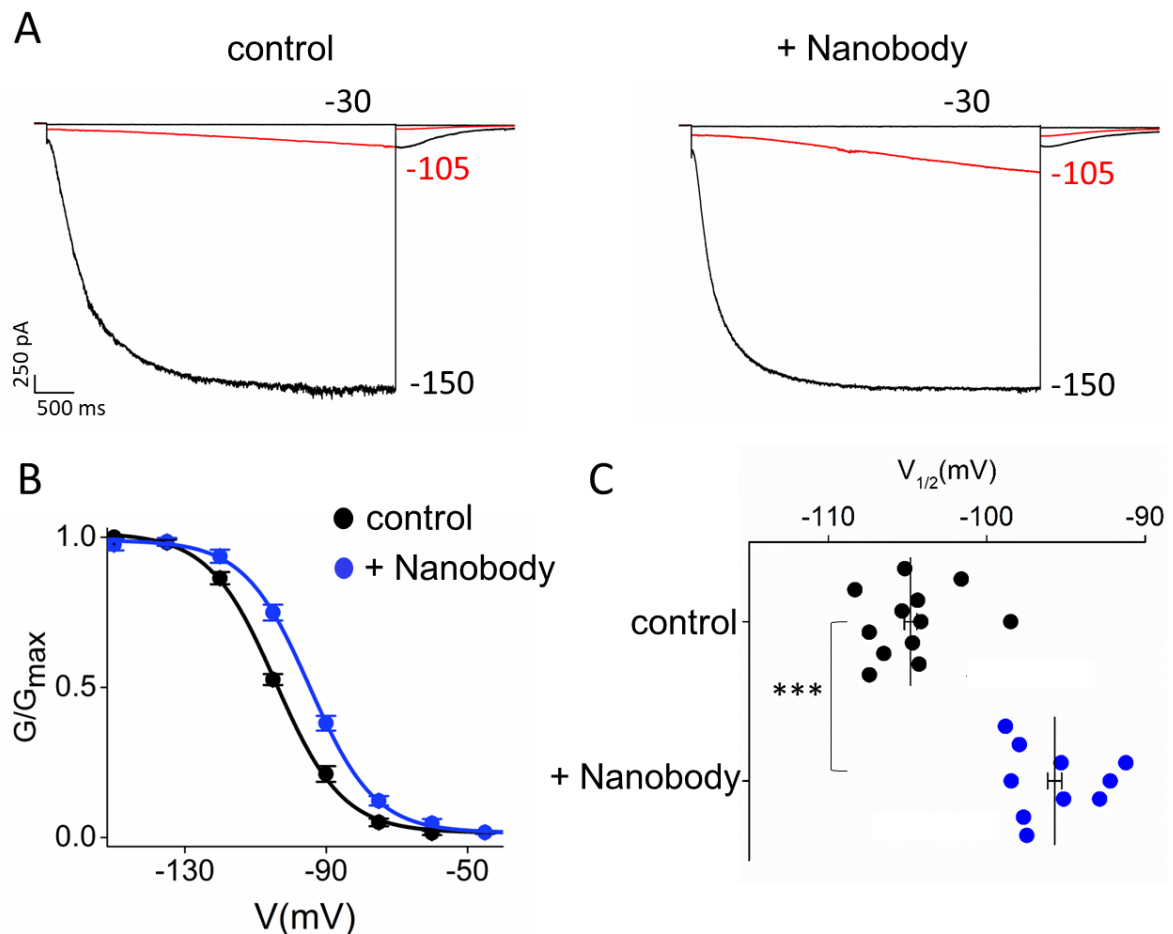


Figure 4.9. Example of modulation of HCN4 current due to a nanobody added from the extracellular side. A. Representative whole-cell HCN4 wt currents recorded, at the indicated voltages, in control solution (left), or pre-treated (right) with 20 μ M nanobody in the extracellular recording solution. **B.** Mean activation curves without (black) and with (blue) nanobody. Lines show data fit to a Boltzmann

function. **C.** Mean $V_{1/2}$ values without (black) and with (blue) nanobody. Data are presented as mean \pm SEM. Number of experiments \geq 10. Statistical analysis performed with T student test (***) $p < 0.001$.

	HCN4-EXTRA	HCN4-INTRA	HCN1-EXTRA	hERG-EXTRA
Nb1		11.1 \pm 1.4 mV	-----	-----
Nb3	8.5 \pm 2mV	-----		-----
Nb5 (20 μ M)	9.1 \pm 1.2 mV	-----		-----
Nb5 (2 μ M)	9.5 \pm 1.5 mV	-----		-----
Nb6	6.8 \pm 1.6 mV	-----	8.4 \pm 1.7 mV	
Nb11	8.7 \pm 1.2 mV	-----	7.3 \pm 1.9 mV	
Nb19			-----	-----
Nb34			-----	-----
Nb60	3.3 \pm 1.3 mV	-----	3.3 \pm 1.2 mV	
Nb66	13.4 \pm 2.9 mV	-----	3.1 \pm 1.2 mV	5.4 \pm 1.1 mV
Nb68			-----	-----

Table 4.2. Summarizing the electrophysiological effects, depolarizing shift in the voltage-dependent opening, exerted by Nbs on HCN4, HCN1 and REG channels. This effect is measured as a Nb-induced shift (mV) on half activation voltages ($V_{1/2}$) calculated as a difference between the value derived from recordings in control conditions and in the presence of 20 μ M Nbs. $V_{1/2}$ values are derived from the fitting with a Boltzmann equation of the tail current amplitudes, plotted against the preconditioning voltages. The red boxes indicate that we did not measure alteration in the $V_{1/2}$ values of HCN current upon Nb addition. In the dark green boxes are reported the shifts on $V_{1/2}$ induced by 20 μ M Nbs. The light green box reports the Nb5-induced shifts on $V_{1/2}$ in the presence of 2 μ M Nb (a ten-time lower concentration compared to the standard one used for all Nbs). Data are presented as mean \pm SEM. Number of experiments \geq 8. Dotted black lines in the white boxes indicate that the condition describing a given column was not tested. Nbs were first tested on HCN4 extracellularly (first column). Those not causing effects on HCN4 current were further tested intracellularly (second column). To

check for the isotype specificity, Nbs were tested on HCN1 (third column) and to hERG, an HCN cognate channel (fourth column).

To broaden our characterization, we assessed a potential HCN isotype-specificity of the Nbs by testing each nanobody also on the HCN1 subtype. Treatment with Nb6, Nb11, Nb60 and Nb66 caused in the same type of assay as in Figure 4.9 a right shift of the HCN1 activation curve. The extent of the effect is reposted in table 4.2. Conversely, treatment with Nb3, Nb5 did not produce any significant effect on the voltage dependency of HCN1, thus making them the only HCN4-specific binders among the Nbs isolated.

Based on these promising results on an HCN4 isoform specificity and on the fact that the yield of purification of Nb5 is significantly higher than that of Nb3, we further characterized the effect of Nb5 at a ten-fold lower concentration (from 20 μ M to 2 μ M) to determine its potentiality as drug. As shown in Table 4.2, the application of 2 μ M Nb5 to the extracellular medium caused the same positive shift of the voltage dependent activation curve of HCN4 that was previously measured at 20 μ M (for a comparison, see Table 4.2). This indicates that 2 μ M can already be considered a saturating concentration and suggests that Nb5 affinity might be in the nanomolar range.

To assess affinity for Nb5 binding, we calculated the K_D of Nb5 for HCN4 by using microscale thermophoresis (MST). MST is a fluorescence-based technique used to visualize and quantify ligand/ receptor interactions in solution (Jerabek-Willemsen et al., 2014; Stinn et al., 2021). Briefly, MST is based on the thermophoresis-dependent depletion of a fluorescently labelled receptor induced by a temperature gradient. This temperature-dependent movement of the receptor can be affected by changes in its size, charge, hydration shell, or conformation caused by the interaction with the ligand. To induce the movement of the receptor, a microscopic temperature gradient ranging from 2–6 °C in a μ l-volume (the diameter of the affected area is about 50 μ m) is induced by an infrared laser (1480 nm) focused through an objective into a glass capillary containing the binding partners (Figure 4.10A). MST monitors the thermophoresis dependent depletion of the fluorescently labeled receptor within the heated area (Figure 4.10B). To do so, fluorophores within this area are excited and their emitted light is collected (Figure 4.10A). In details, the technique requires

to load several capillaries with a constant concentration of the fluorescently labelled receptor, while the concentration of the ligand increases progressively. The system consecutively scans the capillaries to monitor the ligand-dependent changes in the thermophoresis of the fluorescently labelled receptor (Figure 4.10C). These changes, normalized to the fluorescence before the application of the temperature gradient and plotted as a function of ligand concentration, yield a binding curve. From the latter the equilibrium dissociation constant (K_D) is derived (the inflection point of the curve) (figure 4.10D).

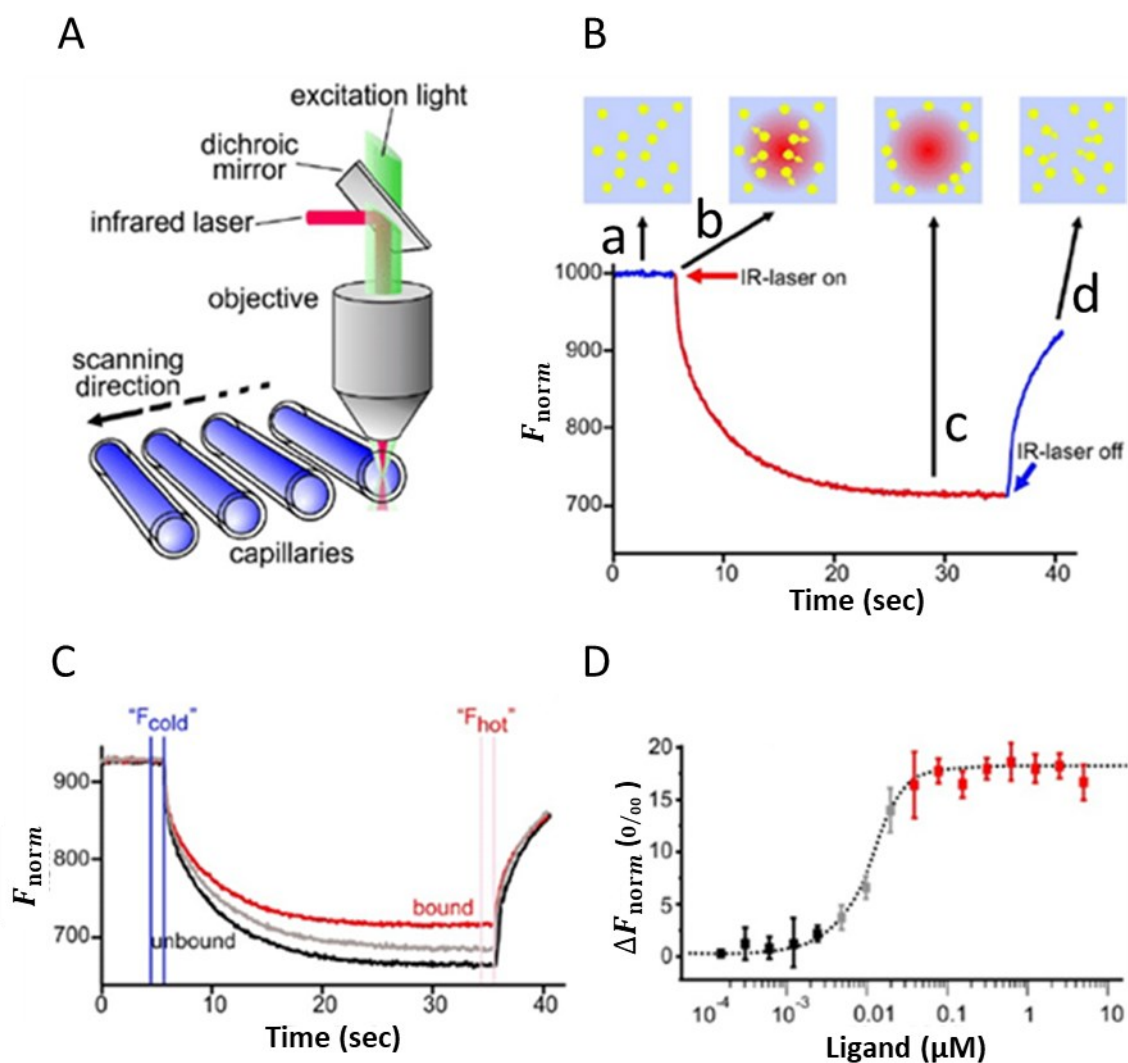



Figure 4.10. MST experiment. **A.** Schematic representation of MST optics. The fluorescence inside the capillaries is excited through the objective. The emitted light is collected using the same object. A



dedicated IR laser used to produce a microscopic temperature gradient to heat the samples. **B.** Thermophoretic movement of molecules from the locally heated region to the outer cold region which reduced the local concentration of molecules. The molecules diffuse back when the laser is returned off. The time dependent fluorescence is recorded by the system. The black arrowheads corresponded to the a) initial fluorescence recorded by the MST; b) change in fluorescence property because of jumping in the temperature; c) steady state in which the fluorescence intensity reaches a plateau; d) back-diffusion in which the molecules back diffuse after laser turns off. **C.** Typical binding experiment showing different MST traces: black trace “unbound” and the red trace “bound” state. **D.** The binding curve is obtained by plotting the change in thermophoresis which is expressed as the change in the normalized fluorescence ($F_{\text{hot}}/F_{\text{cold}}$, where F-values correspond to average fluorescence values between defined areas marked by the red and blue cursors, respectively), over the titration of nonfluorescent ligand (μM). From the binding curve it is possible to derive the equilibrium dissociation constant (K_D), the inflection point of the curve. The figure is adapted from Jerabek-Willemsen et al., 2014.

In our case, the receptor was Nb5. To label it, we used Red-tris-NTA dye. This molecule consists of an NT647 dye covalently bound to a three nitrilotriacetic (NTA) acids (Figure 4.11A). NTA is a potent chelator of divalent cations, specially Ni^{2+} ions. This allows Red-tris-NTA dye to bind with high affinity to His-tags (Figure 4.11B) (Bartoschik et al., 2018). We were choosing this dye because our Nbs possess a His_{x6} -tag fused at their C-terminus, far from the CDR loops, the antigen binding area (for details, see the material and methods, section 4.2.7). Therefore, by labelling Nbs at their C-terminus, we should avoid any disturbance of the dye to the Nb5/HCN4 interaction. It is also worth noting that we employed the red version of the dye as HCN4 possesses a GFP-tag (Saponaro, Bauer, et al., 2021; Saponaro, Sharifzadeh, et al., 2021).

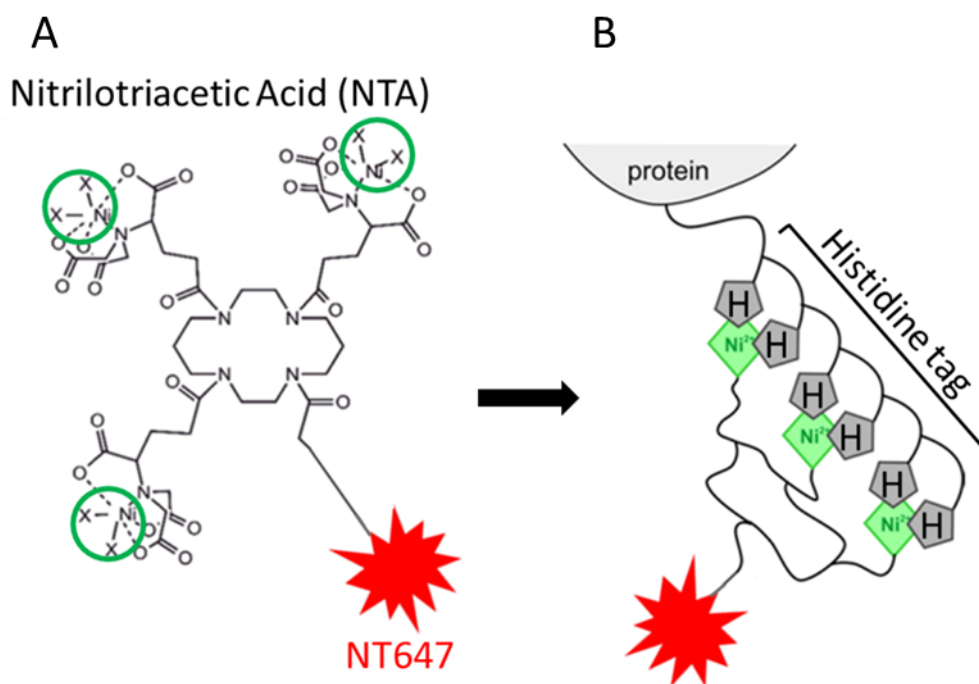


Figure 4.11. Labeling of His-tagged proteins using the RED-tris-NTA dye. **A.** Chemical structure of the tris-Nitrilotriacetic (NTA) acid moiety. In the green circles are highlighted the Ni^{2+} ions coordinated by NTA. NT647 (represented as a red star) is covalently conjugated to NTA via a linker. **B.** Schematic representation of RED-tris-NTA dye bound to a His-tagged protein. Ni^{2+} ions chelated by the three NTA groups allows the dye to tightly interact with the imidazole groups of the side chains of the histidine residues of His-tag. The figure is modified from Bartoschik et al., 2018.

The first step was to identify the optimal condition of Nb labelling, which may vary depending on the position of the His-tag and thus on its exposition to the solvent (Bartoschik et al., 2018). To test whether we could efficiently label Nb5 with Red-His-NTA dye, we performed an MST to calculate the K_D of Red-His-NTA dye for purified Nb5. Indeed, for K_D values below 50nM the labelling is considered possible with high efficiency (Lata et al., 2005). Figure 4.12 shows the MST of RED-tris-NTA binding to Nb5. We prepared 16 capillaries containing RED-tris-NTA at a constant concentration of 50 nM, while the concentration of Nb5 was ranging from 76.3 pM to 2.5 μM . Panel A shows the traces of RED-tris-NTA fluorescence in the presence of increasing concentration of Nb5. Panel B shows the mean normalized fluorescence values as a function of the Nb5 concentration, from which we could derive a K_D of RED-tris-NTA dye for Nb5 of 1.1 ± 1.3 nM (value plus the error associated to the fitting

of the data). This let us conclude that RED-tris-NTA dye efficiently labels Nb5. Since Nbs differ only in the CDR loops 1-3, which in the quaternary structure are far from the C-terminus where the His-tag is fused, we further concluded that the dye could label in a likewise efficient manner also the other Nbs.

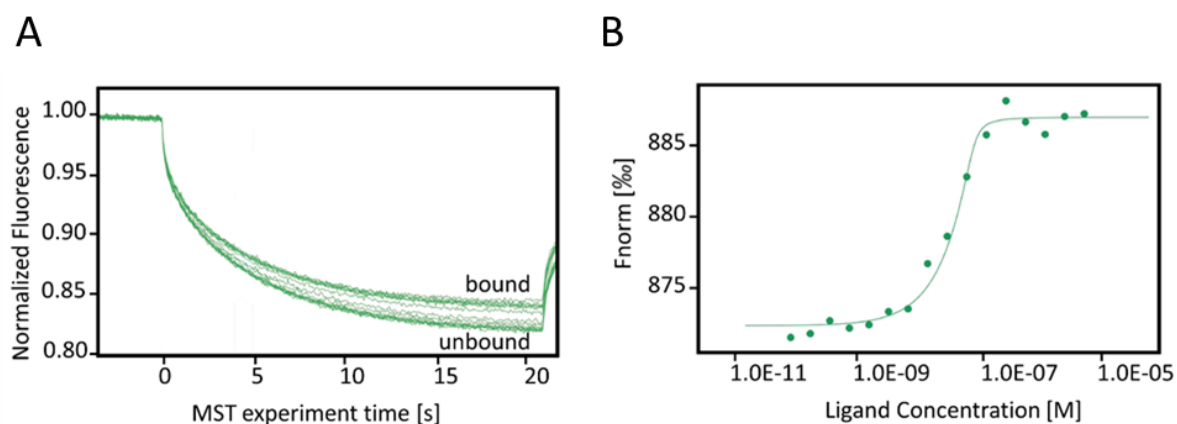


Figure 4.12. MST binding assay of the RED-tris-NTA dye to Nb5. **A.** The MST traces show a progressive decrease on the rate of the temperature-dependent decay of the fluorescence of Red-tris-NTA dye (the receptor) due to a concomitant progressive increase in the Nb5 (the ligand) concentration. **B.** Plotting of the Nb5-dependent thermophoretic changes of RED-tris-NTA dye, expressed as the change in its normalized fluorescence (see Figure 4.10). Data were fitted using the KD model; from which we could derive an equilibrium dissociation constant K_D of 1.1 ± 1.3 nM (the error is derived from the fitting).

Having determined that the RED-tris-NTA can be used to label Nb5, we used the RED-tris-NTA labelled Nb5 (hereafter RED-Nb5) to measure its affinity for the HCN4 protein. It is worth noting that, since Nb5 was selected to bind specifically to HCN4_{OPEN}, the channel was purified to be kept it in this state (Saponaro, Bauer, et al., 2021). We prepared 16 capillaries containing a constant concentration of RED-Nb5 (50 nM), while the concentration of HCN4_{OPEN} was ranging from 30 pM to 1 μ M. Figure 4.13 shows representative MST traces (panel A) and the mean binding curve (panel B), which is the result of three independent experiments. The calculated K_D of Nb5 to HCN4_{OPEN} is 37 nM \pm 3.4 nM. The affinity in the low nanomolar range agrees with the electrophysiological experiments showing that already 2 μ M Nb5 (a tenfold decrease in the concentration respect to the one used for the screening

reported in Table 4.2) caused a full potentiation of the voltage dependent opening of HCN4. Strikingly, Nb5 displays an affinity for its target HCN4 which is considered good for in vivo applications (Debie et al., 2020).

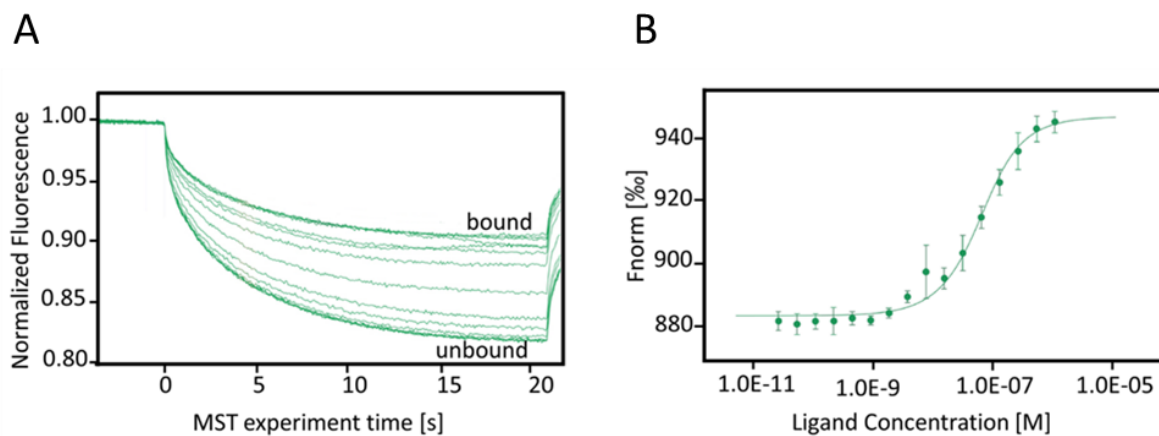



Figure 4.13. MST binding assay of the RED-Nb5 to HCN4_{OPEN}. **A.** The MST traces show a progressive decrease on the rate of the temperature-dependent decay of the RED-Nb5 (the receptor) due to a concomitant progressive increase in the HCN4_{OPEN} (the ligand) concentration. **B.** Plotting of the HCN4_{OPEN}-dependent thermophoretic changes of RED-Nb5, expressed as the change in its normalized fluorescence (see Figure 4.10). Data were fitted using the KD model; from which we could derive an equilibrium dissociation constant K_D of $37 \text{ nM} \pm 3.4 \text{ nM}$. Data are presented as mean \pm SEM. Number of experiments = 3.

Based on these promising results, we tested Nb5 on an HCN4 mutation (K531N following the numbering of our construct, for details, see Saponaro, Bauer, et al., 2021) found in heterozygous form in a bradycardic patient. The pathological state of the patient was most likely caused by a mutant-dependent hyperpolarizing shift in the voltage dependency of HCN4 (Duhme et al., 2013). We reasoned that the Nb5 evoked depolarizing shift of channel activation (see Table 4.2) may rescue this pathological phenotype. For the experimental testing of this hypothesis, we mimicked the heterozygous condition of the patient by co-transfecting HEK293 cells with equal amounts of DNA for wt and K531N HCN4. The data in Figure 4.14 show that the mutation induces in this scenario a significant hyperpolarization in the voltage dependency of the current. This effect is completely rescued by the external



application of 0.2 μM Nb5. At this point it should be mentioned that we used a significantly lower concentration of Nb5 (tenfold less compared to the saturating concentration used with the wt) to revert the pathological phenotype. This is because 2 μM Nb5 was shifting the activation curve toward depolarized potentials which even exceed the value measured for the wt HCN4 in the control.

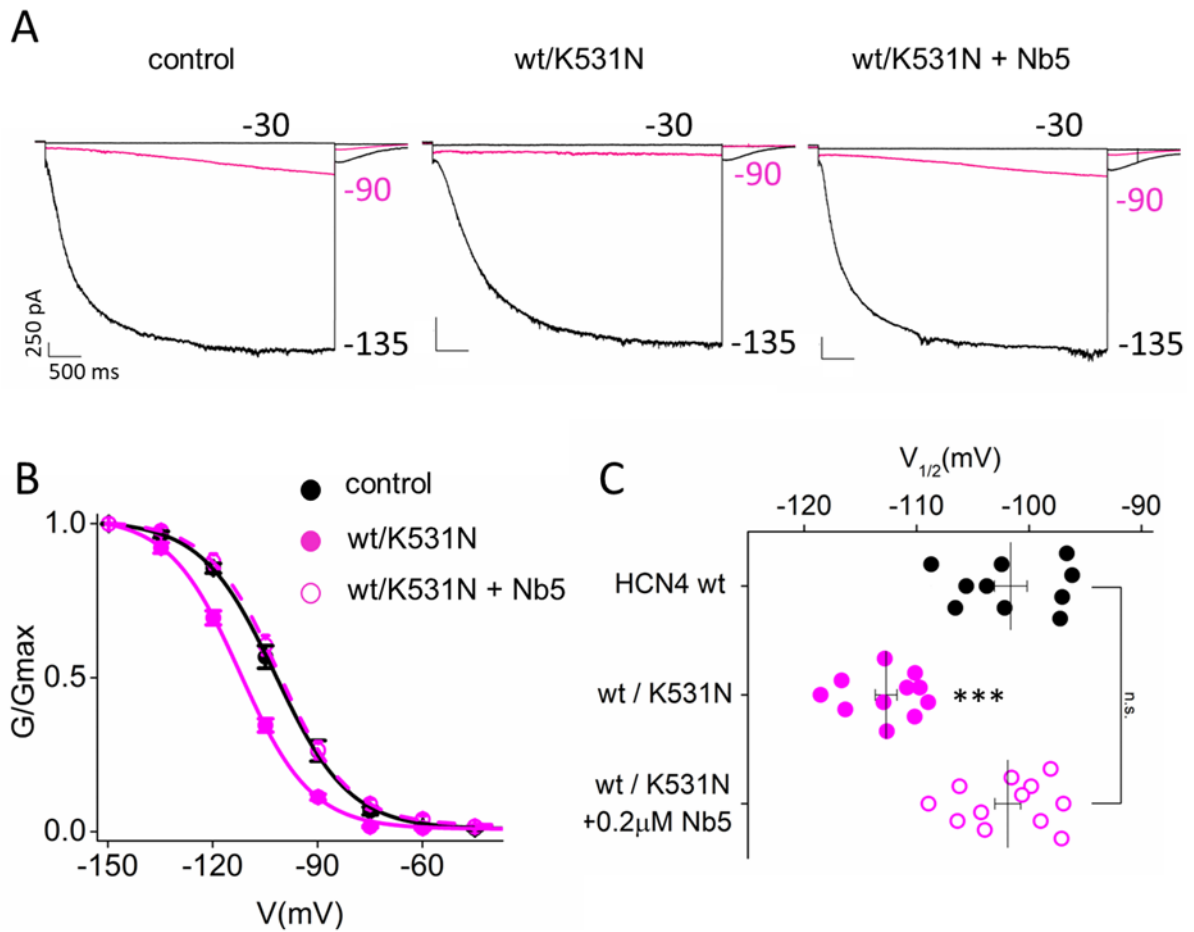


Figure 4.14. Nb5 rescues the pathological effect of a HCN4 mutation found in a bradycardic patient.

A. Representative whole-cell currents, at the indicated voltages, of HCN4 wt homozygous (left, control) and of wt/K531N heterozygous mutant (the condition of the patient) in control solution (center), or pre-treated (right) with 0.2 μ M Nb5 in the extracellular recording solution. **B.** Mean activation curves of HCN4 wt homozygous (black circles, control), wt/K531N heterozygous (magenta filled circles) and wt/K531N heterozygous pre-treated with Nb5 (magenta open circles). Lines show data fit to a Boltzmann function. **C.** Mean $V_{1/2}$ values of HCN4 wt homozygous (black circles, control), wt/K531N heterozygous (magenta filled circles) and wt/K531N heterozygous pre-treated with Nb5 (magenta open circles). Data are presented as mean \pm SEM. Number of experiments \geq 10. Statistical analysis performed with one-way ANOVA, followed by Fisher's test (*** P < 0.001).

In summary, Nb5 has demonstrated to be a promising candidate for future pharmacological applications. To this end, another possible application could be in the treatment of Sinus Node Dysfunction (SND), a type of heart rhythm disorder, which affects

the pacemaker of the heart (sinus node). SND has been associated with a deficit in the I_f current, whose molecular determinant is HCN4. The ability of Nb5 to bind to and positively regulate the voltage dependence opening of HCN4 could be employed to compensate for the partial loss of I_f manifested in several patients displaying SND (Nof et al., 2010).

To understand if Nb6, Nb11, Nb60 and Nb66, which did not discriminate among HCN subtypes (see Table 4.2), were at least selective for channel of the HCN family, we decided to test them on the cardiac hERG channel. hERG is a voltage gated delayed K^+ channel rectifier; it contains six transmembrane domains (S1-S6) with S1-S4 contributing to the voltage sensor domain (VSD) and S5-S6 to the pore-forming unit; the protein assembles to form a tetramer with a central ion conducting pore and the C-terminus contains a cyclic nucleotide binding domain (CNBD). hERG channels share a great degree of homology with HCN channels, even when considering only the pore region (Vandenberg et al., 2012). The hERG channel is known to be widely used for the assessment of proarrhythmic risk of new drugs; blockers obstruct channel functions through different mechanisms, which usually show time-, voltage- and state-dependence (Yao et al., 2005). Because of its characteristics, we were choosing the hERG channel to test our nanobodies for specificity. Nb6, Nb11 and Nb60 do not have any functional effect neither on the activation curve of the channel nor on the total current. Differently, Nb66 causes a shift of the activation curve towards more depolarized potentials, whose value is reported in table 4.2. Given its poor specificity, and since both HCN and hERG channels are co-expressed in the heart, we excluded the use of Nb66 as a possible therapeutic agent and, therefore, we decided not to further investigate its properties.

Of the three Nbs (6, 11 and 60) specific for HCN channels (see Table 4.2), we excluded from further investigations Nb60 because of its modest effect on both HCN1 and HCN4 (see Table 4.2). Instead, Nb6 and 11 show similar robust effects on both HCN1 and HCN4 (see Table 4.2). Nonetheless, since Nb11 displays a low yield of purification, we consider Nb6 the best candidate as a binder of HCN channel family members. Nb6 will be then subjected to further biochemical and functional studies we have done for Nb5.

4.3.5.2 Effect of nanobodies from the intracellular side

Since Nb1, Nb19, Nb34, and Nb68 were not affecting HCN4 currents when applied extracellularly, we further tested them in the intracellular solution. In this condition, only Nb1

affected HCN4 current by causing a depolarizing shift in the voltage dependency of HCN4 (see Table 3.2). Therefore, Nb1 seems to target the intracellular machinery of the channel.

In summary, the seven Nbs which generate either from the extracellular or intracellular side an effect on HCN currents, all cause a depolarizing shift in the voltage dependent opening (see Table 4.2). The same type of positive shift in HCN channel activation is generated by the second messenger cAMP (Robinson & Siegelbaum, 2003; Wahl-Schott & Biel, 2009). Even though none of the Nbs fully recapitulates the agonistic effect of cAMP (see Table 4.2), the convergence of the effect, e.g., a depolarization in the voltage dependency of HCN, caused by both Nbs and the ligand fosters the speculation that Nbs may act on the same molecular mechanism controlled by cAMP. Such a mechanism could be easily understood in the case of Nb1, which acts from the intracellular side, e.g., the side on which the cAMP binding site is located. The same explanation for an action of the remaining Nbs, which act from the extracellular side is less obvious. Nonetheless, it is reasonable to think that also these Nbs could in principle also modulate the cAMP pathway. Indeed, it is known that the transmembrane and the cytosolic regions are interacting in HCN channels (Saponaro, Bauer, et al., 2021); there is good evidence for reciprocal influence between the VSD and the cytosolic cAMP pathway (Chen et al., 2007; Kusch et al., 2010; Porro et al., 2019; Thon et al., 2015; S. Wu et al., 2011). In this light, future studies will be conducted to define the pathway of action of Nb5 (the HCN4-specific binder), Nb6 (the specific binder of HCN channels family members) and Nb1 (the unique intracellular binder), exploring the hypothesis of a possible convergence of the Nbs on the cAMP signaling. These studies will include: i) crosslinking experiments between HCN4 and NBs followed by mass spectrometry analysis to identify the Nb binding site on the channel; ii) electrophysiological recordings with cAMP to clarify whether the three Nbs act on the regulatory pathway controlled by the ligand.

4.3.6 Monitoring the interaction of Nb19, 34 and 68 with HCN4 using biochemical assays

Lastly, for what concerns Nb19, Nb34, and Nb68, for which we did not see any electrophysiological effects (see Table 4.2), we performed a biochemical validation of their ability to binding to HCN4. To this end, we employed MST. In their case, we did not obtain of a full binding curve as in the case of Nb5 (see Figure 4.13). Instead, we employed a faster MST protocol, typically used to screen for ligand binding to a target receptor: In this so-called

binding check assay only two conditions are used: The fluorescently labelled receptor alone and in the presence of an excess of ligand. To this end, we first labelled Nb19, Nb34, and Nb68 with RED-tris-NTA dye thanks to their C-terminal His-tag as previously done with Nb5 (for details, see material and methods, section 4.2.12). We then used the labelled nanobodies as receptors of the assay at a concentration of 50 nM; the concentration of HCN4_{OPEN} as ligand was 1 μ M, the highest concentration used in the binding test with Nb5 (see Figure 4.13). The conditions were chosen in order to assure an excess of ligand for saturating the receptor. The Nb5 was used as a positive control in the assay. Figure 4.15A shows two sets of MST traces corresponding to the labelled Nbs alone (marked as Unbound) and in the presence of an excess of HCN4_{OPEN} (marked as Bound). The analysis of these traces generates two homogeneous sets of data (panel B). In the case of Nb5 (the control), as expected, an excess of HCN4_{OPEN} induces a significant increase in the fluorescence, which is a sign of a decrease in the mobility of Nb5 due to its binding to the partner. The fold of increase in the fluorescence of Nb19, Nb34, and Nb68 is identical to the one of Nb5. This indicates that Nb19, Nb34, and Nb68 bind to the purified HCN4_{OPEN}.

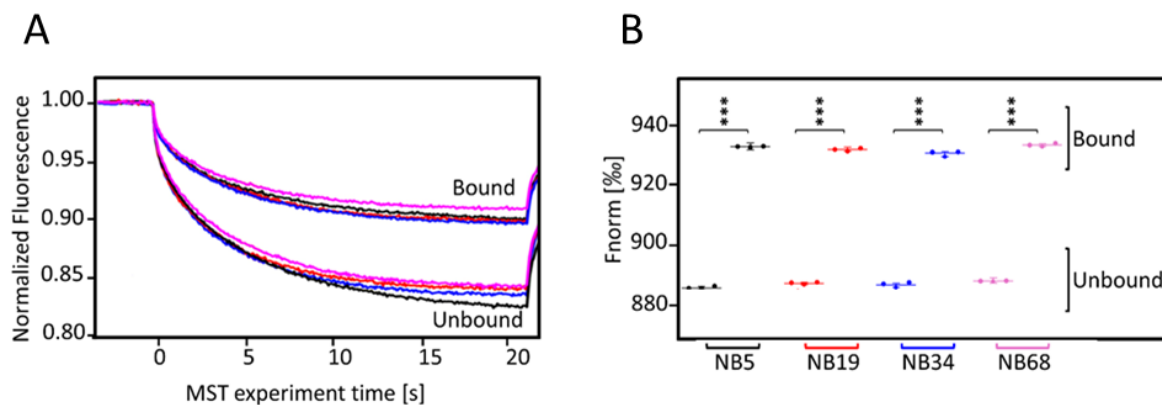



Figure 4.15. MST binding check assay. **A.** The MST traces of RED-Nbs (black for Nb5, red for Nb19, blue for Nb34 and pink for Nb68) in the absence (Unbound) and in the presence of HCN4_{OPEN} (Bound). **B.** Mean normalized fluorescence values in the absence (Unbound) and in the presence of HCN4_{OPEN} (Bound). Data are presented as mean \pm SEM. Number of experiments = 3. Statistical analysis performed with one-way ANOVA, followed by Fisher's test (***P < 0.0001).



While this assay suggests binding of the Nbs to HCN4, it bears no information on whether they interact like Nb5 or Nb6 with the extracellular side of the channel or like Nb1 from the intracellular side. To test if Nb19, Nb34, and Nb68 bind to HCN4 extracellularly, we designed a FACS-based assay where HEK293F cells over-expressing GFP-HCN4 channels were incubated with Nb5; the latter was labelled with the RED-tris-NTA dye before analysis (for details, see material and methods, section 4.2.13). We then sorted cells for both green and red fluorescence. In this way we could select HEK cells 1) expressing GFP-HCN4 and cell 2) decorated with the RED-Nb5 as a result of binding to the channel extracellularly. In a control experiment we found that an efficient labelling with the RED-tris-NTA dye requires 0.05% Tween-20. Therefore, the solution of the labelled protein should contain such a detergent, which is known to affect the stability of the cell membrane, even at a concentration as low as 0.05% (Eskandani et al., 2013; Hua et al., 2018). To avoid an unspecific side effect of the detergent, Nb5 had to be labeled in a Tween-20-free solution. As expected, this affected the efficiency of labelling. Figure 4.16 show the MST binding assay of RED-tris-NTA to Nb5 in the absence of Tween-20, where the traces are indeed disturbed (Figure 4.16). Because of this low resolution and disturbance of the fluorescence signal the binding curve cannot be concluded. This is most likely because in the absence of Tween-20, non-ionic surfactant widely used as an emulsifier and stabilizer of organic compounds as RED-tris-NTA, the dye is not well dissolved in aqueous solution. This results in a scenario in which at high Nb5 concentrations the non-properly dissolved RED-tris-NTA tends to nonspecifically associate with the His-tag of the Nb. This causes the recorded aggregation/precipitation phenomena in Figure 4.16. This significant decrease in the labelling efficiency has to be considered during the analysis of the FACS experiments. Indeed, only a small fraction of Nb5 is actually labelled. Hence the percentage of GFP-HCN4 expressing cells decorated with Nb5 will be underrepresented.

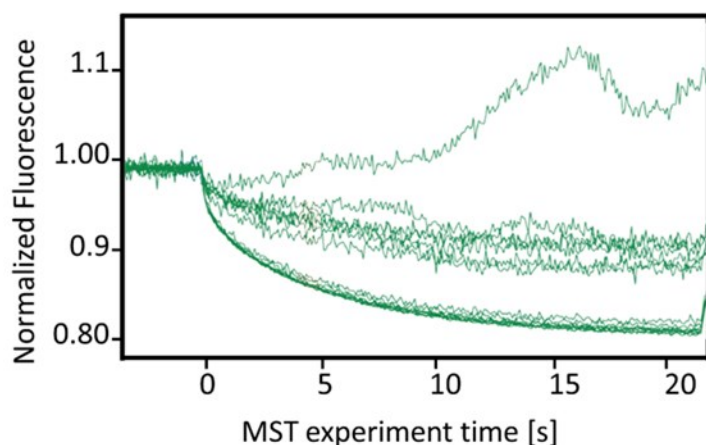


Figure 4.16. Labeling of Nb5 in a Tween-20-free solution. The MST traces show a decrease on the rate of the temperature-dependent decay of the fluorescence of Red-tris-NTA dye (the receptor) due to a concomitant progressive increase in the Nb5 (the ligand) concentration. At high Nb5 concentrations the signal becomes

unstable, most likely because of RED-tris-NTA is not-well dissolved in the absence of Tween-20 and thus tends to improperly associate with the His-tag of Nb5, causing aggregation/precipitation phenomena.

The results of the FACS are shown in the Figure 4.17. First, we ruled out eventual non-specific bindings of RED-tris-NTA-labelled Nbs to HEK cells. To do so, we incubated GFP-expressing cells with RED-Nb5. As shown in panel A, we did not sort cells which contained both green and red labels, indicating that Nb5 does not bind to HEK293 cells in a non-specific manner. Since Nb sequences are highly conserved, except for the CDR loops (the antigen binding site, see Figure 4.6B), we concluded that also other Nbs will behave in the same way as Nb5 when incubated with HEK293F cells. The pre-incubation of cells expressing GFP-HCN4 with RED-Nb5 caused a small, but significant portion of the green labeled cells which also display a red signal (6.5%, Figure 4.17B). This indicates that RED-Nb5 binds to the extracellular portion of the channel. This agrees well with the functional data on Nb5 (see Table 4.2) and prompted us to proceed with this FACS-based assay to screen for the eventual extracellular binding of Nb19, 34 and 68 to HCN4 (respectively panel C-E). In all three cases we could detect a small, but significant fraction of GFP-HCN4 expressing cells decorated with the three RED-tris-NTA-labelled Nbs, as in the case of the control Nb5 (see panel B for a comparison).

Based on these data, we can confirm that Nb19, Nb34, and Nb68 bind to HCN4 and that this binding occurs on the extracellular side. After establishing this protocol further FACS assays can be performed with HEK293 cells expressing HCN1 and HCN2 to investigate their isotype selectivity. Those Nbs that will turn out in this assay as non-selective for HCN4, will be

further tested on hERG expressing cells to check for their specificity for the HCN family member.

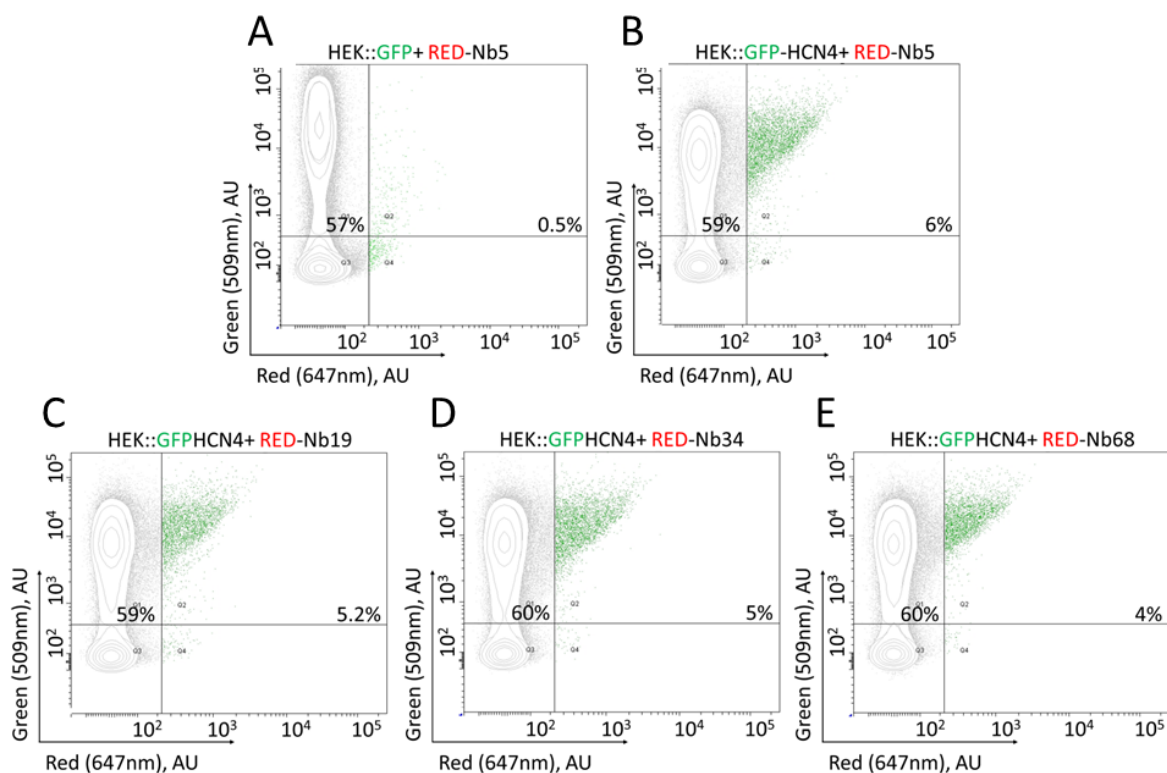



Figure 4.17. Testing Nb19, 34, 68 binding to HCN4 from its extracellular side. A-E. FACS contour plots showing double gate signals (red in the x axis – 647 nm and green in the y axis – 509 nm). The percentage of green positive cells is about 60% in all the transfections shown. On note that cells not emitting green light are either not positive for the red light too, or if so, the percentage is not significant. **A.** GFP transfected HEK293F cells were pre-incubated with RED-Nb5 and then subjected to an analytical FACS analysis. The absence of double red- and green-positive cells indicates that the RED-Nb5 does not aspecifically interacts with the cells. **B.** GFP-HCN4 transfected HEK293F cells pre-incubated with RED-Nb5 and then subjected to an analytical FACS analysis, which shows that 6.5% of green positive cells are also positive for the red signal. **C-E.** GFP-HCN4 transfected HEK293F cells pre-incubated with RED-Nb19 (C), 34 (D) and 68 (E) and then subjected to an analytical FACS. The assay shows that 5.2% (C), 5% (D), and 4% (E) of green positive cells are also positive for the red signal.

4.3.7 Conclusions

Nanobodies (Nbs) are promising molecules in both biotechnology and pharmacology. Indeed, they combine the beneficial properties of small molecules and monoclonal antibodies such as high affinity and selectivity for the target. It is worth noting that Nb are already employed in clinics (Morrison, 2019).

By taking advantage of an available yeast display platform of nanobody library (McMahon et al., 2018), and of our ability to purify the HCN4 channel with the pore in the open and closed conformation (Saponaro, Bauer, et al., 2021; Saponaro, Sharifzadeh, et al., 2021), we set a protocol for the selection of Nbs able to bind and to modulate HCN4 channels. With this protocol we identified ten independent hits. As summarized in Table 4.2, seven of them affect the voltage dependent gating of HCN4 by shifting its opening towards more depolarized potentials. Six act from the extracellular side (3, 5, 6, 11, 60, 66) and one intracellularly (Nb1). Of these, four are not HCN4 specific, as they modulate also HCN1 currents (6, 11, 60, 66). Nonetheless, even these four Nbs appear to be specific for the HCN family, as they do not act on the cognate channel hERG. Only one of the candidates (Nb66) acts also on the hERG channel. Hence Nb66 seems not to be HCN selective. This overall quite stringent selectivity of the Nbs toward the family of HCN channels is a sign for the success of the procedure of Nb selection. Moreover, we are not surprised that the selectivity for the HCN4 subtype is not a predominant feature of the Nbs characterized up to now. Indeed, HCN channel subtypes are highly conserved in both their core transmembrane and cytosolic regions; on the amino acid level they are 80–90% identical (Santoro et al., 1998). Nonetheless, our protocol of selection led us to identify Nb3 and Nb5 as selective modulators of the HCN4 isoform. At this point it should be mentioned that the characterization of the isotype specificity has not yet been completed for Nb1, 19, 34, and 68, so that now we cannot exclude that these Nbs will also work on other HCN isotypes.

Nb5 already represents a good candidate for future pharmacological treatments of HCN4-linked diseases. Indeed, it displays four crucial features of a feasible protein-based drug candidate. It exhibits: 1) a high yield of expression/purification; 2) selectivity for an isoform and 3) the high affinity for the target and finally 4) the activity from the extracellular side. In some prove of concept studies, we have demonstrated the ability of Nb5 to abolish the




pathological effect of an HCN4 mutation identified in a bradycardic patient (Duhme et al., 2013). Future perspectives will regard the testing of Nb5 on native HCN4 current, i.e., by applying the Nb on SAN cells.

Even though we have selected Nbs specifically targeting HCN4 with the open pore, none of them acted as a pore blocker or reduces/inhibits the channel current. It is also worth noting that our functional/cellular data indicate that, at least for the Nbs that interact with HCN channels from the extracellular side, they are binding to channels in the closed state. In electrophysiological recordings, Nbs are added to the extracellular solution ten minutes before the recordings. In this condition the membrane potential of HEK293 cells is about -10 mV, e.g., a condition under which HCN channels are closed. Also, in the FACS assays, cells are incubated with labelled Nbs in PBS buffer. Also in this condition the membrane potential of the cells is only around -20 mV e.g a voltage at which HCN channels are closed (Porro et al., 2019). Future biochemical studies, e.g., MST binding assays between labelled Nbs and HCN4 with the closed pore, will further validate this indication.


How can we explain the discrepancy between a stringent selection of Nbs positively targeting HCN4 with the open pore and the isolation of several Nbs apparently interacting with the closed state of the channels?

A possible explanation comes from the fact that the conformational changes at the level of the extracellular vestibule of the pore of HCN4 (Saponaro, Bauer, et al., 2021) may have not caused enough modifications to the solvent exposed surface of the pore to become a defined target for a conformational selective binders. We thought to overcome this limit by using Nbs instead of conventional antibodies. Indeed, Nbs are significantly smaller compared to the fab fragments, the domains of canonical antibodies bearing the antigen binding surface. This is the reason why Nb are typically used to target narrow spaces not reachable by conventional antibodies, such as the clefts of enzyme's catalytic sites and the even pore of ion channels (De Genst et al., 2006; Lauwereys et al., 1998). From our functional characterization of the selected Nbs, this approach did not work for the HCN4 channel. Anyhow, there is still the possibility that the remaining Nbs, Nb19, 34, and 68, which do not modify the biophysical properties of HCN4 but still interact with the channel from the extracellular side, may bind close to the pore. We already know from the electrophysiological



data that they do not occlude the pore. This does not imply that they do not interact in its proximity. Indeed, the small size of a Nb (about 15 kDa) can limit its ability of occluding a large extracellular vestibule as the one of the tetrameric HCN channels. In agreement with this, a recent report showed that monomeric nanobodies selected for blocking the pore of a trimeric ion channel were poorly efficient. Only their dimeric tandem version succeeded in occluding the pore (Danquah et al., 2016). Following this strategy, any candidate Nb among Nb19, 34, and 68, that will bind in proximity of the extracellular vestibule of the pore will be tested as dimeric, or even tetrameric tandems, depending on their binding stoichiometry. This enlargement of their size might possibly lead to an effective occlusion of the HCN4 pore, thus generating protein-based blockers.

A key question that needs to be addressed in relation to Nb action is its binding site. This can be roughly solved by chemically crosslinking Nbs to purified HCN4 and then by analyzing the complex by mass spectrometry. This procedure will identify the primary sequences of Nb and HCN4 involved in the interaction. A more detailed analysis will require a 3D structure of the HCN4-Nb complex via single particle cryo-EM. The identification of the binding site will help to understand three main open questions: 1) the source of the isotype specificity; 2) why we did not select pore blockers; 2) the modulatory effects on HCN current exerted by Nbs. Concerning the latter question, we were surprised to have selected only potentiators of the voltage dependent opening of HCN channels. With no indication on where the Nbs interact with the channel protein, we can only report the fact that this positive effect on the voltage dependency exerted by Nbs resembles the one of the natural ligand cAMP (Wainger et al., 2001). Since the action of the Nbs does not fully recapitulate the response of the channel to cAMP it remains unclear if both modulations are based on the same mechanism. At first glance the fact that most NBs act from the extracellular side but cAMP from the cytosolic side seem even to exclude a common mode of action. But, since we know from the literature that there is a reciprocal influence between the VSD and the cytosolic cAMP pathway and that VSD movement influences the affinity of the CNBD for cAMP (Chen et al., 2007; Kusch et al., 2010; Porro et al., 2019; Thon et al., 2015; S. Wu et al., 2011), we can even speculate that Nbs may act on the same molecular pathway of cAMP. Further studies will address this question.



Finally, it is worth noting that the three Nbs which are not affecting the biophysical properties of HCN4 current are still specifically interacting with HCN proteins from the extracellular side. While these Nbs might be less interesting developing pore blockers they offer a great opportunity for a labelling of HCN channels. Also from a pharmacological perspective, they might be useful for targeting and tethering proteins and/or drugs to the extracellular side of HCN channels (Shields et al., 2017). Depending on the specificity of the Nbs this could result in an HCN4 isoform specific targeting or general HCN channels specific targeting.

References

- Altomare, C., Terragni, B., Brioschi, C., Milanesi, R., Pagliuca, C., Viscomi, C., Moroni, A., Baruscotti, M., & DiFrancesco, D. (2003). Heteromeric HCN1-HCN4 channels: A comparison with native pacemaker channels from the rabbit sinoatrial node. *Journal of Physiology*, 549(2), 347–359. <https://doi.org/10.1113/jphysiol.2002.027698>
- Alvarez-Baron, C. P., Klenchin, V. A., & Chanda, B. (2018). Minimal molecular determinants of isoform-specific differences in efficacy in the HCN channel family. *Journal of General Physiology*, 150(8), 1203–1213. <https://doi.org/10.1085/jgp.201812031>
- Bartoschik, T., Galinec, S., Kleusch, C., Walkiewicz, K., Breitsprecher, D., Weigert, S., Muller, Y. A., You, C., Piehler, J., Vercruyse, T., Daelemans, D., & Tschammer, N. (2018). Near-native, site-specific and purification-free protein labeling for quantitative protein interaction analysis by MicroScale Thermophoresis. *Scientific Reports*, 8(1), 1–10. <https://doi.org/10.1038/s41598-018-23154-3>
- Baruscotti, M., Bottelli, G., Milanesi, R., DiFrancesco, J. C., & DiFrancesco, D. (2010). HCN-related channelopathies. *Pflugers Archiv European Journal of Physiology*, 460(2), 405–415. <https://doi.org/10.1007/s00424-010-0810-8>
- Baruscotti, M., Bucchi, A., Barbuti, A., & DiFrancesco, D. (2012). Funny current and cardiac rhythm: insights from HCN knockout and transgenic mouse models. *Frontiers in Physiology*, 3, 240.
- Baruscotti, M., Bucchi, A., Milanesi, R., Paina, M., Barbuti, A., Gnecci-Ruscione, T., Bianco, E., Vitali-Serdoz, L., Cappato, R., & DiFrancesco, D. (2017). A gain-of-function mutation in the cardiac pacemaker HCN4 channel increasing cAMP sensitivity is associated with familial Inappropriate Sinus Tachycardia. *European Heart Journal*, 38(4), 280–288.
- Baruscotti, M., & DiFrancesco, D. (2004). Pacemaker channels. *Annals of the New York Academy of Sciences*, 1015(1), 111–121.
- Biel, M., Wahl-Schott, C., Michalakis, S., & Zong, X. (2009). Hyperpolarization-activated cation channels: From genes to function. *Physiological Reviews*, 89(3), 847–885. <https://doi.org/10.1152/physrev.00029.2008>
- Billen, B., Vincke, C., Hansen, R., Devoogdt, N., Muyldermans, S., Adriaensens, P., & Guedens, W. (2017). Cytoplasmic versus periplasmic expression of site-specifically and bioorthogonally functionalized nanobodies using expressed protein ligation. *Protein Expression and Purification*, 133, 25–34. <https://doi.org/10.1016/j.pep.2017.02.009>
- Bolívar, J. J., Tapia, D., Arenas, G., Castanon-Arreola, M., Torres, H., & Galarraga, E. (2008). A hyperpolarization-activated, cyclic nucleotide-gated, (I_h-like) cationic current and HCN gene expression in renal inner medullary collecting duct cells. *American Journal of Physiology-Cell Physiology*, 294(4), C893–C906.
- Bucchi, A., Baruscotti, M., Nardini, M., Barbuti, A., Micheloni, S., Bolognesi, M., & DiFrancesco, D. (2013). Identification of the Molecular Site of Ivabradine Binding to HCN4 Channels. *PLoS ONE*, 8(1), 1–12. <https://doi.org/10.1371/journal.pone.0053132>
- Burke, D., Howells, J., & Tomlinson, S. E. (2013). Hcn channels: Function and clinical implications. *Neurology*, 81(5), 513–514. <https://doi.org/10.1212/01.wnl.0000433163.22224.2c>
- Campostrini, G., DiFrancesco, J. C., Castellotti, B., Milanesi, R., Gnecci-Ruscione, T., Bonzanni, M., Bucchi, A., Baruscotti, M., Ferrarese, C., Franceschetti, S., Canafoglia, L., Ragona, F., Freri, E., Labate, A., Gambardella, A., Costa, C., Gellera, C., Granata, T., Barbuti, A., &

-
- Difrancesco, D. (2018). A loss-of-function HCN4 mutation associated with familial benign myoclonic epilepsy in infancy causes increased neuronal excitability. *Frontiers in Molecular Neuroscience*, 11(August), 1–15. <https://doi.org/10.3389/fnmol.2018.00269>
- Cervetto, L., Demontis, G. C., & Gargini, C. (2007). Cellular mechanisms underlying the pharmacological induction of phosphenes. *British Journal of Pharmacology*, 150(4), 383–390. <https://doi.org/10.1038/sj.bjp.0706998>
- Chen, S., Wang, J., & Siegelbaum, S. A. (2001). Properties of hyperpolarization-activated pacemaker current defined by coassembly of HCN1 and HCN2 subunits and basal modulation by cyclic nucleotide. *The Journal of General Physiology*, 117(5), 491–504.
- Chen, S., Wang, J., Zhou, L., George, M. S., & Siegelbaum, S. A. (2007). Voltage sensor movement and cAMP binding allosterically regulate an inherently voltage-independent closed-open transition in HCN channels. *Journal of General Physiology*, 129(2), 175–188. <https://doi.org/10.1085/jgp.200609585>
- Danquah, W., Catherine, M. S., Rissiek, B., Pinto, C., Arnau, S. P., Amadi, M., Iacenda, D., Knop, J. H., Hammel, A., Bergmann, P., Schwarz, N., Assunção, J., Rotthier, W., Haag, F., Tolosa, E., Bannas, P., Eric, B. G., Magnus, T., Laeremans, T., ... Friedrich, K. N. (2016). Nanobodies that block gating of the P2X7 ion channel ameliorate inflammation. *Science Translational Medicine*, 8(366). <https://doi.org/10.1126/scitranslmed.aaf8463>
- De Genst, E., Silence, K., Decanniere, K., Conrath, K., Loris, R., Kinne, J., Muyldermans, S., & Wyns, L. (2006). Molecular basis for the preferential cleft recognition by dromedary heavy-chain antibodies. *Proceedings of the National Academy of Sciences of the United States of America*, 103(12), 4586–4591. <https://doi.org/10.1073/pnas.0505379103>
- Debie, P., Lafont, C., Defrise, M., Hansen, I., van Willigen, D. M., van Leeuwen, F. W. B., Gijssbers, R., D’Huyvetter, M., Devoogdt, N., Lahoutte, T., Mollard, P., & Hernot, S. (2020). Size and affinity kinetics of nanobodies influence targeting and penetration of solid tumours. *Journal of Controlled Release*, 317(September 2019), 34–42. <https://doi.org/10.1016/j.jconrel.2019.11.014>
- Di Francesco, D. (2015). HCN4, sinus bradycardia and atrial fibrillation. *Arrhythmia and Electrophysiology Review*, 4(1), 9–13. <https://doi.org/10.15420/aer.2015.4.1.9>
- Difrancesco, D. (2013). Funny channel gene mutations associated with arrhythmias. *Journal of Physiology*, 591(17), 4117–4124. <https://doi.org/10.1113/jphysiol.2013.253765>
- DiFrancesco, D. (1993). Pacemaker mechanisms in cardiac tissue. *Annual Review of Physiology*, 55(1), 455–472.
- DiFrancesco, D. (2006). Funny channels in the control of cardiac rhythm and mode of action of selective blockers. *Pharmacological Research*, 53(5), 399–406.
- DiFrancesco, J. C., Barbuti, A., Milanesi, R., Coco, S., Bucchi, A., Bottelli, G., Ferrarese, C., Franceschetti, S., Terragni, B., Baruscotti, M., & DiFrancesco, D. (2011). Recessive loss-of-function mutation in the pacemaker HCN2 Channel causing increased neuronal excitability in a patient with idiopathic generalized epilepsy. *Journal of Neuroscience*, 31(48), 17327–17337. <https://doi.org/10.1523/JNEUROSCI.3727-11.2011>
- DiFrancesco, J. C., & DiFrancesco, D. (2015). Dysfunctional HCN ion channels in neurological diseases. *Frontiers in Cellular Neuroscience*, 9(March), 1–10. <https://doi.org/10.3389/fncel.2015.00071>
- Duhme, N., Schweizer, P. A., Thomas, D., Barends, T. R. M., Schlichting, I., Draguhn, A., Bruehl, C., Katus, H. A., & Koenen, M. (2013). Altered HCN4 channel C-linker interaction is

- associated with familial tachycardia – bradycardia syndrome and atrial fibrillation. 2768–2775. <https://doi.org/10.1093/eurheartj/ehs391>
- El-Kholy, W., MacDonald, P. E., Fox, J. M., Bhattacharjee, A., Xue, T., Gao, X., Zhang, Y., Stieber, J., Li, R. A., & Tsushima, R. G. (2007). Hyperpolarization-activated cyclic nucleotide-gated channels in pancreatic β -cells. *Molecular Endocrinology*, 21(3), 753–764.
- Emery, E. C., Young, G. T., Berrocoso, E. M., Chen, L., & McNaughton, P. A. (2011). HCN2 ion channels play a central role in inflammatory and neuropathic pain. *Science*, 333(6048), 1462–1466.
- Emery, E. C., Young, G. T., & McNaughton, P. A. (2012). HCN2 ion channels: An emerging role as the pacemakers of pain. *Trends in Pharmacological Sciences*, 33(8), 456–463. <https://doi.org/10.1016/j.tips.2012.04.004>
- Eskandani, M., Hamishehkar, H., & Dolatabadi, J. E. N. (2013). Cyto/genotoxicity study of polyoxyethylene (20) sorbitan monolaurate (tween 20). *DNA and Cell Biology*, 32(9), 498–503. <https://doi.org/10.1089/dna.2013.2059>
- Fenske, S., Mader, R., Scharr, A., Pappas, C., Cao-Ehler, X., Michalakis, S., Shaltiel, L., Weidinger, M., Stieber, J., & Feil, S. (2011). HCN3 contributes to the ventricular action potential waveform in the murine heart. *Circulation Research*, 109(9), 1015–1023.
- Flajnik, M. F., Deschacht, N., & Muylers, S. (2011). A case of convergence: Why did a simple alternative to canonical antibodies arise in Sharks and Camels? *PLoS Biology*, 9(8). <https://doi.org/10.1371/journal.pbio.1001120>
- Flynn, G. E., & Zagotta, W. N. (2018). Insights into the molecular mechanism for hyperpolarization-dependent activation of HCN channels. *Proceedings of the National Academy of Sciences of the United States of America*, 115(34), E8086–E8095. <https://doi.org/10.1073/pnas.1805596115>
- Fürst, O., & D’Avanzo, N. (2015). Isoform dependent regulation of human HCN channels by cholesterol. *Scientific Reports*, 5, 1–12. <https://doi.org/10.1038/srep14270>
- Fyk-Kolodziej, B., & Pourcho, R. G. (2007). Differential distribution of hyperpolarization-activated and cyclic nucleotide-gated channels in cone bipolar cells of the rat retina. *Journal of Comparative Neurology*, 501(6), 891–903.
- Gareth, R., Physiological, T. H. E., Of, S., Firing, R., Role, T. H. E., Hcn, T. H. E., Family, G., Patterns, E., The, O. F., Genes, H. C. N., Molecular, P., For, B., Low, T. H. E., Selectivity, I. O. N., Nucleotide, C., & Of, M. (2005). The HCN Gene Family : Molecular Basis of the Hyperpolarization-Activated ABSTRACT : AND THE ROLE OF I h. 868, 1–23.
- Gibson, D. G., Young, L., Chuang, R. Y., Venter, J. C., Hutchison, C. A., & Smith, H. O. (2009). Enzymatic assembly of DNA molecules up to several hundred kilobases. *Nature Methods*, 6(5), 343–345. <https://doi.org/10.1038/nmeth.1318>
- Gross, C., Saponaro, A., Santoro, B., Moroni, A., Thiel, G., & Hamacher, K. (2018). Mechanical transduction of cytoplasmic-to-transmembrane-domain movements in a hyperpolarization-activated cyclic nucleotide-gated cation channel. *Journal of Biological Chemistry*, 293(33), 12908–12918. <https://doi.org/10.1074/jbc.RA118.002139>
- Hamers-Casterman, C., Atarhouch, T., Muylers, S. al, Robinson, G., Hammers, C., Songa, E. B., Bendahman, N., & Hammers, R. (1993). Naturally occurring antibodies devoid of light chains. *Nature*, 363(6428), 446–448.
- Hayoz, S., Tiwari, P. B., Piszczek, G., Üren, A., & Brelidze, T. I. (2017). Investigating cyclic nucleotide and cyclic dinucleotide binding to HCN channels by surface plasmon

- resonance. *PLoS ONE*, 12(9), 1–20. <https://doi.org/10.1371/journal.pone.0185359>
- He, P., Deng, J., Zhong, X., Zhou, Z., Song, B., & Li, L. (2012). Identification of a hyperpolarization-activated cyclic nucleotide-gated channel and its subtypes in the urinary bladder of the rat. *Urology*, 79(6), 1411–e7.
- Herrmann, S., Hofmann, F., Stieber, J., & Ludwig, A. (2012). HCN channels in the heart: Lessons from mouse mutants. *British Journal of Pharmacology*, 166(2), 501–509. <https://doi.org/10.1111/j.1476-5381.2011.01798.x>
- Herrmann, S., Layh, B., & Ludwig, A. (2011). Novel insights into the distribution of cardiac HCN channels: an expression study in the mouse heart. *Journal of Molecular and Cellular Cardiology*, 51(6), 997–1006.
- Herrmann, S., Schnorr, S., & Ludwig, A. (2015). Hcn channels—modulators of cardiac and neuronal excitability. *International Journal of Molecular Sciences*, 16(1), 1429–1447. <https://doi.org/10.3390/ijms16011429>
- Holmgren, M., Shin, K. S., & Yellen, G. (1998). The activation gate of a voltage-gated K⁺ channel can be trapped in the open state by an intersubunit metal bridge. *Neuron*, 21(3), 617–621.
- Hua, T., Zhang, X., Tang, B., Chang, C., Liu, G., Feng, L., Yu, Y., Zhang, D., & Hou, J. (2018). Tween-20 transiently changes the surface morphology of PK-15 cells and improves PCV2 infection. *BMC Veterinary Research*, 14(1), 1–8. <https://doi.org/10.1186/s12917-018-1457-5>
- Ishii, T. M., Takano, M., Xie, L.-H., Noma, A., & Ohmori, H. (1999). Molecular characterization of the hyperpolarization-activated cation channel in rabbit heart sinoatrial node. *Journal of Biological Chemistry*, 274(18), 12835–12839.
- Jerabek-Willemsen, M., André, T., Wanner, R., Roth, H. M., Duhr, S., Baaske, P., & Breitsprecher, D. (2014). MicroScale Thermophoresis: Interaction analysis and beyond. *Journal of Molecular Structure*, 1077, 101–113. <https://doi.org/10.1016/j.molstruc.2014.03.009>
- Jung, S., Bullis, J. B., Lau, I. H., Jones, T. D., Warner, L. N., & Poolos, N. P. (2010). Downregulation of dendritic HCN channel gating in epilepsy is mediated by altered phosphorylation signaling. *Journal of Neuroscience*, 30(19), 6678–6688. <https://doi.org/10.1523/JNEUROSCI.1290-10.2010>
- Kanner, S. A., Shuja, Z., Choudhury, P., Jain, A., & Colecraft, H. M. (2020). Targeted deubiquitination rescues distinct trafficking-deficient ion channelopathies. *Nature Methods*, 17(12), 1245–1253. <https://doi.org/10.1038/s41592-020-00992-6>
- Kariuki, C. K., & Magez, S. (2021). Improving the yield of recalcitrant Nanobodies® by simple modifications to the standard protocol. *Protein Expression and Purification*, 185. <https://doi.org/10.1016/j.pep.2021.105906>
- Kopec, W., Köpfer, D. A., Vickery, O. N., Bondarenko, A. S., Jansen, T. L. C., De Groot, B. L., & Zachariae, U. (2018). Direct knock-on of desolvated ions governs strict ion selectivity in K⁺ channels. *Nature Chemistry*, 10(8), 813–820.
- Kusch, J., Biskup, C., Thon, S., Schulz, E., Nache, V., Zimmer, T., Schwede, F., & Benndorf, K. (2010). Interdependence of receptor activation and ligand binding in hcn2 pacemaker channels. *Neuron*, 67(1), 75–85. <https://doi.org/10.1016/j.neuron.2010.05.022>
- Kusch, J., Thon, S., Schulz, E., Biskup, C., Nache, V., Zimmer, T., Seifert, R., Schwede, F., & Benndorf, K. (2012). How subunits cooperate in cAMP-induced activation of

-
- homotetrameric HCN2 channels. *Nature Chemical Biology*, 8(2), 162–169.
- Lata, S., Reichel, A., Brock, R., Tampé, R., & Piehler, J. (2005). High-affinity adaptors for switchable recognition of histidine-tagged proteins. *Journal of the American Chemical Society*, 127(29), 10205–10215. <https://doi.org/10.1021/ja050690c>
- Lauwereys, M., Ghahroudi, M. A., Desmyter, A., Kinne, J., Hölzer, W., De Genst, E., Wyns, L., & Muyldermans, S. (1998). Potent enzyme inhibitors derived from dromedary heavy-chain antibodies. *EMBO Journal*, 17(13), 3512–3520. <https://doi.org/10.1093/emboj/17.13.3512>
- Lee, C. H., & MacKinnon, R. (2017). Structures of the Human HCN1 Hyperpolarization-Activated Channel. *Cell*, 168(1–2), 111–120.e11. <https://doi.org/10.1016/j.cell.2016.12.023>
- Lee, C. H., & MacKinnon, R. (2019). Voltage Sensor Movements during Hyperpolarization in the HCN Channel. *Cell*, 179(7), 1582–1589.e7. <https://doi.org/10.1016/j.cell.2019.11.006>
- Liston, C. (2019). Targeting pacemaker channels in depression. *Science Translational Medicine*, 11(477), eaaw5318.
- Liu, B., & Yang, D. (2022). Easily Established and Multifunctional Synthetic Nanobody Libraries as Research Tools. *International Journal of Molecular Sciences*, 23(3). <https://doi.org/10.3390/ijms23031482>
- Lolicato, M., Bucchi, A., Arrigoni, C., Zucca, S., Nardini, M., Schroeder, I., Simmons, K., Aquila, M., Difrancesco, D., Bolognesi, M., Schwede, F., Kashin, D., Fishwick, C. W. G., Johnson, A. P., Thiel, G., & Moroni, A. (2014). Cyclic dinucleotides bind the C-linker of HCN4 to control channel cAMP responsiveness. *Nature Chemical Biology*, 10(6), 457–462. <https://doi.org/10.1038/nchembio.1521>
- Lolicato, M., Nardini, M., Gazzarrini, S., Möller, S., Bertinetti, D., Herberg, F. W., Bolognesi, M., Martin, H., Fasolini, M., Bertrand, J. A., Arrigoni, C., Thiel, G., & Moroni, A. (2011). Tetramerization dynamics of C-terminal domain underlies isoform-specific cAMP gating in hyperpolarization-activated cyclic nucleotide-gated channels. *Journal of Biological Chemistry*, 286(52), 44811–44820. <https://doi.org/10.1074/jbc.M111.297606>
- Marini, C., Porro, A., Rastetter, A., Dalle, C., Rivolta, I., Bauer, D., Oegema, R., Nava, C., Parrini, E., Mei, D., Mercer, C., Dhamija, R., Chambers, C., Coubes, C., Thévenon, J., Kuentz, P., Julia, S., Pasquier, L., Dubourg, C., ... Depienne, C. (2018). HCN1 mutation spectrum: From neonatal epileptic encephalopathy to benign generalized epilepsy and beyond. *Brain*, 141(11), 3160–3178. <https://doi.org/10.1093/brain/awy263>
- Marionneau, C., Couette, B., Liu, J., Li, H., Mangoni, M. E., Nargeot, J., Lei, M., Escande, D., & Demolombe, S. (2005). Specific pattern of ionic channel gene expression associated with pacemaker activity in the mouse heart. *Journal of Physiology*, 562(1), 223–234. <https://doi.org/10.1113/jphysiol.2004.074047>
- Maslanka, R., Kwolek-Mirek, M., & Zadrag-Tecza, R. (2018). Autofluorescence of yeast *Saccharomyces cerevisiae* cells caused by glucose metabolism products and its methodological implications. *Journal of Microbiological Methods*, 146(January), 55–60. <https://doi.org/10.1016/j.mimet.2018.01.017>
- McMahon, C., Baier, A. S., Pascolutti, R., Wegrecki, M., Zheng, S., Ong, J. X., Erlandson, S. C., Hilger, D., Rasmussen, S. G. F., Ring, A. M., Manglik, A., & Kruse, A. C. (2018). Yeast surface display platform for rapid discovery of conformationally selective nanobodies. *Nature Structural and Molecular Biology*, 25(3), 289–296.

- <https://doi.org/10.1038/s41594-018-0028-6>
- Miltenyi, S., Müller, W., Weichel, W., & Radbruch, A. (1990). High gradient magnetic cell separation with MACS. *Cytometry*, 11(2), 231–238. <https://doi.org/10.1002/cyto.990110203>
- Momin, A., Cadiou, H., Mason, A., & Mcnaughton, P. A. (2008). Role of the hyperpolarization-activated current Ih in somatosensory neurons. *Journal of Physiology*, 586(24), 5911–5929. <https://doi.org/10.1113/jphysiol.2008.163154>
- Moosmang, S., Biel, M., Hofmann, F., & Ludwig, A. (1999). Differential distribution of four hyperpolarization-activated cation channels in mouse brain.
- Moroni, A., Barbuti, A., Altomare, C., Viscomi, C., Morgan, J., Baruscotti, M., & DiFrancesco, D. (2000). Kinetic and ionic properties of the human HCN2 pacemaker channel. *Pflügers Archiv European Journal of Physiology*, 439(5), 618–626. <https://doi.org/10.1007/s004240050985>
- Morrison, C. (2019). Nanobody approval gives domain antibodies a boost. 18(July), 485–487.
- Nji, E., Chatzikyriakidou, Y., Landreh, M., & Drew, D. (2018). An engineered thermal-shift screen reveals specific lipid preferences of eukaryotic and prokaryotic membrane proteins. *Nature Communications*, 9(1). <https://doi.org/10.1038/s41467-018-06702-3>
- Noam, Y., Bernard, C., & Baram, T. Z. (2011). Towards an integrated view of HCN channel role in epilepsy. *Current Opinion in Neurobiology*, 21(6), 873–879.
- Nof, E., Antzelevitch, C., & Glikson, M. (2010). The contribution of HCN4 to normal sinus node function in humans and animal models. *PACE - Pacing and Clinical Electrophysiology*, 33(1), 100–106. <https://doi.org/10.1111/j.1540-8159.2009.02563.x>
- Notomi, T., & Shigemoto, R. (2004). Immunohistochemical localization of Ih channel subunits, HCN1–4, in the rat brain. *Journal of Comparative Neurology*, 471(3), 241–276.
- Novella Romanelli, M., Sartiani, L., Masi, A., Mannaioni, G., Manetti, D., Mugelli, A., & Cerbai, E. (2016). HCN Channels Modulators: The Need for Selectivity. *Current Topics in Medicinal Chemistry*, 16(16). <https://doi.org/10.2174/1568026616999160315130832>
- Pape, H.-C., & McCormick, D. A. (1989). Noradrenaline and serotonin selectively modulate thalamic burst firing by enhancing a hyperpolarization-activated cation current. *Nature*, 340(6236), 715–718.
- Porro, A., Abbandonato, G., Veronesi, V., Russo, A., Binda, A., Antolini, L., Granata, T., Castellotti, B., Marini, C., Moroni, A., DiFrancesco, J. C., & Rivolta, I. (2021). Do the functional properties of HCN1 mutants correlate with the clinical features in epileptic patients? *Progress in Biophysics and Molecular Biology*, 166, 147–155. <https://doi.org/10.1016/j.pbiomolbio.2021.07.008>
- Porro, A., Saponaro, A., Gasparri, F., Bauer, D., Gross, C., Pisoni, M., Abbandonato, G., Hamacher, K., Santoro, B., Thiel, G., & Moroni, A. (2019). The HCN domain couples voltage gating and cAMP response in hyperpolarization-activated cyclic nucleotide-gated channels. *ELife*, 8, 1–23. <https://doi.org/10.7554/eLife.49672>
- Porro, A., Thiel, G., Moroni, A., & Saponaro, A. (2020). cyclic AMP Regulation and Its Command in the Pacemaker Channel HCN4. *Frontiers in Physiology*, 11, 771. <https://doi.org/10.3389/fphys.2020.00771>
- Postea, O., & Biel, M. (2011). Exploring HCN channels as novel drug targets. *Nature Reviews Drug Discovery*, 10(12), 903–914.
- Reid, C. A., Phillips, A. M., & Petrou, S. (2012). HCN channelopathies: Pathophysiology in

-
- genetic epilepsy and therapeutic implications. *British Journal of Pharmacology*, 165(1), 49–56. <https://doi.org/10.1111/j.1476-5381.2011.01507.x>
- Robinson, R. B., & Siegelbaum, S. A. (2003). Hyperpolarization-Activated Cation Currents: From Molecules to Physiological Function. *Annual Review of Physiology*, 65(4), 453–480. <https://doi.org/10.1146/annurev.physiol.65.092101.142734>
- Santoro, B., Chen, S., Lüthi, A., Pavlidis, P., Shumyatsky, G. P., Tibbs, G. R., & Siegelbaum, S. A. (2000). Molecular and functional heterogeneity of hyperpolarization-activated pacemaker channels in the mouse CNS. *Journal of Neuroscience*, 20(14), 5264–5275. <https://doi.org/10.1523/jneurosci.20-14-05264.2000>
- Santoro, B., Liu, D. T., Yao, H., Bartsch, D., Kandel, E. R., Siegelbaum, S. A., & Tibbs, G. R. (1998). Identification of a gene encoding a hyperpolarization-activated pacemaker channel of brain. *Cell*, 93(5), 717–729.
- Santoro, B., & Shah, M. M. (2020). Hyperpolarization-Activated Cyclic Nucleotide-Gated Channels as Drug Targets for Neurological Disorders.
- Saponaro, A., Bauer, D., Giese, M. H., Swuec, P., Porro, A., Gasparri, F., Sharifzadeh, A. S., Chaves-Sanjuan, A., Alberio, L., Parisi, G., Cerutti, G., Clarke, O. B., Hamacher, K., Colecraft, H. M., Mancía, F., Hendrickson, W. A., Siegelbaum, S. A., DiFrancesco, D., Bolognesi, M., ... Moroni, A. (2021). Gating movements and ion permeation in HCN4 pacemaker channels. *Molecular Cell*, 81(14), 2929–2943.e6. <https://doi.org/10.1016/j.molcel.2021.05.033>
- Saponaro, A., Cantini, F., Porro, A., Bucchi, A., DiFrancesco, D., Maione, V., Donadoni, C., Introini, B., Mesirca, P., Mangoni, M. E., Thiel, G., Banci, L., Santoro, B., & Moroni, A. (2018). A synthetic peptide that prevents camp regulation in mammalian hyperpolarization-activated cyclic nucleotide-gated (HCN) channels. *ELife*, 7, 1–22. <https://doi.org/10.7554/eLife.35753>
- Saponaro, A., Pauleta, S. R., Cantini, F., Matzapetakis, M., & Hammann, C. (2014). Structural basis for the mutual antagonism of cAMP and TRIP8b in regulating HCN channel function. *PNAS*, 111(40), 14577–14582. <https://doi.org/10.1073/pnas.1410389111>
- Saponaro, A., Sharifzadeh, A. S., & Moroni, A. (2021). Detection of ligand binding to purified HCN channels using fluorescence-based size exclusion chromatography. In *Ion Channels Part A* (1st ed., Vol. 652). Elsevier Inc. <https://doi.org/10.1016/bs.mie.2021.01.043>
- Sartiani, L., Mannaioni, G., Masi, A., Romanelli, M. N., & Cerbai, E. (2017). The hyperpolarization-activated cyclic nucleotide-gated channels: from biophysics to pharmacology of a unique family of ion channels. *Pharmacological Reviews*, 69(4), 354–395.
- Shields, B. C., Kahuno, E., Kim, C., Apostolides, P. F., Brown, J., Lindo, S., Mensh, B. D., Dudman, J. T., Lavis, L. D., & Tadross, M. R. (2017). Deconstructing behavioral neuropharmacology with cellular specificity. *Science*, 356(6352), 2161–2166. <https://doi.org/10.1126/science.aaj2161>
- Srinivasan, L., Alzogaray, V., Selvakumar, D., Nathan, S., Yoder, J. B., Wright, K. M., Klinke, S., Nwafor, J. N., Labanda, M. S., Goldbaum, F. A., Schön, A., Freire, E., Tomaselli, G. F., Amzel, L. M., Ben-Johny, M., & Gabelli, S. B. (2022). Development of high-affinity nanobodies specific for NaV1.4 and NaV1.5 voltage-gated sodium channel isoforms. *Journal of Biological Chemistry*, 298(4), 1–16. <https://doi.org/10.1016/j.jbc.2022.101763>
- Stieber, J., Stöckl, G., Herrmann, S., Hassfurth, B., & Hofmann, F. (2005). Functional expression of the human HCN3 channel. *Journal of Biological Chemistry*, 280(41), 34635–34643.

- <https://doi.org/10.1074/jbc.M502508200>
- Stinn, A., Furkert, J., Kaufmann, S. H. E., Moura-Alves, P., & Kolbe, M. (2021). Novel method for quantifying ahr-ligand binding affinities using microscale thermophoresis. *Biosensors*, 11(3). <https://doi.org/10.3390/bios11030060>
- Stortelers, C., Pinto-Espinoza, C., Van Hoorick, D., & Koch-Nolte, F. (2018). Modulating ion channel function with antibodies and nanobodies. *Current Opinion in Immunology*, 52, 18–26. <https://doi.org/10.1016/j.coi.2018.02.003>
- Tanguay, J., Callahan, K. M., & D’Avanzo, N. (2019). Characterization of drug binding within the HCN1 channel pore. *Scientific Reports*, 9(1), 1–14. <https://doi.org/10.1038/s41598-018-37116-2>
- Thon, S., Schulz, E., Kusch, J., & Benndorf, K. (2015). Conformational Flip of Nonactivated HCN2 Channel Subunits Evoked by Cyclic Nucleotides. *Biophysical Journal*, 109(11), 2268–2276. <https://doi.org/10.1016/j.bpj.2015.08.054>
- Ueda, K., Hirano, Y., Higashiuesato, Y., Aizawa, Y., Hayashi, T., Inagaki, N., Tana, T., Ohya, Y., Takishita, S., Muratani, H., Hiraoka, M., & Kimura, A. (2009). Role of HCN4 channel in preventing ventricular arrhythmia. *Journal of Human Genetics*, 54(2), 115–121. <https://doi.org/10.1038/jhg.2008.16>
- Vandenberg, J. I., Perry, M. D., Perrin, M. J., Mann, S. A., Ke, Y., & Hill, A. P. (2012). hERG K(+) channels: structure, function, and clinical significance. *Physiological Reviews*, 92(3), 1393–1478. <https://doi.org/10.1152/physrev.00036.2011>
- Verrier, R. L., Bonatti, R., Silva, A. F. G., Batatinha, J. A. P., Nearing, B. D., Liu, G., Rajamani, S., Zeng, D., & Belardinelli, L. (2014). If inhibition in the atrioventricular node by ivabradine causes rate-dependent slowing of conduction and reduces ventricular rate during atrial fibrillation. *Heart Rhythm*, 11(12), 2288–2296.
- Wahl-Schott, C., & Biel, M. (2009). HCN channels: Structure, cellular regulation and physiological function. *Cellular and Molecular Life Sciences*, 66(3), 470–494. <https://doi.org/10.1007/s00018-008-8525-0>
- Wahl-Schott, C., Fenske, S., & Biel, M. (2014). HCN channels: new roles in sinoatrial node function. *Current Opinion in Pharmacology*, 15, 83–90.
- Wainger, B. J., DeGennaro, M., Santoro, B., Siegelbaum, S. A., & Tibbs, G. R. (2001). Molecular mechanism of cAMP modulation of HCN pacemaker channels. *Nature*, 411(6839), 805–810.
- Weißgraeber, S., Saponaro, A., Thiel, G., & Hamacher, K. (2017). A reduced mechanical model for cAMP-modulated gating in HCN channels. *Scientific Reports*, 7(January), 1–9. <https://doi.org/10.1038/srep40168>
- William N. Zagotta, Nelson B. Olivier, Kevin D. Black, Edgar C. Young, Rich Olson², & Eric Gouaux. (2003). Structural basis for modulation and agonist specificity of HCN pacemaker channels. *Nature*, 425(6954), 196–200. <https://doi.org/10.1038/nature01932.1>
- Wu, J., Sun, L., Chen, X., Du, F., Shi, H., Chen, C., & Chen, Z. J. (2013). Cyclic GMP-AMP is an endogenous second messenger in innate immune signaling by cytosolic DNA. *Science (New York, N.Y.)*, 339(6121), 826–830. <https://doi.org/10.1126/science.1229963>
- Wu, S., Vysotskaya, Z. V., Xu, X., Xie, C., Liu, Q., & Zhou, L. (2011). State-dependent cAMP binding to functioning HCN channels studied by patch-clamp fluorometry. *Biophysical Journal*, 100(5), 1226–1232. <https://doi.org/10.1016/j.bpj.2011.01.034>
- Wu, Y., Chen, Z., Sigworth, F. J., & Canessa, C. M. (2021). Structure and analysis of nanobody

-
- binding to the human *ASIC1a* ion channel. *eLife*, 10, 1–20.
<https://doi.org/10.7554/eLife.67115>
- Wynia-Smith, S. L., Gillian-Daniel, A. L., Satyshur, K. A., & Robertson, G. A. (2008). hERG gating microdomains defined by S6 mutagenesis and molecular modeling. *The Journal of General Physiology*, 132(5), 507–520.
- Xu, H., Li, L., Deng, B., Hong, W., Li, R., Guo, Z., Hou, J., Govinden, R., & Chenia, H. Y. (2022). Construction of a T7 phage display nanobody library for bio-panning and identification of chicken dendritic cell-specific binding nanobodies. *Scientific Reports*, 12(1), 1–11.
<https://doi.org/10.1038/s41598-022-16378-x>
- Yao, J. A., Du, X., Lu, D., Baker, R. L., Daharsh, E., & Atterson, P. (2005). Estimation of potency of HERG channel blockers: Impact of voltage protocol and temperature. *Journal of Pharmacological and Toxicological Methods*, 52(1), 146–153.
<https://doi.org/10.1016/j.vascn.2005.04.008>
- Young, G. T., Emery, E. C., Mooney, E. R., Tsantoulas, C., & McNaughton, P. A. (2014). Inflammatory and neuropathic pain are rapidly suppressed by peripheral block of hyperpolarisation-activated cyclic nucleotide-gated ion channels. *PAIN*[®], 155(9), 1708–1719.

Declaration of own work

Part I and part II

I have elaborated the procedure for the expression of eukaryotic membrane proteins Hyperpolarization Activated and cyclic Nucleotide regulated (HCN4) pacemaker channel, in mammalian HEK293F cells.

I have set the protocol for the purification of eukaryotic membrane proteins, HCN pacemaker channel from the isolated membrane. I have performed the respective protein purifications and quality controls and I have provided the protein for the Cryo-EM studies.

I have been setting a protocol for performing fluorescent thermal shift assay and adapting a screening system, based on this assay, to detect binding of small molecules to the purified GFP-tagged HCN4 protein. I have used this binding protocol to detect the interaction of full-length HCN4 protein with cyclic dinucleotides, a new class of second messengers, which regulate the activity of HCN4. These data are not yet published.

Part III:

I have performed all experiments, data analysis, and data presentation in this chapter with the exception of the functional tests by electrophysiology. These experiments and related data analysis were performed by Roberta Castelli in the frame of a master thesis, which I partially supervised.

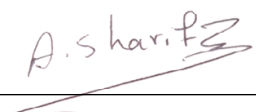
EHRENWÖRTLICHE ERKLÄRUNG

Ich erkläre hiermit ehrenwörtlich, dass ich die vorliegende Arbeit entsprechend den Regeln guter wissenschaftlicher Praxis selbstständig und ohne unzulässige Hilfe Dritter angefertigt habe.

Sämtliche aus fremden Quellen direkt oder indirekt übernommenen Gedanken sowie sämtliche von Anderen direkt oder indirekt übernommenen Daten, Techniken und Materialien sind als solche kenntlich gemacht. Die Arbeit wurde bisher bei keiner anderen Hochschule zu Prüfungszwecken eingereicht.

Die eingereichte elektronische Version stimmt mit der schriftlichen Version überein.

Milano, 22.01.2023



Atiyehsadat Sharifzadeh

CURRICULUM VITAE

Name Atiyehsadat Sharifzadeh
Date of birth 23/07/1979
Place of birth Golpayegan - Iran

Education

Since 01.01.2019 **PhD thesis** (Dr. rer. nat.)
Technische Universität Darmstadt
Fachbereich Biologie

01.10.2016 – 15.10.2018 **Master**
University of Milan
Molecular Biology of the Cell

10.01.2002 – 22.07.2006 **Bachelor**
Bu-Ali Sina University of Hamedan (Iran)
General Biology

Conferences and seminars

- 11-14/09/2022 - 25th National Congress, Italian Society of Pure and Applied Biophysics (SIBPA). Poster presentations: (1) Isolation of state-dependent nanobodies against HCN4 channels using a yeast surface display platform; (2) Detection of cyclic di-GMP binding to purified HCN4 pacemaker channel. San Miniato (Pisa), Italy
- 8/02/2022 - 3rd Chembion Online Symposium, Westfälische. Poster presentation: Detection of cyclic di-GMP binding to purified HCN4 pacemaker channel. Wilhelms-Universität Münster, Germany (Online)

-
- 22-26/02/2021 - 65th Annual Meeting of the Biophysical Society. Abstract: Monitoring ligand binding to purified HCN4 channel proteins (Online)
 - 10/01/2020 - noMAGIC Winter Retreat 2020; A Biochemical assay to detect ligand binding in purified full length HCN4 channels. Technische Universität Darmstadt, Germany
 - 10-12/09/2018 - noMAGIC International Symposium: Ion channel design using experimental and computational inputs (participation). Gargnano (BS) Italy

List of publications

- Saponaro A., Bauer D., Giese M.H., Swuec P., Porro A., Gasparri F., Sharifzadeh A.S., Chaves-Sanjuan A., Alberio A., Parisi G., Cerutti G., Clarke O.B., Hamacher K., Colecraft H.M., Mancina F., Hendrickson W.A., Siegelbaum S.A., DiFrancesco D., Bolognesi M., Thiel G., Santoro B., Moroni A. "Gating movements and ion permeation in HCN4 pacemaker channels". Mol Cell. 2021 81(14):2929-2943.e6. doi: 10.1016/j.molcel.2021.05.033.
- Saponaro A., Sharifzadeh A.S., Moroni A. "Detection of ligand binding to purified HCN channels using fluorescence-based size exclusion chromatography". Methods Enzymol. 2021; 652:105-123. doi: 10.1016/bs.mie.2021.01.043.